Mitigating Impacts of High Wind Energy Penetration through Energy Storage and Demand Response

Hamideh Bitaraf

Dissertation submitted to the Faculty of the Virginia Polytechnic Institute and State University in partial fulfillment of the requirements for the degree of

DOCTOR OF PHILOSOPHY

in

Electrical Engineering

Saifur Rahman

Manisa Pipattanasomporn

Lamine Mili

Guoqiang Yu

Alireza Haghighat

March 18, 2016

Arlington, Virginia

Key Words: High wind energy penetration, Energy storage, Demand response

Mitigating Impacts of High Wind Energy Penetration through Energy Storage and Demand Response

Hamideh Bitaraf

Abstract

High renewable energy penetration is a goal for many countries to increase energy security and reduce carbon emissions from conventional power plants. Wind energy is one of leading sources among different renewable resources. However, high wind energy penetration in the system brings new challenges to the electric power system due to its variable and stochastic nature, and non-correlation between wind and load profiles. The term non-correlation is used in this research refers to the fact that wind or any other renewable generation, which is nature driven, does not follow the load like conventional power plants.

Wind spill is a challenge to utilities with high wind energy penetration levels. This occurs from situations mentioned above and the fact that wind generation sometimes exceeds the servable load minus must-run generation. In these cases there is no option but to curtail non-usable wind generation. This dissertation presents grid-scale energy storage and demand response options as an optimization problem to minimize spilled wind energy. Even after managing this spilled wind energy, there is still a challenge in a system with high wind energy penetration coming from wind power forecast error.

Wind power forecast error is handled by having more back-up energy and spilling the non-usable wind power. This research offers a way to use the grid-scale energy storage units to mitigate impacts of wind power forecast error. A signal processing method is proposed to decompose the fluctuating wind power forecast error signal, based on the fact that each energy storage or conventional unit is more efficient to operate within specific cycling regimes. Finally, an algorithm is proposed to schedule energy storage for mitigating both impacts.

Mitigating Impacts of High Wind Energy Penetration through Energy Storage and Demand Response

Hamideh Bitaraf

General Audience Abstract

Wind energy is increasing to achieve the goal of environmental policies for less carbon emissions. High wind energy penetration in the electric power system brings new challenges because its generation depends on the wind speed. This makes renewable energy sources, including the wind energy, different from conventional power plants that follow the load profile.

Spilled wind energy is a challenge that occurs when wind power exceeds the load minus the must-run generation. In these cases there is no option rather than spilling the excess of wind generation. Energy storage technologies can be scheduled to store this excess of generation and then release it later. Load profile can be changed in such a way to decrease this spillage. This is achievable if customers change their demand based on incentive contracts they have with utilities or respond to the signal sent by utilities (This is called demand response). This dissertation presents the scheduling of energy storage and demand response to minimize spilled wind energy.

The wind power forecast error is another challenge due to the stochastic nature of this renewable energy. This research offers an algorithm to schedule energy storage units for mitigating impacts of wind power forecast error. The proposed algorithm is based on the fact that wind power forecast error signal is a very fluctuating signal and each energy storage unit is more efficient to operate within specific cycling regimes. Finally, an algorithm is proposed to use energy storage for mitigating both impacts coming from high wind energy penetration.

Acknowledgments

First, I would like to thank God to give me strength, hope, and patience to be able to complete my Ph.D. degree requirement. This became an important life journey as well, since I left my beloved family to come abroad for fulfilling my dreams.

I would like to express my gratitude to my advisor, Dr. Saifur Rahman, whose continuous support, guidance, and patience made this research work possible for me. He taught me to become an independent researcher while always questioning the applicability of proposed solutions in real world problems. His discipline, hard work, and deep knowledge set a good example for me to learn from. He will be always my role model not just as a great professor and advisor, but also as an outstanding person in academic, social, and personal life. I will always be grateful to him for giving me wise and precious advice in academic and non-academic matters.

I would like to thank Dr. Manisa Pipattanasomporn for her valuable contribution to my Ph.D. research. Her kind personality, patience, and smile have made Advanced Research Institute (ARI) a very friendly place to work in. I would like to thank Dr. Lamine Mili, Dr. Guaqiang Yu, and Dr. Alireza Haghighat who served as members of my committee. Thank you for your support, and great comments that helped me, improve my work from different perspectives.

Working at ARI has been a great experience for me. I would like to thank all my friends at ARI as Shibani, Avijit, Desong, and Prachi, who made my Ph.D. life fun and enjoyable. I would like to thank Yonael and Afroze for their support and kindness. I would like to thank Haya, who has been like a close sister to me, for her selfless friendship, as well as teaching me to be strong.

I would like to thank my parents, Zahra Mansouri and Habibolah Bitaraf. I would not have been able to do all of this without their unlimited support, encouragement, friendship, and love. My parents are not only my role models, but also my first, honest, and selfless friends in my life.

I would like to thank my dearest husband, Alireza Mirdamadi, who has lightened up my life with his endless support, patience, and love. He is the one who listened to me when I was confused and gave me great advices from his own Ph.D. experience. Words are not enough to express all my gratitude and love to my husband.

I would like to thank my sisters, Maryam and Tahereh, and their families for their support and encouragement. They have brought more joy and happiness to my life with their precious, lovely, and cute kids, Yusuf and Delsa.

Lastly, I would like to thank U.S. National Science Foundation (NSF grant number OISE-1104023) that partly supported this dissertation.

To my Mother, Zahra Mansouri, my lifetime kindest support to fulfill my dreams,
my Father, Habibolah Bitaraf, my lifetime inspiration to dream big,
my Husband, Alireza Mirdamadi, who brings love, hope, and happiness to my life,
and my Sisters, Maryam and Tahereh, my lifetime friends.

Table of Contents

List of Figures

List of Tables

1. Introduction

1.1 Background

High wind energy penetration is a goal for future scenarios influencing from many energy and environmental policies. Denmark, Portugal and Spain are top three countries, which have the highest percentage of annual wind energy generation to their total electricity consumption [1]. In Denmark wind power provided 33.2% of its annual electricity consumption in 2013 and is expected to reach 50% by 2020 [1], [2]. U.S. annual wind energy generation in 2012 was 3.5% [1]. Wind power is approaching 10% of the state's total electricity generation in Texas. Iowa is producing 25% of its power from wind energy [1]. 80% of the total U.S. electricity generation in 2050 can be supplied by renewable generation combined with a more flexible electric system [3].

Stability and reliability challenges occur due to uncertain and variable characteristics of wind resources [3]. In a system with high level of wind energy penetration, wind spill energy and negative electricity prices occur when there is an excess of wind generation. The negative price in an electricity market can appear due to the high level of inflexible generation, and production tax credit for renewable generation [4]. In cases where wind generation is more than load minus must-run generation (e.g., large nuclear power plants), the excess of wind energy needs to be spilled to keep the balance between demand and supply. This challenge can be mitigated by increasing flexible resources in the system, such as energy storage technologies and demand response resources. It is important to note that it is possible to manage the variable and stochastic generation of renewable sources by cycling intermediate power plants, but the downside of this strategy is fatigue and increased rates of maintenance for them.

Scheduling energy storage and demand response to minimize the cost function has been studied in [100]. The state of the art of this research compared to [100] is to model detailed characteristics of different energy storage technologies such as idle time, as well as modeling demand response and its rebound effect to minimize the spillage of wind

energy. The demand response modeled in this research is based on the contract that customers allow the utility to reduce their demand for limited times and duration to get incentive payments. The frequency change is the signal which demand responds to in this research, because it varies by the mismatch between total load and total generation. This mismatch is due to the wind power forecast error or the highly variable source of wind generation.

Uncertainty of wind power output poses a new challenge to power system operation, which is the wind power forecast error. Solutions to overcome this challenge may include improvement in wind power forecasting, sub-hourly scheduling, system reserve increase, or deployment of energy storage technologies. Energy storage technologies can absorb (charge) excess of wind power when the actual wind power output is more than the forecasted one, to reduce wind output curtailment. They can also inject (discharge) required power when the actual wind power is less than the forecasted one, to reduce required back-up generation. Proper sizing and scheduling of energy storage units can help reducing spilled wind energy and required back-up generation. Scheduling energy storage to mitigate impacts of wind power forecast error by Discrete Fourier Transform has been studied in [57] for a general energy storage model. Another state of the art of this research is to study other signal processing methods like Discrete Wavelet Transform while modeling detailed characteristics of each energy storage technology.

1.2 Objectives and Scope of the Dissertation

The objective of this dissertation is to propose a planning tool for electric utility operators, evaluating impacts of different grid-scale energy storage technologies and demand response options on mitigating high wind energy penetration challenges. Spilled wind energy is a challenge due to the lack of correlation between load and wind profiles, which increases in the existence of must-run generation, such as nuclear power plants. Energy storage can absorb the excess of wind energy to help total generation meets the load during low wind output periods. The term non-correlation is used in this research to refer to the fact that wind or any other renewable generation does not follow the load like conventional power plants as their generation is nature driven. Demand response can be

scheduled in such a way that the rebound effect coincides with high wind energy output periods. Hence, energy storage and demand response can be scheduled to minimize wind energy spillage.

The question is how to schedule different energy storage technologies and demand response programs to guarantee the balance between load and generation, while minimizing spilled wind energy, in a system with high wind energy penetration. Other energy sources to supply the load are must-run generation such as nuclear power plants, and conventional generation units including coal and gas-fired power plants. This question is answered in Task 1, by solving a mixed integer linear programming problem while presenting a detailed modeling of each energy storage technology, and demand response, as well as, nuclear, coal, and gas-fired power plants.

Wind power forecast error is another challenge beside the non-correlation between wind and load profiles. This challenge may results in more spilled wind energy and required back-up generation, which is addressed in Task 2 by defining an algorithm based on signal processing techniques. The novelty is to decompose the wind power forecast error signal to components appropriate for controlling each energy storage technology.

Finally, energy storage technologies are operated to mitigate both mentioned challenges (non-correlation between wind and load profiles, and wind power forecast error) by using the proposed technique discussed in Task 1, and Task 2. This idea is explained in Task 3 to update the operation of pre-scheduled energy storage technologies, which were scheduled to minimize spilled wind energy due to the non-correlation, for mitigating the impacts of wind power forecast error.

The proposed work includes following tasks:

Task 1: Schedule grid-scale energy storage and demand response at the transmission level to mitigate spilled wind energy due to the non-correlation between wind and load profiles.

a) Define a mixed integer linear programming (MILP) problem in MATLAB to be solved by IBM CPLEX using real-world load and wind data.

b) Define constraints to include detailed characteristics of grid-scale energy storage technologies including compressed air energy storage (CAES), adjustable and fixed speed pumped hydro energy storage (PHES) systems, and large scale batteries such as NaS, Lead acid, and Vanadium redox.
c) Define constraints to represent different demand response scenarios while considering the rebound effect at the transmission level. Three different rebound effect scenarios are considered for the energy ratio of rebound effect to demand response of 50%, 100%, and 150%.
d) Solve MILP for different combinations of energy storage and demand response options. The global objective function is to minimize spilled wind energy due to the non-correlation between wind and load profiles in the existence of must-run generation units as nuclear power plants.
e) Analyze the impact of different generation mixes, energy storage technologies, and demand response on reducing spilled wind energy.

Task 2: Propose an algorithm to schedule grid-scale energy storage units for mitigating the impact of wind power forecast error.

a) Develop an algorithm based on signal processing techniques to decompose the wind power forecast error signal to components appropriate for scheduling hybrid configuration of grid-scale energy storage technologies including CAES, and NaS battery.
b) Propose an algorithm that considers detailed characteristics of CAES, and NaS battery to follow control signals derived by the proposed signal processing techniques.
c) Study the impact of different combinations of energy storage technologies on reducing spilled wind energy and required back-up generation.
d) Analyze the cycle life of NaS batteries and the impact of using CAES in a hybrid energy storage combination with NaS battery on increasing the NaS battery cycle life.
e) Evaluate the impact of considering a frequency bias constant on reducing spilled wind energy and required back up generation.

Task 3: Present an algorithm for optimal operation of energy storage that addresses both applications – minimizing spilled wind energy and mitigating wind power forecast errors. The idea is to update day-ahead operation of energy storage technologies based on Task 1 by the algorithm presented in Task 2, to mitigate the wind power forecast error challenge.

a) First, schedule the day-ahead operation of energy storage to minimize wind spillage due to the non-correlation between load profile and day-ahead wind power forecast using MILP.
b) Update energy storage operation in hour ahead by using signal processing techniques to mitigate errors between the day-ahead wind power forecast, and the hour-ahead wind power forecast.
c) Update energy storage operation in 5 minutes ahead by using signal processing techniques to mitigate errors between the hour-ahead wind power forecast, and the actual wind power output.
d) Compare the final wind spillage and the back-up generation for different energy storage units when their operation is not updated, with the case that their operation is updated based on the proposed algorithm.
e) Demonstrate the convexity of the problem by plotting results using different initial conditions

1.3 Contributions

Contributions of each three tasks are defined briefly as follows.

1.3.1 Energy Storage and Demand Response Scheduling to Mitigate Wind Power Spillage

Mixed integer linear programming (MILP) model is proposed for scheduling large-scale energy storage units and different demand response options at the transmission level to mitigate high wind penetration challenges. The contribution of this research is the consideration of detailed characteristics of each energy storage technology into the

proposed MILP model. For example, the required idle time for CAES to switch between charging and discharging modes has not been considered in the literature. DR modeling which also includes rebound effect at the transmission level is one of the contributions of this research. The idea is to schedule demand response in such a way that rebound effect occurs during high wind generation periods. The objective of scheduling energy storage and demand response is to reduce wind spillage. This MILP model is solved by IBM CPLEX for different scenarios of energy storage technologies and DR.

1.3.2 Mitigating Impacts of Wind Power Forecast Error by Energy Storage Based on Signal Processing Techniques

An algorithm is proposed based on signal processing methods to decompose the wind power forecast error signal to time-varying periodic components. These components are used to schedule the hybrid configuration of grid-scale energy storage units. Two signal processing approaches including Discrete Fourier Transform (DFT) and Discrete Wavelet Transform (DWT) are considered in this research. The wind power forecast error signal is decomposed to intra-hour, intra-day and slow-cycling components to control NaS, CAES, and conventional units, respectively. The slow-cycling component is followed by conventional generators which are more efficient when operating close to their rated capacity. The trade-off between installing more energy storage units and decreasing the wind spillage, back-up energy and the standard deviation of residual wind power forecast error signal is analyzed. NaS life cycle analysis and CAES contribution on increasing NaS life-time are studied. The impact of considering the frequency bias constant to allow small frequency deviations on reducing wind spillage and required back-up energy is also investigated.

1.3.3. Mitigating Spilled wind energy and Wind Power Forecast Error by Updating Energy Storage Scheduling

An algorithm is proposed to update day-ahead energy storage scheduling presented in Task 1 by using signal processing method presented in Task 2, to reduce the error among

day-ahead, and hour-ahead wind power forecast with actual wind power. This algorithm updates energy storage scheduling based on wind power forecast errors. Then, the performance of this algorithm is analyzed based on final spilled wind energy and required back-up generation for different number of energy storage units, and day-ahead wind power forecast.

2. Literature Search

This chapter summarizes the literature search into four categories, including high wind energy penetration challenges, energy storage sizing and control, demand response, and coordination of demand response and energy storage. Each category contains basic knowledge and in-depth information about the research conducted in respective areas.

2.1 High Wind Energy Penetration Challenges

There are major technical barriers that can be mitigated with flexible resources as demand response and energy storage at high renewable energy penetration level in the system. These barriers can be listed as follows [9].

1. The geographic sites for renewable energy resources are not particularly at the same place with load centers. Hence, the usefulness of renewable resources is limited to the available transmission capacity.
2. Because of zero fuel cost, renewable resources are usually held at their maximum available output. Hence, they cannot be considered as up-reserve for outages. This limits the utilization of renewable generations compared to conventional units that provides up-reserve to the system.
3. Since wind and load profiles are not correlated, at high wind penetration scenarios there are times when load minus wind becomes less than must-run generation such as large coal and nuclear power plants. Hence, in this case the excess of wind generation needs to be spilled.
4. Wind power forecast error is also a challenge in high wind penetration scenarios. This barrier requires more reserve in the system when the actual wind is less than the forecasted one. Wind spill occurs when the actual wind exceeds the forecasted generation.

Following solutions can mitigate these challenges [9].

1. Wind Forecasting: Day-ahead forecast can be used for unit commitment. Short-term forecasts are required to schedule the quick-start generators or energy storage units with high ramp rates.

2. Fast Dispatch and Sub-Hourly Scheduling: This can help the system mitigate the variability of wind generation. When generators are set for longer dispatch as an hour, then they are not available to adjust their generation for balancing. With faster dispatch, load and generation can be matched while reducing the need for more expensive regulation services.
3. Reserve Management: Reserve capacity can be used to mitigate challenges regarding wind generation variability in addition to other contingencies. Another way to deal with the variability of wind power is to limit its ramping. Tools associated for controlling ramps are low cost and have been used in Electric Reliability Council of Texas (ERCOT), Ireland, Germany and Hawaii.
4. Energy Storage: Grid-scale energy storage technologies can help mitigate high wind penetration challenges. Since they are not a source of generation, they can absorb the excess of wind energy and discharge when there is a need for more wind energy. These technologies have high ramp rates, and power and energy capacity ratings that can be used to address wind variability, uncertainty.
5. Demand response: Demand response brings flexibility to the load which can be used to solve high wind penetration challenges. Demand response can be used as reserve, and for ancillary services and peak reduction.
6. Flexible generation: Natural gas combustion turbines, hydropower plants, and internal combustion engines are the most flexible generators. On the other hand, Nuclear and coal base-load power plants are the least flexible (or inflexible) generators which are designed to operate at a constant level.

Curtailment of wind energy is becoming more widespread as renewable energy penetration increases. This curtailment happens due to transmission congestion and excess generation during low load periods that cause base load power plants reach their minimum threshold of generation. Hence, wind curtailment is used for maintaining the energy balance. A summary of frequency and reasons for curtailment by several utilities and grid operators is provided in Table 2-1. Curtailment levels are in the range of 1% to 4% of wind generation, but higher levels have occurred in Electric Reliability Council of Texas (ERCOT) as shown in Fig. 2-1[11]. Grid Operators deploy many strategies to minimize renewable energy curtailment, as summarized in Table 2-2.

Table 2-1 Summary of Curtailment Levels and Reasons [11]

Utility/Grid Operator	**Wind and Solar Curtailment Levels Frequency**	**Primary Reasons for Curtailment**
Alberta Electric System Operator (AESO)	Infrequent Oversupply;	transmission constraints, high wind ramps
Arizona Public Service (APS)	Infrequent	Local transmission outages or constraints
Bonneville Power Administration (BPA)	Varies by year; less than 2% of wind production	Balancing issues related to exhaustion of reserves; oversupply
California Independent System Operator (CAISO)	Infrequent; not tracked	Oversupply; transmission constraints, congestion
Electric Reliability Council of Texas (ERCOT)	Varies by year; 2% to 4% in 2012–2013, but higher in previous years	Transmission constraints; oversupply, new transmission lagged wind capacity
Hawaiian Electric Co. (HECO), Hawaii Electric Light Co., (HELCO) and Maui Electric Co. (MECO)	Substantial curtailment on Maui and the island of Hawaii	Oversupply in low load periods and balancing challenges
ISO New England (ISO-NE)	Infrequent, but some plants experienced substantial curtailment Local transmission constraints;	oversupply; voltage control; other (wildlife protection, ice formations)
Midcontinent ISO (MISO)	1%–4% of wind generation	Transmission congestion; oversupply handled by downward dispatch
NV Energy	Infrequent; 6–7 occasions per year	Oversupply; local transmission outages

PacifiCorp	Much less than 1% of total wind production	Transmission congestion; avoid area control error (ACE) violations
PJM Interconnection	Not tracked	Local transmission constraints
Puget Sound Energy (PSE)	Infrequent in PSE balancing area and not tracked	PSE wind subject to BPA's curtailment protocols related to balancing and oversupply
Salt River Project	Very infrequent	Transmission issues and maintenance
Sacramento Municipal Utility District (SMUD)	Not tracked	SMUD not affected by curtailments
Southwest Power Pool (SPP)	Some wind generators report high levels	Local transmission constraints, expansion of wind outpaced new transmission build-out
Tucson Electric Power	Very infrequent	Local outages
Western Area Power Administration (WAPA)	None	None
Public Service Company of Colorado (PSCO)	1%–2% of wind generation	Oversupply; transmission constraints
Southwest Power Pool (SPP)	Some wind generators report high levels	Local transmission constraints, expansion of wind outpaced new transmission build-out
Tucson Electric Power	Very infrequent	Local outages
Western Area Power Administration (WAPA)	None	None
Public Service Company of Colorado (PSCO)	1%–2% of wind generation	Oversupply; transmission constraints

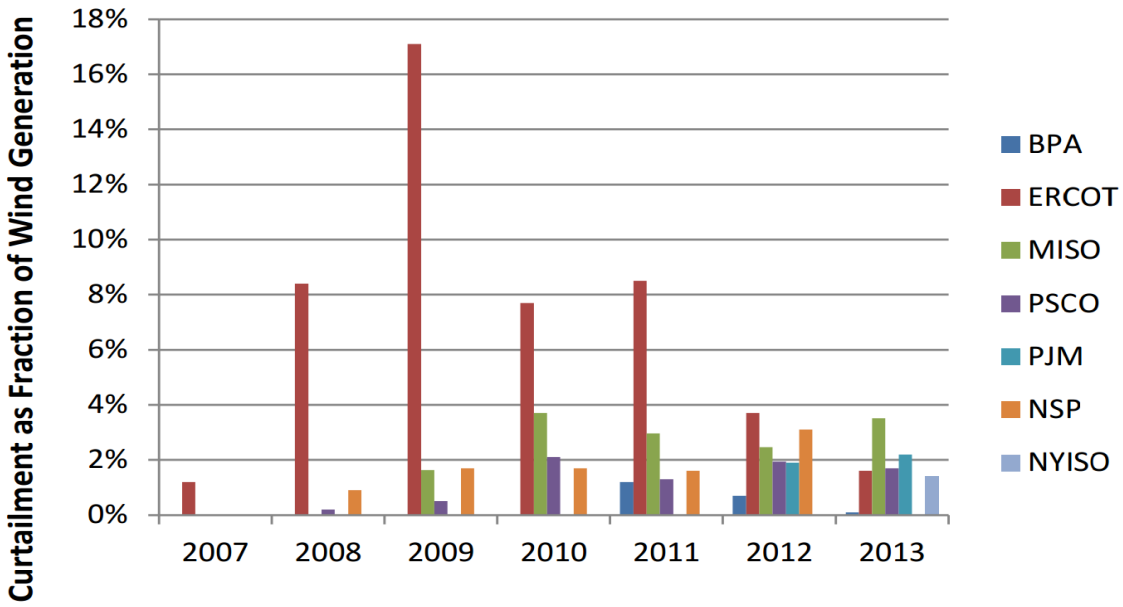

Fig. 2-1. Curtailment levels by region, 2007–2012 [11]

Table 2-2 Strategies that Mitigate Wind and Solar Energy Curtailment [11]

Strategy	**Utility/Grid Operator**
Automation (i.e., AGC)	ERCOT, PSCO
Use curtailed generators for positive reserves	PSCO
Reduction of minimum generation levels	HECO (Maui)
Increase scheduling frequency	WAPA (adopting)
Economic dispatch	ERCOT, MISO, SPP (adopting)
Negative pricing	CAISO, ERCOT, MISO, PJM, ISO-NE (adopting)
Energy imbalance market	CAISO, PacifiCorp
Wind power ramp management system	AESO
Increase transmission capacity	ISO-NE, ERCOT, MISO, PJM, SPP
Improve forecasting	ISO-NE, PSCO, NV Energy, SMUD

2.2 Grid-Scale Energy Storage

Electricity cannot be stored directly and requires to be converted to other forms of energy. These forms of energy includes chemical energy (batteries), kinetic energy (flywheels and compressed air), gravitational potential energy (pumped hydroelectric), and also magnetic field (capacitors). There are two main terms that define energy storage as rated power and energy capacity. Each application such as power quality or load shifting requires special range of power or energy capacity to fulfill their goals. Other factors of energy storage technologies are efficiency, response time, discharge duration, discharge frequency, and depth of discharge.

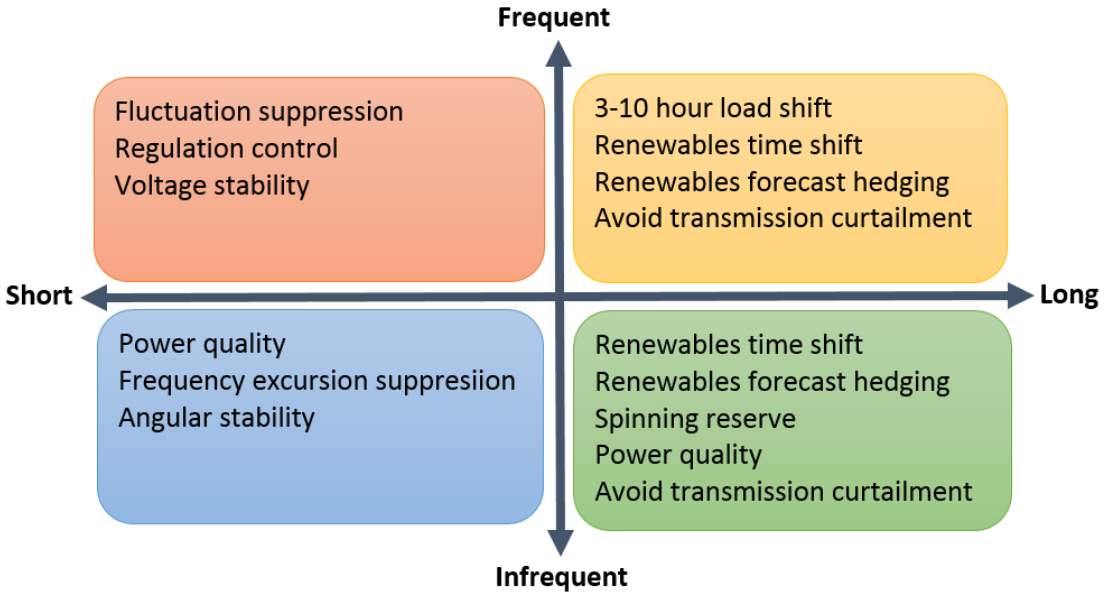

Fig. 2-2. Energy Storage Applications Based on Discharge Duration and Frequency [12]

Each energy storage application requires specific type of energy storage technology. These applications can be divided into long and short duration categories by considering the discharge time. It can also be categorized into frequent and infrequent applications based on the discharge frequency. Fig. 2-2 summarizes energy storage applications in each category.

Long duration category needs enough rated energy capacity. On the other hand, short duration application requires enough rated power capacity for sudden charge and

discharge requests. Infrequent application uses storage few times a year, but frequent applications require energy storage to cycle frequently.

2.2.1 Grid-Scale Energy Storage Technologies

Grid-scale energy storage technologies can be categorized into mechanical as pumped hydro energy storage (PHES), compressed air energy storage (CAES), flywheel energy storage, and electrochemical ones as large-scale batteries. Batteries can be categorized as conventional batteries including Lead Acid (PbA), Nickel Cadmium (NiCad) and Lithium Ion (Li-Ion), high temperature batteries as Sodium Sulfur (NaS) and ZEBRA (NaNiCl), and flow batteries like Vanadium Redox (VRB) and Zinc Bromine (ZnBr). The energy storage capacity in U.S by 2011 is shown in Fig. 2-3. As shown, pumped hydro energy storage is the majority among other types of grid-scale energy storage technologies.

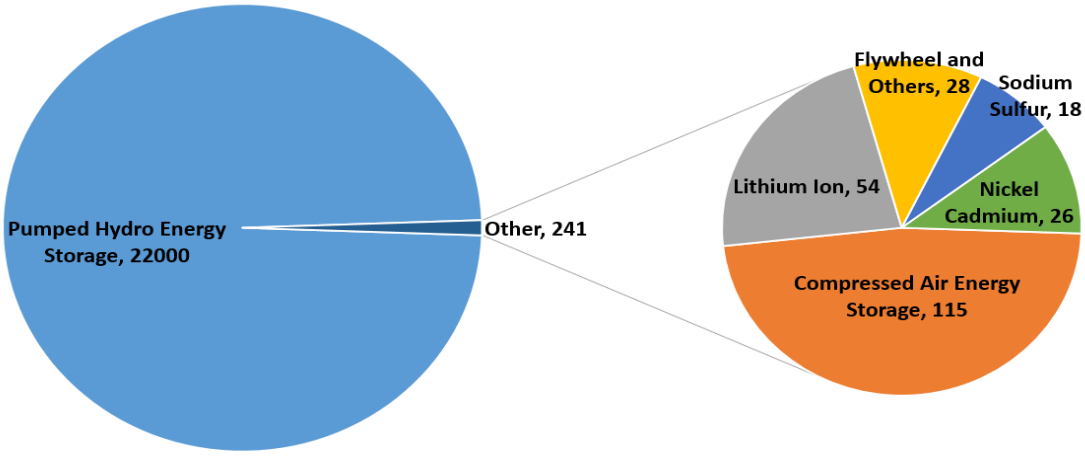

Fig. 2-3. Energy Storage Capacity (MW) in US by 2011 [12]

A. Pumped Hydro Energy Storage

Pumped Hydro Energy Storage (PHES) is the most mature technology among other grid-scale energy storage units. The existing PHES projects in US are shown in Fig.2-4. PHES

projects may have negative impacts on environment and ecosystem. They are also limited to special geographic situation to design upper and lower reservoirs.

The concept behind PHES is to convert electrical energy to potential energy by pumping water from lower reservoir to higher reservoir. Hence, the electricity is generated when the water from higher reservoir is released to lower reservoir to rotate turbine. The simple PHES topology is depicted in Fig. 2-5.

The technical characteristics of PHES are shown in Table 2-3. Most of the PHES projects involve two reservoirs, but recently there are other designs suggesting one reservoir to be underground while the other one is aboveground. This can alleviate the geographical barriers of building PHES projects. The new designs suggest using rivers as above ground reservoir and underground pipes as the lower reservoir as shown in Fig. 2-6. Another PHES design is based on two water-filled cylindrical shafts in the ground as depicted in Fig. 2-6.

Fig. 2-4. Pumped Hydro Existing Projects in US (2009) [13]

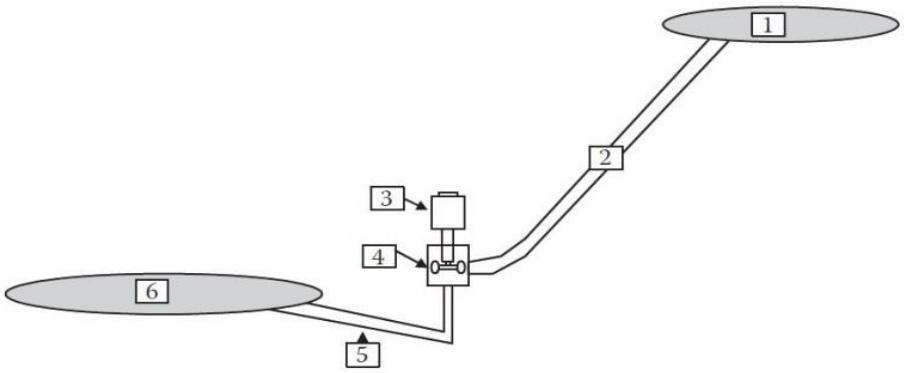

Object#	Name
1	Upper Reservoir or Forebay
2	Penstock
3	Motor Generator
4	Pump Turbine
5	Tail Race
6	Lower Reservoir or Afterbay

Fig. 2-5. PHES Technology [13]

Table 2-3 PHES Technical Characteristics [12]

PHES	Capacity (MWh)	Power (MW)	Duration (hrs)	Efficiency (%)	Lifetime (Cycles)
Small	1,680-5,300	280-530	6-10	80-82	>13,000
Large	5,400-14,000	900-1,400	6-10	80-82	>13,000

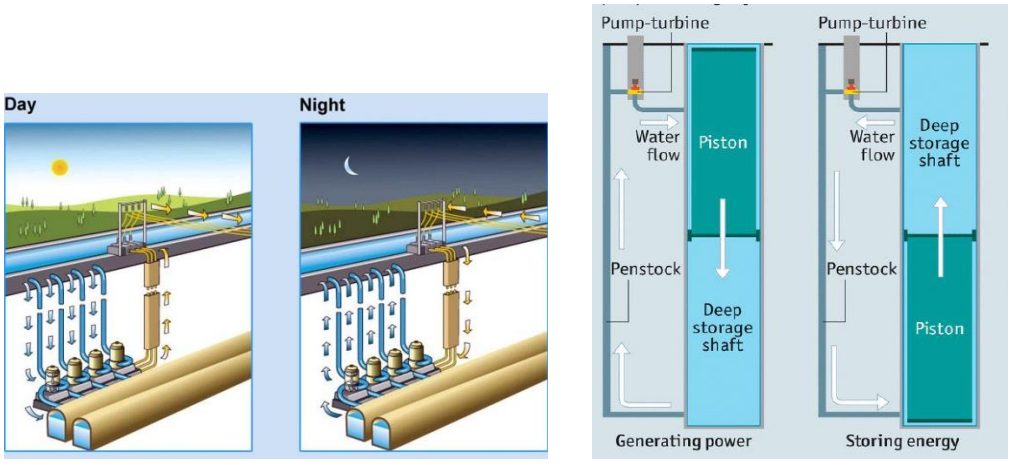

Fig. 2-6. Riverbank PHES Technology [13] and Gravity Power-Grid Scale Energy Storage [14]

Pumped hydro energy storage can be categorized in two groups based on the range of pumping and generation powers, as follows:

1) Fixed speed (single speed) pumped hydro energy storage: This type of energy storage can only pump at the rated power capacity. The generating power range is between 100% and 50% of rated power capacity. As a result, it is not suitable when energy storage is supposed to change its pumping or generating power such as smoothing the wind power output [117].
2) Adjustable speed pumped hydro energy storage: This type of pumped hydro energy storage is able to pump in a range between 100% and 40% of rated power capacity. Its generating power is also adjustable between 1005 and 30% of rated power capacity. This adjustable characteristic is very critical when energy storage is used to cope up with variable and uncertain renewable power generation [117].

B. Compressed Air Energy Storage

CAES technology was first developed in 1978, located in Huntrof, Germany. It was used to store off-peak energy from nuclear power plant. It has a storage capacity of 11 million cubic feet or 290 MW. It takes 12 hours to charge and up to 4 hours to discharge at maximum capacity with 10 hours of exponentially declining power output. The second one was built in 1991 in McIntosh, Alabama. The McIntosh facility has a capacity of 19 million cubic feet, or 110 MW, with a maximum 26 hours output. It is now used for load management, peaking power, ramping duty and spinning reserve. A proposal has been under development in Norton, Ohio for 800 MW CAES. There are several plans to develop a 540 MW CAES is Matagorda County, Texas and 268 MW CAES in Dallas Center, Iowa [13].

The basic technology of CAES is shown in Fig. 2-4. CAES operates like conventional gas turbines while its compression and expansion are not simultaneous. The compressor stores the energy as compressed air inside a cavern. The electricity is then generated by reheating and mixing the compressed air with fuel and passing through an expansion turbine. Various type of caverns as salt, porous and hard rock can be used to form the

CAES cavern. Also, hydrogen, natural gas, gasified biomass and oil can be used as the fuel.

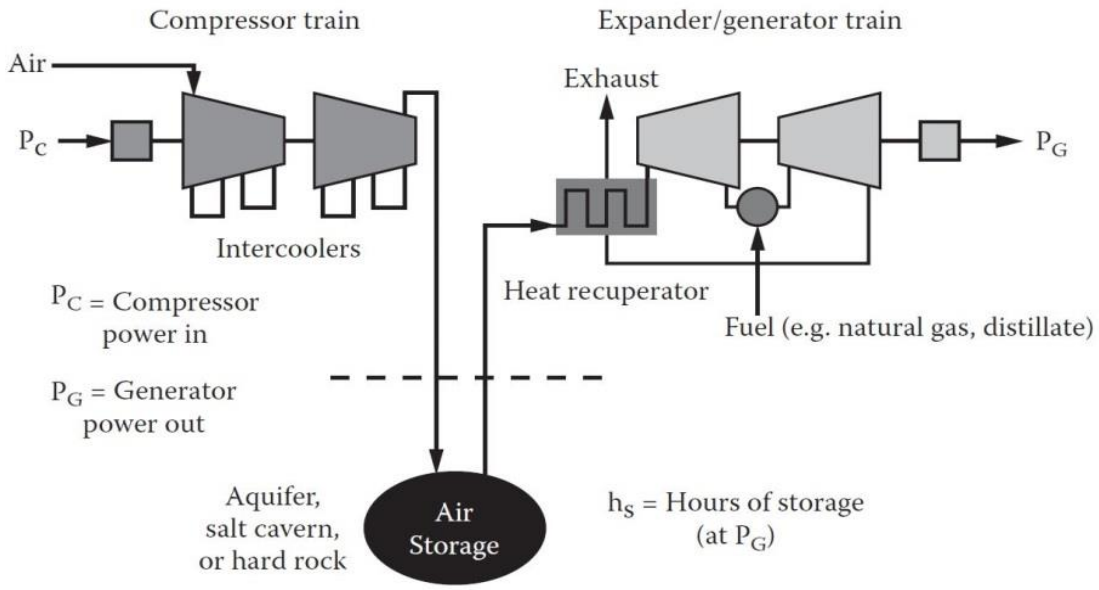

Fig. 2-7. CAES Basic Technology [13]

Table 2-4. CAES Technical Characteristics [12]

CAES	Size	Capacity (MWh)	Power (MW)	Duration (hrs)	Lifetime (Cycles)
Under ground	Small	1,080	135	8	>13,000
	Large	2,700	135	20	>10,000
Above ground	Small	250	50	5	>10,000

Typical characteristics of CAES as aboveground and underground are summarized in Table 2-3. As shown the duration of storage in CAES can last for 20 hours which results in large energy capacity. According to the operation of CAES, the switch from one operating mode to the other requires at least 20 minutes idle time [13]. This switch over time may have a negative impact when CAES is used as a balancing resource coupled with fluctuating wind generation. The reason for this switch over time is because turbines are called upon to initiate both generation and compression. Although this can be

eliminated by new designs that decouple generation and compression, but it is necessary to model this characteristic while using it to mitigate wind generation challenges.

C. Large-Scale Batteries

Chemical energy storage technologies (batteries) are among grid-scale energy storage units that can help alleviate the wind integration challenges. A battery contains different electrochemical cells. Electrons are generated from the anode (the negative electrode) to do external work. Positive ions migrated inside the cathode (positive electrode) and electrons migrate through the external circuit. The electrolyte allows the ions migration.

The characteristics of Lead-Acid, NaS, Li-Ion and Vanadium Redox batteries are summarized in Table 2-5. NAS battery is commercially available in Japan for over 10 years by NGK Insulators, Ltd, marketed globally, 300 MW (1800 MWh) worldwide, over 170 projects [14]. More than 20 MW of NAS Batteries have been installed in North America, as shown in Fig. 2-8. NaS battery characteristics are summarized in Table 2-6. NaS battery modules are shown in Fig. 2-9.

Table 2-5. Grid-Scale Battery Characteristics [13]

	Lead–Acid	**NaS**	**Li Ion**	**Vanadium Redox**
Anode	Pb	Na	C	$V^{2+} \leftrightarrow V^{3+}$
Cathode	PbO_2	S	$LiCoO_2$	$V^{4+} \leftrightarrow V^{5+}$
Electrolyte	H_2SO_4	β-alumina	Organic solvent	H_2SO_4
Open circuit voltage	2.1	2.1	4.1	2.1
Specific energy (Wh/kg)	10 to 35	133 to 202	150	20 to 30
Energy density (Wh/L)	50 to 90	285 to 345	400	30
Discharge profile	Flat	Flat	Sloping	Flat

Specific power (W)	35 to 50	36 to 60	80 to 130	110
Cycle life (cycles)	200 to 700	2500 to 4500	1000	12000
Advantages	Low cost, good high rate	Potential low cost, high cycle life, high energy, goof power density, high efficiency	High specific energy and energy density, low self-discharge, long cycle life	High energy efficiency, high charge rate, low replacement cost
Limitations	Limited energy density, hydrogen evolution	Thermal management safety, seal and freeze-thaw durability	Low rate	Cross mixing of electrolytes

Table 2-6. NaS Characteristics [14]

Power Capacity	1 MW
Energy Capacity	6 MWh
Service Life	15-year
Cycle Life	2500 cycles at 100% DOD – 4500 at 90% – 6500 at 65%
Ambient Temp	-20 to +45 C
Ramp Rate	prompt response (full power charge to discharge in 2 millisecond)
Efficiency	AC:75%, DC:85%
Self-Discharge	No
Energy Density	~1500 ft2/MW, 25 MW/Acre

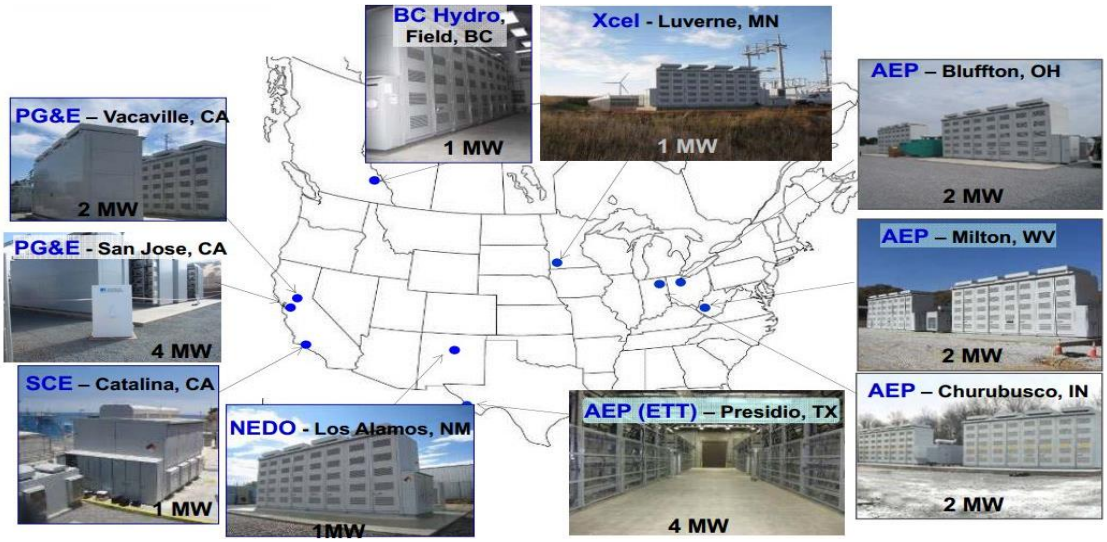

Fig. 2-8. NaS Battery Projects in North America [14]

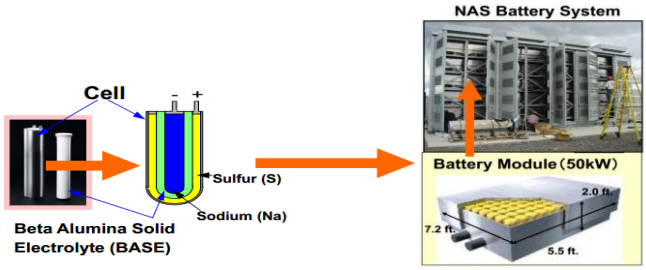

Fig. 2-9. NaS Battery System [14]

Large scale batteries have high ramp rate and efficiency comparing to mechanical energy storage technologies. The important factor that needs to be taken into consideration for planning and operation of these types of energy storage technologies are their life cycle. This parameter determines that when large-scale batteries are required to change based on their performance. Each type of batteries have different life cycle as shown in Table 2-5. Vanadium Redox has the highest cycle life (12000 cycles) and Lead acid has the lowest cycle life (200-700 cycles). Advantage and disadvantage of each battery is also listed in Table 2-5. For example, NaS battery has high energy and power capacity but has some thermal safety problems.

Pure sodium spontaneously burns in contact with air and moisture, thus NaS battery must be protected from water and oxidizing atmospheres. On September 21, 2011, NGK-manufactured NaS batteries for storing electricity installed at the Tsukuba, Japan, and

plant caught fire. Following the incident, NGK temporarily suspended production of NaS [15]. There are upcoming new technologies in the grid-scale battery energy storage units with advanced characteristics by various companies. One of the upcoming battery technologies is Durathon Battery by General Electric Company, which is based on combination of sodium and nickel.

2.2.2 Grid-Scale Energy Storage Literature Review

In the literature, planning energy storage technology is categorized into two main approaches: optimization methods and signal processing approaches. The first approach models the system behavior by defining various constraints to size and schedule energy storage. The second approach is based on decomposing the fluctuating signal (e.g., wind power forecast error signal) into components that are suitable to control energy storage technologies. The literature can also be categorized into two other groups based on energy storage applications. The first category provides frequency regulation, ramp rates and mitigating forecast error in the real-time market. The second category is used in the day-ahead electricity market while providing arbitrage to electric power system.

A. Optimization and Probabilistic Approaches

The problem of sizing energy storage units can be solved by optimization approaches considering investment, operation and penalty costs [16]-[21] to maximize the revenue or smooth out the wind farm output. Sizing energy storage that makes combined wind and storage output meet the predicted hour-ahead or day-ahead forecast has been addressed in [22]-[25]. A variety of heuristic optimization methods [26]-[29] and Game Theory approaches [30]-[31] have been used to solve the energy storage sizing in a system with high wind energy penetration. Sizing energy storage based on pre-compensation and post-compensation approaches to minimize hourly wind power forecast error was proposed in [32]. Sizing Li-Ion batteries based on statistical analysis of wind power forecast error has been addressed in [10].

Some papers address both variability and uncertainty of wind generation by providing extra reserve in the system for forecast error [34]. Sizing energy storage to manage hourly energy imbalance charges has been addressed in [35]. The trade-off between energy storage size and unserved energy due to the wind power forecast error has been studied in [36]. This study neglected any specific energy storage characteristics, for example wind ramp rates and wind spill. The impact of additional energy storage as PHES to minimize thermal unit operational costs for reducing the wind spill in excess of wind generation scenarios has been investigated in [37].

Planning grid-scale energy storage units requires a suitable market infrastructure that has been discussed in [38]-[40]. Planning and operating battery storage in a system with high wind penetration by dynamic programming in the hourly electricity market has been studied in [39] to compensate for the wind hourly forecast error. The operation of independently-operated energy storage with high wind energy penetration has been investigated in [41]. This study has used stochastic optimization to maximize the profit of energy storage operation in day-ahead and hour-ahead markets. Also, the tradeoff between energy storage capacity and total revenue in the market was addressed. The comparison between centralized and distributed energy storage scheduling in a day-ahead market has been addressed in [42]. The authors of [42], and [42] have scheduled distributed energy storage units at the aggregator level to minimize generation costs. The results indicate that centralized energy storage reduces peak load and system operating costs further than distributed energy storage systems.

Optimal sizing of the wind-solar-battery hybrid system to minimize investment and operational costs, while satisfying reliability and operating reserve constraints, has been studied in [43]. The authors of [43] have used this battery to compensate for the deficiency of wind and solar power. It is also used to smooth out the power injected to the grid by applying a second order filter. Optimal power flow and control strategies to smooth wind farm output with reliability evaluations have been addressed in [44]-[46]. Day-ahead unit commitment in a wind-coal intensive power system is studied considering both variability and uncertainty of wind energy [47].

The multi agent approach has been studied in [48]-[50] to consider battery characteristics and operational costs in a hybrid energy system. Classical and intelligent approaches for tracking the maximum generation of wind output while minimizing its variability has been proposed in [51]. Planning energy storage for a micro-grid with wind farms considering the reliability indices to minimize overall costs has been investigated in [52]. The contribution of this paper is finding the expansion planning of energy storage for a 10-year plan while considering the battery lifetime constraint.

Required reserve in a system with high wind penetration was addressed in [53]-[55] while considering the reserve provided by interconnections. Temporal and non-temporal methods to evaluate the size of required energy storage units for wind output ramp rates have been investigated in [56].

B. Signal Processing Approaches

The problem of hybrid energy storage sizing can be solved by signal processing approaches based on the concept that the efficient operation of energy storage and conventional units depends on their cycling. This concept for mitigating wind power forecast error is proposed in [57] using Discrete Fourier Transform (DFT). The issue of capacity planning of energy storage and diesel generators based on DFT to supply a load in a micro grid with high wind penetration has been addressed in [58]. Discrete Wavelet Transform (DWT) was used for data filtering of day-ahead electricity price forecasting in [59]. DWT has also been used to control storage for smoothing the fluctuation of wind farm output [60]. These papers determine the rated power and energy capacity of energy storage to be able to follow decomposed components completely. Hence, they lead to oversizing the energy storage for following infrequent values while neglecting the standard deviation of decomposed components. Also, the approach presented in the literature does not consider specific types of energy storage technology while neglecting its properties, for instance efficiency, ramp rate, depth of discharge and required idle time to switch between charge and discharge modes.

The idea of combining different renewable generation types to alleviate their challenges has been addressed in [61] . This paper combines wind and concentrating solar power plants (CSP) since CSP has the potential of energy storage and will reduce the required reserve for the system. Wind and solar energy can also be combined since solar reaches its maximum generation at daytime and wind usually reaches its maximum generation at night time.

2.3 Demand Response

According to the Federal Energy Regulatory Commission [62], demand response (DR) is:

"Changes in electric usage by end-use customers from their normal consumption patterns in response to changes in the price of electricity over time, or to incentive payments designed to induce lower electricity use at times of high wholesale market prices or when system reliability is jeopardized."

DR includes all intentional modifications to consumption patterns of electricity of induce customers that are intended to alter the timing, level of instantaneous demand, or the total electricity consumption. DR can play different roles in electric power system planning and operation as shown in Fig. 2-7. As shown, DR effective time horizon for planning varies between years to less than 15 minutes. DR can be categorized into two main groups as price-based demand response and incentive-based demand response as shown in Table 2-6. The first category happens due to the change in price signal. The second is established by utilities, load serving entities, or a regional grid operator. They give customers load reduction incentives that are separate from, or additional to, their retail electricity rate, which may be fixed or time-varying.

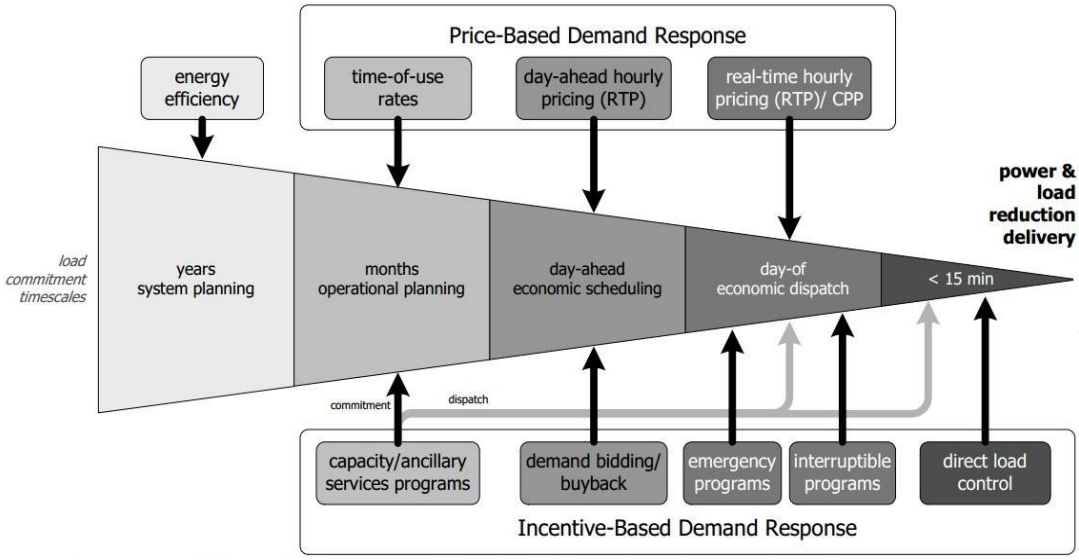

Fig. 2-10. Role of DR in Electric Power System Planning and Operations [62]

Table 2-7. Demand Response Options [62]

Price-based options	**Incentive-based options**
• *Time-of-use (TOU):* a rate with different unit prices for usage during different blocks of time, usually defined for a 24 hour day. TOU rates reflect the average cost of generating and delivering power during those time periods. • *Real-time pricing (RTP):* a rate in which the price for electricity typically fluctuates hourly reflecting changes in the wholesale price of electricity. Customers are typically notified of RTP prices on a day-ahead or hour-ahead basis. • *Critical Peak Pricing (CPP):* CPP rates are a hybrid of the TOU and	• *Direct load control:* a program by which the program operator remotely shuts down or cycles a customer's electrical equipment (e.g. air conditioner, water heater) on short notice. • Direct load control programs are primarily offered to residential or small commercial customers. • *Interruptible/curtailable (I/C) service*: curtailment options integrated into retail tariffs that provide a rate discount or bill credit for agreeing to reduce load during system contingencies. Penalties maybe assessed for failure to curtail. Interruptible programs have traditionally been offered only to the largest industrial

RTP design. The basic rate structure is TOU. However, provision is made for replacing the normal peak price with a much higher CPP event price under specified trigger conditions (e.g., when system reliability is compromised or supply prices are very high).	(or commercial) customers. • *Demand Bidding/Buyback Programs:* customers offer bids to curtail based on wholesale electricity market prices or an equivalent. Mainly offered to large customers (e.g., one megawatt [MW] and over). • *Emergency Demand Response Programs*: programs that provide incentive payments to customers for load reductions during periods when reserve shortfalls arise. • *Capacity Market Programs:* customers offer load curtailments as system capacity to replace conventional generation or delivery resources. Customers typically receive day-of notice of events. Incentives usually consist of up-front reservation payments, and face penalties for failure to curtail when called upon to do so. • *Ancillary Services Market Programs*: customers bid load curtailments in ISO/RTO markets as operating reserves. If their bids are accepted, they are paid the market price for committing to be on standby. If their load curtailments are needed, they are called by the ISO/RTO, and may be paid the spot market energy price.

Table 2-8. Total Demand Response Potential in the U.S. [63]-[65]

	The potential demand response resource contribution from all U.S. demand response programs (MW)	Percentage of U.S. peak load
2008	41,000	5.8 %
2010	58,000	7.6 %
2012	72,000	9.2 %

The potential DR in U.S. is evaluated 9.2% in 2012 [65]. DR evaluations for three years are shown in Table 2-7. There are some field experiments of demand response in U.S. For instance, ISO New England is planning to fully integrate demand response resources in 2017. The PJM's small customer pilot program operates an integrated load management system that serves the need of rural electric cooperatives located throughout the PJM control area. This integrated system comprises 45,000 load control switches and delivers an estimated 35 MW of load reduction in summer (50 MW in winter) through control of residential electric water heaters, water pumps, and electric thermal storage space heaters [66]-[72].

DR needs a market infrastructure to participate in the day-ahead and the real-time electricity markets. The optimal DR aggregation in the energy and reserve market has been fully investigated in [74]-[75]. DR exchange in stochastic day-ahead scheduling with wind generation has been discussed in [77]. This paper schedules DR in a two-step optimization approach to find the locational marginal price and then schedules DR for maximizing the social welfare. The statistical behavior of large aggregators of small loads may work well with wind and solar integration. The communication network to aggregate DR is studied in [78]. DR can participate also in real time to provide ramp rates and frequency stabilization [79]-[81]. The security-constrained unit commitment for hourly DR as load shifting and load reduction is proposed in [83]-[84]. DR cost analysis with wind integration by decision tree approach has been addressed in [85]-[86]. Scheduling DR and conventional units to maximize the social welfare while restricting the frequency and quantity of wind power deficiency have been investigated in [87].

A state-queuing model to analyze thermostatically controlled appliances is proposed for providing regulation services in [88]-[90]. There is much research focusing on the control methods of heating/cooling systems as fuzzy controllers [90], fuzzy adaptive controllers [91] neural network controllers [93] and active controllers [94] to minimize the total system cost. Typically, a 100% cycling strategy is employed with water heating controls since most water heaters have a tank with sufficient capacity to last several hours during control [96].

A common phenomenon after demand response is called "Rebound Effect" or an immediate spike (restrike) in power consumption when the thermostat set point is back to normal operation [97]. When interrupted water heaters are allowed to return to normal, the payback demand can be several times greater than the amount shed. "This is due to the fact that the control signal in the population model synchronizes all loads, resulting in a loss of diversification, which takes some time to be re-established." [96]. For instance, there is a threat of rebound peaks in which facilities delay their demands to avoid the peak, but causes a new peak when trying to satisfy those delayed demand. The analysis in [96] indicates an average consumption reduction per household of approximately 0.5 kWh/h during disconnection, and an additional average increase in consumption the following hour, due to the payback effect, that may reach up to 0.28 kWh/h per household. Thus, rebound effect energy is 56% of the load reduction energy based on the research proposed in [96]. The demonstration of demand response and rebound effect is shown in Fig. 2-11.

When consumers reduce their consumption during peak pricing events (or due to direct load control), a significant portion of the load is shifted to subsequent hours. Air conditioners are typically cycled or thermostats are set back in order to reduce consumption during DR events. Once the event period ends, the thermostats are returned to their original set point. At this point the ambient temperature will be above the original set point, resulting in an increase in the air conditioner usage as it "catches up" and returns the temperature to the "normal" range. This catching up process results in an increase in load following the DR event. For low levels of participation in DR programs, the impact of the rebound effect is likely to be small. As participation increases, it is

necessary for utilities that are managing DR programs to update their load forecasts, accounting for the rebound effect. Otherwise, there may be a shortage of generation available for the rebound effect.

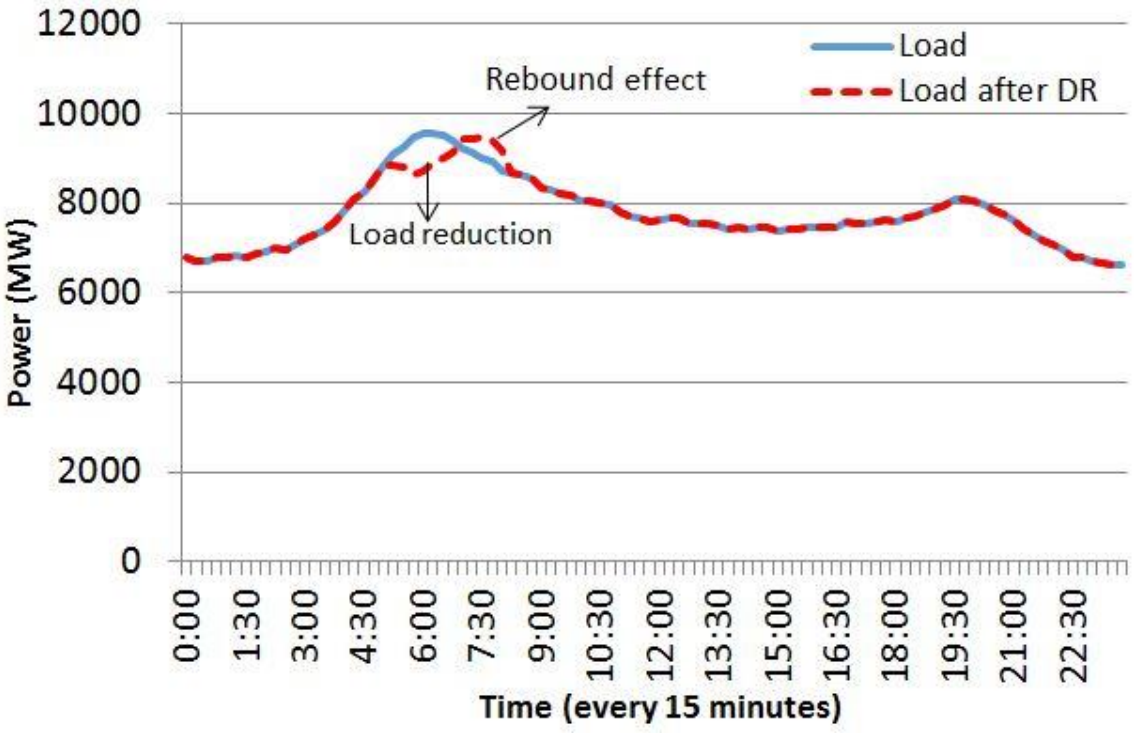

Fig. 2-11. DR and rebound effect demonstration in a typical daily load profile

By controlling DR strategies to return to normal condition slowly, demand restrike can be avoided. However, without special forethought, HVAC systems tend to use extra energy following DR events to bring systems back to normal condition. The simple case to manage rebound effect is where the DR event ends or can be postponed until the building is unoccupied. Also other strategies that allow HVAC equipment to slowly ramp up or otherwise limit power usage during the post DR event can be used to manage negative impacts of the rebound effect [98].

2.4 Coordination of Energy Storage and DR

While utilizing energy storage and DR to accommodate wind power has been extensively investigated separately, the coordination of energy storage and DR operation still deserves more research efforts. Coordination of energy storage and DR to mitigate high

wind penetration challenges as smoothing out the tie line power or decreasing the carbon emission has been addressed in [99]and [100] respectively. The multi-agent approach has been proposed in [101] to minimize the cost and peak load by managing DR and energy storage on the distribution system level. Simple models for coordination of DR and ES for a micro grid case study are presented in [102]-[103] to minimize the total operational cost of the system with high renewable penetration levels. Coordination of energy storage and demand response in an energy hub for combined heat and power (CHP) is investigated in [104], minimizing both electricity and gas consumption costs. Optimal demand response with energy storage management has also been addressed in [105] to find a control policy for an entity by convex optimization. These papers assume very simple models for battery energy storage and demand response resources neglecting detailed characteristics of each technology.

2.5 Knowledge Gaps and Contributions

High wind energy penetration challenges at the system level can be categorized into two main groups: wind intermittency and wind power forecast error. Wind intermittency leads to the non-correlation between load and wind profiles, which can be mitigated by energy storage units and demand response implementation. Impacts of wind power forecast error can be alleviated by using energy storage units, back up reserve and spilling excess wind power. These two areas are the focus of this research. The knowledge gaps and the contributions based on the literature review, discussed in previous sections, are addressed as following three bullets, each of this is addressed in subsequent chapters..

- The non-correlation between load and wind profiles, in existence of must-run generation, leads to spilled wind energy. Wind spill occurs when load minus must-run generations is less than wind power. There are various stochastic and heuristic approaches that address this challenge by using demand response and energy storage units. Energy storage and demand response coordination to minimize spilled wind energy is novel as presented in this research. Modeling detailed characteristics of grid-scale energy storage technologies, including CAES, PHES, and large scale batteries such as NaS, Lead acid, and Vanadium

redox batteries, is the contribution of this work. DR modeling including rebound effect at the transmission level is presented in this research. Studying the impact of rebound effect on minimizing spilled wind energy is another contribution of this work.

- Signal processing techniques are proposed in this research to schedule energy storage units for mitigating the impact of wind power forecast error. The advantage of these techniques as compared to other methods is their ability to extract control signals appropriate for cycling each energy storage technology. The contribution of this research over literature is considering all detailed characteristics of energy storage technologies (e.g., idle time to switch between charge and discharge modes). The trade-off between increasing the number of energy storage units and reducing spilled wind energy and back up generation is discussed. The life cycle analysis of grid-scale batteries and the impact of hybrid configuration of grid-scale energy storage technologies on increasing their lifetime have also been investigated in this research. The impact of considering frequency bias constant on reducing spilled wind energy and back up generation is also analyzed.

- Extra Reserve constraints are added in the literature to address the wind power forecast error challenge in the optimization problem. This constraint implies that system reserve has the capability to mitigate the wind power forecast error or any other contingencies in the system, such as generation outage. This research presents an algorithm to update the energy storage day-ahead scheduling in two steps for mitigating the forecast error among day-ahead wind power forecast, hour-ahead wind power forecast, and 5 minutes ahead (actual) wind power. The impact of updating day-ahead energy storage scheduling is discussed extensively on final required back-up generation and spilled wind energy.

3. Energy Storage and Demand Response Scheduling

Wind spill is a challenge due to the non-correlation between load and wind profiles in existence of must-run generation units. This happens mainly when wind generation exceeds load minus must-run generation (e.g., large nuclear power plants). In such situations the non-usable wind generation is curtailed. The key to solving this problem is to use grid-scale energy storage units and implement demand response to curtail loads. This chapter models different types of large-scale energy storage technologies and demand response scenarios while considering the rebound effect.

The over-arching objective is to minimize spilled wind energy. This problem is formulated as a mixed integer linear programming in IBM CPLEX. The uniqueness in this approach is that the impact of the rebound effect on the system load shape is considered, thereby scheduling DR such that the rebound period aligns itself with high wind output period. This helps to consume more wind energy, consequently minimizing the spilled wind energy. To showcase the applicability of the proposed approach, a case study based on the real world 15-minute interval wind and load data obtained from the Bonneville Power Administration (BPA) in 2013 is presented.

The contributions of this work can be summarized as follows:

- Present a pure technical analysis and objective function to minimize spilled wind energy for different energy storage and DR scenarios.
- Analyze the impact of different generation mixes on reducing wind spill energy. This has been achieved by detailed modeling of nuclear, coal, and natural gas generation units.
- Model detailed characteristics of large scale energy storage units such as CAES, both fixed speed and variable speed PHES units, and NaS, Lead acid, and vanadium redox batteries.
- Model DR rebound effect such that its rebound is aligned with high wind output period to reduce spilled wind energy. This is achieved by simulating different

scenarios for DR quantity as well as the ratio of rebound effect energy to DR energy.

- Investigate the impact of scheduling both energy storage and DR on reducing spilled wind energy and required energy storage size.

The rest of this chapter is organized as follows: system modeling, case study and discussion, and conclusion.

3.1. System Modeling

The whole system topology is depicted in Fig. 3-1. Generation is provided by natural gas, coal, and nuclear power plants as well as a wind farm. Different large-scale batteries (e.g. NaS, Lead acid, and Vanadium redox batteries), CAES, and PHES are considered as energy storage units. Electric water heaters and air conditioners represent devices for deploying DR in Fig. 3-1. Inelastic loads that do not participate in DR programs are also shown in Fig. 3-1.

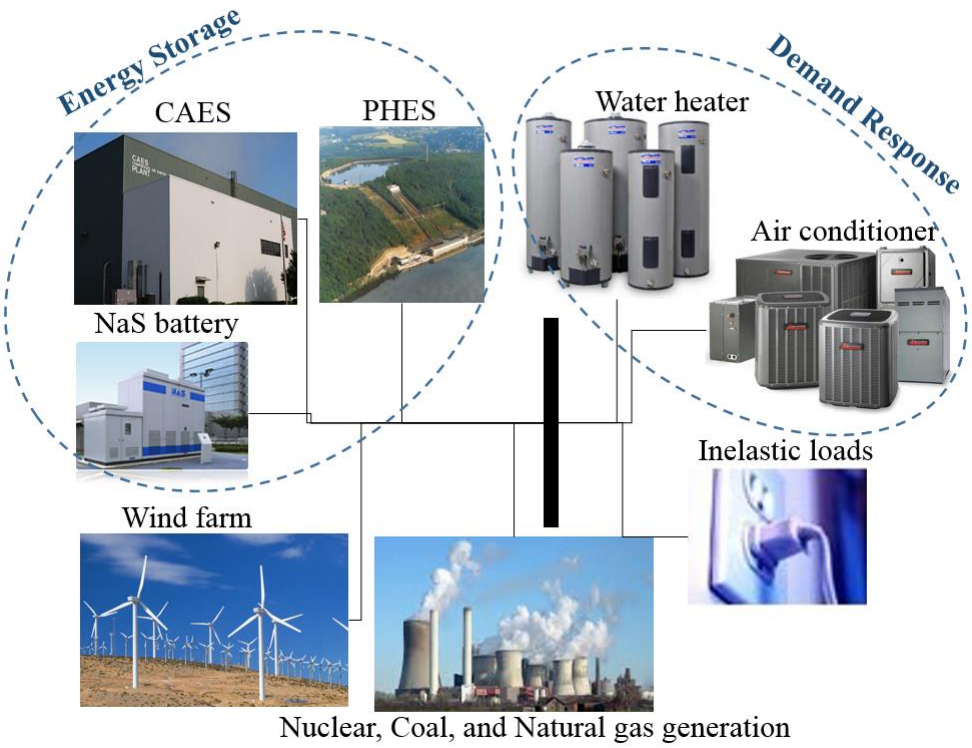

Fig. 3-1. The System Topology

The modeling presented in this research is from the utility operators' point of view, or in other words, transmission level. Transmission lines constraints as thermal limit are neglected in this chapter, assuming there are enough transmission lines available in the system having sufficient capacity to transfer the power from generators to loads, as well as, among energy storage units, generators, and loads.

Modeling of each energy storage, generation units, and demand response are presented by various equality and inequality constraints for a mixed integer linear programming (MILP) as follows.

Energy balance is an equality constraint to keep generation equal to demand at each time interval as shown in Eq. 3-1.

$$p_{l,t} - q_t + q_{rb,t} = p_{w,t} + p_{NG,t} + p_{Coal,t} + p_{Nuc,t} + p_{MSdchg,t} - p_{MSchg,t} + p_{Bdchg,t} - p_{Bchg,t} - p_{ws,t}, \forall t \quad \text{Eq. 3-1}$$

Where,

$p_{l,t}$: Continuous variable denoting the quantity of load at time *t* (MW).

q_t : Continuous variable denoting the load reduction quantity at time *t* (MW).

$q_{rb,t}$: Continuous variable denoting the rebound effect quantity at time *t* (MW).

$p_{w,t}$: Continuous variable denoting the wind power at time *t* (MW).

$p_{NG,t}$: Continuous variable denoting the power of natural gas generation at time *t* (MW).

$p_{Coal,t}$: Continuous variable denoting the power of coal generation at time *t* (MW).

$p_{Nuc,t}$: Continuous variable denoting the power of nuclear generation at time *t* (MW).

$p_{MSdchg,t}$: Continuous variable denoting mechanical energy storage discharging power at time *t* (MW).

$p_{MSchg,t}$: Continuous variable denoting mechanical energy storage charging power at time *t* (MW).

$p_{Bdchg,t}$: Continuous variable denoting the battery discharging power at time *t* (MW).

$p_{Bchg,t}$: Continuous variable denoting the battery charging power at time *t* (MW).

$p_{ws,t}$: Continuous variable denoting the wind spill power at time *t* (MW).

The mechanical energy storage modeling is related to CAES and PHES, while battery modeling is related to NaS, Lead acid, and Vanadium redox batteries. As shown in Eq. 3-1, the rebound effect increases the load while demand response decreases the load at each time interval.

3.1.1 DR Modeling

DR is assumed in this research as a contract between utility and loads at the transmission level to reduce percentage of load with certain maximum amount for limited duration and times. The modeling presented below is defined for load reduction followed by a rebound effect (restrike). The state of the art here is considering the rebound effect and find out its impact on spilled wind energy reduction when there is a high penetration of wind energy in the system.

DR amount is limited to its maximum and minimum bounds as shown in Eq. 3-2.

$$u_t q_t^{\min} \le q_t \le u_t q_t^{\max} \quad \forall t \qquad \text{Eq. 3-2}$$

Where,

t : Index of time intervals

u_t : Binary variable denoting whether load is reduced at time t ; 1 if the demand is reduced, 0 otherwise.

$q_t^{\min}$: Minimum quantity of load reduction at time *t* (MW).

q_t : Continuous variable denoting the quantity of load reduction at time *t* (MW).

$q_t^{\max}$: Maximum quantity of load reduction at time *t* (MW).

The DR ramp rate is another constraint that needs to be considered if the time interval of study is less than an hour. This constraint is shown in Eq. 3-3.

$$-r_t^D \le (q_t - q_{t-1})/\Delta t \le r_t^U, t > 1 \qquad \text{Eq. 3-3}$$

Where,

r_t^D : Ramp down rate limit of DR at time *t* (MW/min).

r_t^U : Ramp up rate limit of DR at time *t* (MW/min).

Δt : Time interval (min).

A constraint of minimum duration of DR, which is based on the contract between utility and loads, is stated as Eq. 3-4.

$$\sum_{t'=t}^{t+T^{\min}-1} u_{t'} \ge T^{\min} y_t \quad \forall t \qquad \text{Eq. 3-4}$$

Where,

u_t : Binary variable denoting whether load is reduced at time t ; 1 if the demand is reduced, 0 otherwise.

y_t : Binary variable denoting the starting indicator of DR at time t ; if $u_t = 1$ and $u_{t-1} = 0$, $y_t = 1$

$T^{\min}$: Minimum DR duration (min)

A constraint that limits the maximum duration of DR, which is based on the contract between utility and loads, is shown in Eq. 3-5.

$$\sum_{t'=t}^{t+T^{\max}-1} z_{t'} \geq y_t \quad \forall t \qquad \text{Eq. 3-5}$$

Where,

z_t : Binary variable denoting the stopping indicator of DR at time t ; if $u_t = 0$ and $u_{t-1} = 1$, $z_t = 1$

$T^{\max}$: Maximum DR duration (min)

A constraint that specifies the minimum duration of 'idle state' from last DR event is stated in Eq. 3-6. This is also known as the recovery time from the last DR event.

$$\sum_{t'=t}^{t+T_D^{\min}-1} \left(1-u_{t'}\right) \geq T_D^{\min} z_t \quad \forall t \qquad \text{Eq. 3-6}$$

Where,

$T_D^{\min}$: Minimum duration of 'idle state' from the last DR event (min).

The constraint that specifies the amount of demand rebound from the last DR event is shown in Eq. 3-7.

$$x_t q_{rb,t}^{\min} \leq q_{rb,t} \leq q_{rb,t}^{\max} \sum_{t'=1}^{T_{rb}} z_{t-t'+1}, \forall t \qquad \text{Eq. 3-7}$$

Where,

$q_{rb,t}$: Continuous variable denoting the rebound effect at time *t* (MW).

$q_{rb,t}^{\min}$: Minimum quantity of the rebound effect at time *t* (MW).

$q_{rb,t}^{\max}$: Maximum quantity of the rebound effect at time *t* (MW).

x_t : Binary variable denoting whether load is rebounded at time t ; 1 if the demand is rebounded, 0 otherwise.

T_{rb} : Duration time of rebound effect profile (min).

The ramping rate limit of the rebound effect is defined in Eq. 3-8.

$$-r_t^D \le q_{rb,t+1} - q_{rb,t} \le r_t^U \quad \text{Eq. 3-8}$$

The relationship between the energy of the rebound effect and the last DR event is shown in Eq. 3-9. This is the ratio of the rebound effect energy to the demand reduction energy caused by calling a DR event. If it is one, it has no change on total load consumption energy. But, if it is less than one, it reduces the overall load consumption. When it is more than one, it increases the total load consumption.

$$\sum_{t=1}^{T} q_{rb,t} \le \lambda_{rb} \sum_{t=1}^{T} q_t \quad \text{Eq. 3-9}$$

Where,

λ_{rb} : The ratio of rebound effect energy to DR energy.

The maximum number of weekly DR events is enforced, as indicated in Eq. 3-10. This can be based on the contract between a utility and homeowners to satisfy their comfort requirement.

$$\sum_{t=1}^{T} y_t \le N_{Weekly} \quad \text{Eq. 3-10}$$

Where,

N_{weekly} : Maximum number of DR events per week.

The maximum number of daily DR events is another constraint that is shown in Eq. 3-11.

$$\sum_{t=1}^{Daily} y_t \le N_{Daily} \quad \text{Eq. 3-11}$$

Where,

N_{daily} : Maximum number of DR events per day.

The relationships among binary variables of DR are shown in Eq. 3-12 and Eq. 3-13. Eq. 3-12 defines the relationship between the starting and stopping indicators of DR. Eq. 3-13 states that stopping and starting indicators of DR happens only once at a time.

$$y_t - z_t = u_t - u_{t-1} \quad \forall t \qquad \text{Eq. 3-12}$$

$$y_t + z_t \leq 1 \quad \forall t \qquad \text{Eq. 3-13}$$

The relationship among binary variables of DR and the rebound effect as shown in Eq. 3-14 indicates that the rebound effect starts right after the DR event ends.

$$\sum_{t=1}^{t'} z_t = x_{t'}, t' = T_R : T \qquad \text{Eq. 3-14}$$

3.1.2 Mechanical Energy Storage Modeling

This section describes the incorporation of detailed characteristics of mechanical energy storage units including PHES and CAES into the MILP formulation. The state-of-the-art modeling methods for both CAES and PHES take into account the required idle time to switch between charge and discharge modes. This constraint is not addressed nor modeled in the literature. Since the problem is solved by MILP, this constraint is presented by linear constraints while defining extra binary variables. Modeling of mechanical energy storage units are presented as follows.

The final state of charge equals to the initial state of charge every week as shown in Eq. 3-15. This constraint insures that energy storage is not a source of generation.

$$\sum_{t'}^{weekly} (p_{MSchg,t'} \eta_{MS} - p_{MSdchg,t'}) \Delta t = 0 \qquad \text{Eq. 3-15}$$

Where,

$p_{MSchg,t}$: Continuous variable denoting mechanical energy storage charging power at time *t* (MW).

$p_{MSdchg,t}$: Continuous variable denoting mechanical energy storage discharging power at time *t* (MW).

η_{MS} : Mechanical energy storage roundtrip efficiency (%).

Δt : Time interval (min).

Mechanical energy storage can operate in one mode at a time, charge, discharge, or idle, which is stated in Eq. 3-16.

$$\alpha_{MS,t} + \beta_{MS,t} + \gamma_{MS,t} = 1, \forall t \quad \text{Eq. 3-16}$$

Where,

$\alpha_{MS,t}$: Binary variable denoting whether mechanical energy storage is charged at time t ; 1 if charge, 0 otherwise.

$\beta_{MS,t}$: Binary variable denoting whether mechanical energy storage is discharged at time t ; 1 if discharge, 0 otherwise.

$\gamma_{MS,t}$: Binary variable denoting whether mechanical energy storage is idle at time t ; 1 if idle, 0 otherwise.

The relationship among start and stop of idle time and idle mode indicator are presented in Eq. 3-17 and Eq. 3-18.

$$\rho_{MS,t} - \varphi_{MS,t} = \gamma_{MS,t} - \gamma_{MS,t-1}, t > 1 \quad \text{Eq. 3-17}$$

$$\rho_{MS,t} + \varphi_{MS,t} \leq 1, \forall t \quad \text{Eq. 3-18}$$

Where,

$\rho_{MS,t}$: Binary variable denoting the starting indicator of the idle mode at time t ; if $\gamma_{MX,t} = 1$ and $\gamma_{MX,t-1} = 0$, then $\rho_{MX,t} = 1$.

$\varphi_{MS,t}$: Binary variable denoting the stopping indicator of the idle mode at time t ; if $\gamma_{MX,t} = 0$ and $\gamma_{MX,t-1} = 1$, then $\varphi_{MX,t} = 1$.

The relationship among binary variables indicating that if the mode of operation changes it should remain idle is shown in Eq. 3-19 and Eq. 3-20.

$$\rho_{MS,t} - \varphi_{MS,t} = \alpha_{MS,t-1} - \alpha_{MS,t} + \beta_{MS,t-1} - \beta_{MS,t}, t > 1 \quad \text{Eq. 3-19}$$

$$-1 \le (\alpha_{MS,t-1} - \alpha_{MS,t}) + (\beta_{MS,t-1} - \beta_{MS,t}) \le 1, t > 1 \quad \text{Eq. 3-20}$$

Charging and discharging powers are limited to the rated power of energy storage as shown in Eq. 3-21 and Eq. 3-22, respectively.

$$P_{MS} N_{MS} \alpha_{MS,t} \mu_{MSchg}^{\min} \le p_{MSchg,t} \le P_{MS} N_{MS} \alpha_{MS,t}, \forall t \quad \text{Eq. 3-21}$$

$$P_{MS} N_{MS} \beta_{MS,t} \mu_{MSdchg}^{\min} \le p_{MSdchg,t} \le P_{MS} N_{MS} \beta_{MS,t}, \forall t \quad \text{Eq. 3-22}$$

Where,

P_{MS} : Rated power capacity for mechanical energy storage (MW).

N_{MS} : Number of mechanical energy storage.

The minimum required idle time for mechanical energy storage technologies to switch mode is formulated as Eq.3-23.

$$\sum_{t'=t}^{t+T_{MS}^{\min}-1} \gamma_{MS,t'} \ge T_{MS}^{\min} \rho_{MS,t}, \forall t \quad \text{Eq. 3-23}$$

Where,

$T_{MS}^{\min}$: Minimum duration of idle mode for mechanical energy storage (min).

State of charge is limited to the storage energy rating as shown in Eq. 3-24. Maximum and minimum quantities for the state of charge are assumed to be 1 and 0, respectively for mechanical energy storage technologies.

$$0 \le \frac{\sum_{t'=1}^{k}(p_{MSchg,t'}\eta_{MS} - p_{MSdchg,t'})\Delta t}{E_{MS}N_{MS}} + SOC_{MS}^{i} \le 1, k = 1:T \quad \text{Eq. 3-24}$$

Where,

E_{MS} : Rated energy capacity of mechanical energy storage (MWh).

SoC_{MS}^{i} : Initial state of charge of mechanical energy storage (%).

Rate of change of storage output is limited to the storage ramp rate as stated in Eq. 3-25.

$$-dP_{MS}N_{MS} \le \frac{(p_{MSchg,t} - p_{MSdchg,t}) - (p_{MSchg,t-1} - p_{MSdchg,t-1})}{\Delta t} \le dP_{MS}N_{MS}, t > 1$$

Eq. 3-25

Where,

dP_{MS} : Energy storage ramp rate for mechanical energy storage (MW/min).

3.1.3 Large Scale Battery Modeling

As mentioned before, large scale batteries considered in this research are NaS battery, Lead acid battery, and Vanadium redox battery. Large scale batteries are modeled by defining following equality and inequality constraints based on their operational characteristics.

Final state of charge equals to the initial state of charge every day as shown in Eq. 3-26. Since large scale battery is not a source of energy, it is scheduled to return to its initial state of charge every day, or in other words, refill daily.

$$\sum_{t'}^{Daily}(p_{Bchg,t'}\eta_{B} - p_{Bdchg,t'})\Delta t = 0 \quad \text{Eq. 3-26}$$

Where,

$p_{Bchg,t}$: Continuous variable denoting quantity of charging power of battery at time *t* (MW).

$p_{Bdchg,t}$: Continuous variable denoting quantity of discharging power of battery at time *t* (MW).

η_B : Roundtrip efficiency of battery (%).

Δt : Time interval (min).

Charge and discharge power quantities are limited to the rated power of energy storage as shown in Eq. 3-27.

$$0 \le p_{Bchg,t}, p_{Bdchg,t} \le P_B N_B, \forall t \qquad \text{Eq. 3-27}$$

Where,

N_B : Number of large scale batteries

P_B : Rated power capacity of large scale battery (MW)

State of the charge is limited to the energy capacity of large scale battery as shown in Eq.3-28 and Eq. 3-29. The maximum and minimum state of charge is defined between 0 and 1 to avoid overfilling or depleting the battery technology.

$$SOC_{B,t} = \frac{\sum_{t'=1}^{t} (p_{Bchg,t'} \eta_B - p_{Bdchg,t'}) \Delta t}{E_B N_B} + SOC_B^i \qquad \text{Eq. 3-28}$$

$$SOC_B^{\min} \le SOC_{B,t} \le SOC_B^{\max}, t = 1:T \qquad \text{Eq. 3-29}$$

Where,

$SoC_{B,t}$: State of charge of large scale battery at time *t* (%).

E_B : Rated energy capacity of large scale battery (MWh).

$SoC_B^{\max}$: Maximum state of charge of large scale battery (%).

$SoC_B^{\min}$: Minimum state of charge of large scale battery (%).

3.1.4 Equivalent Natural Gas Unit Modeling

A natural gas-fired generator is modeled by defining following equality and inequality constraints for it associated binary and continuous variables.

Power limit:

$$P_{NG}^{\min} u_{NG,t} \leq p_{NG,t} \leq P_{NG}^{\max} u_{NG,t}, \forall t \quad \text{Eq. 3-30}$$

Where,

$P_{NG}^{\min}$: Minimum stable operation power of natural gas generation unit (MW).

$P_{NG}^{\max}$: Maximum stable operation power of natural gas generation unit (MW).

$u_{NG,t}$: Binary variable denoting whether natural gas unit is on or off at time t; 1 if on, 0 otherwise

The relationship among binary variables can be written as:

$$y_{NG,t} - z_{NG,t} = u_{NG,t} - u_{NG,t-1}, t > 1 \quad \text{Eq. 3-31}$$

$$y_{NG,t} + z_{NG,t} \leq 1, \forall t \quad \text{Eq. 3-32}$$

Where,

$y_{NG,t}$: Binary variable denoting the starting indicator of generation unit at time *t*; if $u_{NG,t} = 1$ and $u_{NG,t-1} = 0$, then $y_{NG,t} = 1$.

$z_{NG,t}$: Binary variable denoting the stopping indicator of natural gas unit at time *t*; if $u_{NG,t} = 0$ and $u_{NG,t-1} = 1$, then $z_{NG,t} = 1$.

Ramp rate limit:

$$-dP_{NG} \le (p_{NG,t} - p_{NG,t-1}) / \Delta t \le dP_{NG}, \forall t \qquad \text{Eq. 3-33}$$

Where,

dP_{NG} : Natural gas unit ramp rate (MW/min).

Minimum up time constraint:

$$\sum_{t'=t}^{t+T_{NG,up}^{\min}-1} u_{NG,t'} \ge T_{NG,up}^{\min} y_{NG,t}, \forall t \qquad \text{Eq. 3-34}$$

Where,

$T_{NG,up}^{\min}$: Minimum up time of the natural gas generation unit (min).

Minimum down time constraint:

$$\sum_{t'=t}^{t+T_{NG,dn}^{\min}-1} (1-u_{NG,t'}) \ge T_{NG,dn}^{\min} z_{NG,t}, \forall t \qquad \text{Eq. 3-35}$$

Where,

$T_{NG,dn}^{\min}$: Minimum down time of the natural gas generation unit (min).

3.1.5 Equivalent Coal Unit Modeling

A coal-fired generator is modeled by defining following equality and inequality constraints for it associated binary and continuous variables. The extra constraint for modeling a coal-fired generator as compared to a natural gas-fired unit is the capacity factor constraint that is required for the economic operation of coal power plants.

Power limit:

$$P_{Coal}^{\min} u_{Coal,t} \le p_{Coal,t} \le P_{Coal}^{\max} u_{Coal,t}, \forall t \quad \text{Eq. 3-36}$$

Where,

$P_{Coal}^{\min}$: Minimum stable operation power of coal generation unit (MW).

$P_{Coal}^{\max}$: Maximum stable operation power of coal generation unit (MW).

$u_{Coal,t}$: Binary variable denoting whether coal unit is on or off at time t; 1 if on, 0 otherwise.

The relationship among binary variables is defined as:

$$y_{Coal,t} - z_{Coal,t} = u_{Coal,t} - u_{Coal,t-1}, t > 1 \quad \text{Eq. 3-37}$$

$$y_{Coal,t} + z_{Coal,t} \le 1, \forall t \quad \text{Eq. 3-38}$$

Where,

$y_{Coal,t}$: Binary variable denoting the starting indicator of coal generation unit at time *t*; if $u_{Coal,t} = 1$ and $u_{Coal,t-1} = 0$, then $y_{Coal,t} = 1$

$z_{Coal,t}$: Binary variable denoting the stopping indicator of coal generation unit at time *t*; if $u_{Coal,t} = 0$ and $u_{Coal,t-1} = 1$, then $z_{Coal,t} = 1$

Ramp rate limit:

$$-dP_{Coal} \le (p_{Coal,t} - p_{Coal,t-1}) / \Delta t \le dP_{Coal}, \forall t \quad \text{Eq. 3-39}$$

Where,

dP_{Coal} : Coal generation unit ramp rate (MW/min).

Minimum up time constraint:

$$\sum_{t'=t}^{t+T_{Coal,up}^{\min}-1} u_{Coal,t'} \geq T_{Coal,up}^{\min} y_{Coal,t}, \forall t \qquad \text{Eq. 3-40}$$

Where,

$T_{Coal,up}^{\min}$: Minimum up time of the coal generation unit (min).

Minimum down time constraint:

$$\sum_{t'=t}^{t+T_{Coal,dn}^{\min}-1} (1-u_{Coal,t'}) \geq T_{Coal,dn}^{\min} z_{Coal,t}, \forall t \qquad \text{Eq. 3-41}$$

Where,

$T_{Coal,dn}^{\min}$: Minimum down time of the coal generation unit (min).

Capacity factor constraint:

$$CF_{coal}^{\min} \leq \frac{\sum_{t=1}^{T} p_{coal,t}}{P_{Coal}^{\max} \Delta T} \leq CF_{coal}^{\max} \qquad \text{Eq. 3-42}$$

Where,

$CF_{Coal}^{\min}$: Minimum capacity factor of the coal generation unit (%).

$CF_{Coal}^{\min}$: Maximum capacity factor of the coal generation unit (%).

ΔT : Total duration of simulation (min).

3.1.6 Equivalent Nuclear Unit Modeling

A nuclear generation unit has a technical barrier related to its inability to be turned off and on frequently. Hence, it is considered to be on while having minimum stable operation. As a result it does not have minimum required up and down time either. The nuclear generation modeling is presented with following constraints.

Power limit:

$$P_{Nuc}^{\min} \le p_{Nuc,t} \le P_{Nuc}^{\max}, \forall t \qquad \text{Eq. 3-43}$$

Where,

$P_{Nuc}^{\min}$: Minimum stable operation power of nuclear generation unit (MW).

$P_{Nuc}^{\max}$: Maximum stable operation power of nuclear generation unit (MW).

Ramp rate limit:

$$-dP_{Nuc} \le (p_{Nuc,t} - p_{Nuc,t-1})/\Delta t \le dP_{Nuc}, \forall t \qquad \text{Eq. 3-44}$$

Where,

dP_{Nuc} : Nuclear generation unit ramp rate (MW/min).

Capacity factor constraint:

$$CF_{nuc}^{\min} \le \frac{\sum_{t=1}^{T} p_{nuc,t}}{P_{nuc}^{\max} \Delta T} \le CF_{nuc}^{\max} \qquad \text{Eq. 3-45}$$

Where,

$CF_{Nuc}^{\min}$: Minimum capacity factor of the nuclear generation unit (%).

$CF_{Nuc}^{\min}$: Maximum capacity factor of the nuclear generation unit (%)

3.1.7 Objective Function

The objective function is to minimize spilled wind energy as shown in Eq. 3-46. This is chosen to study the impact of energy storage and demand response at the transmission level while skipping all economic evaluations. Since energy storage and demand response are assumed to be available flexible resources in control of utility operators, they appear in constraints, not the objective function.

$$\textit{Minimize} \qquad \sum_{t=1}^{T} p_{ws,t} \qquad \text{Eq. 3-46}$$

3.2 Results and Discussions

To showcase the applicability of the proposed approach, different case studies based on real world wind and load data in 15-minute time intervals - obtained from the Bonneville Power Administration (BPA) in 2013 - are used [54]. BPA peak load in 2013 was 10.6 GW, and installed wind capacity is 4.5 GW. The wind energy penetration level is 20% in BPA, while neglecting net interchange. BPA load is scaled up to meet the projected load in 2040 using the average growth rate of 0.8% per year from 2013 to 2040 [106]. Wind data is also scaled up in the same ratio to remain at the level of 20% wind energy penetration.

The mixed integer linear programming (MILP) is modeled in MATLAB and solved by IBM CPLEX with the time horizon of one year with 15-minute time resolution. Since the optimization constraints are defined independent for each week, the optimization problem is simulated for fifty-two weeks (one year) separately and results are the summation of the fifty-two week period.

Parameters for modeling the generation mix by fuel type are presented in Table 3-1. Nuclear power plants can ramp down by 20% of its nominal capacity in an hour, but ramping up the same amount takes up to 6 to 8 hours [107]. The economic operation of nuclear power plant requires the capacity factor to be within the range of 100% to 75%. Coal power plants have 1.5-3% of its nominal capacity ramp rate per minute, and their economic operation enforces their capacity factor to remain between 45% and 70%. Natural Gas units are peaking power plants and their ramp rate is limited to 8% of capacity per minute. The maintenance and forced outage rates of conventional power plants have been neglected in this study.

Minimum stable operation of nuclear generation is at 80% of its nominal capacity, while minimum operation of natural gas and coal units are at 20% and 30% of their rated

capacity, respectively. As shown in Table 3-1, the minimum up or down time for natural gas and coal units are 2 hours and 12 hours, respectively. According to the inability to shutdown of nuclear units, this yields no down time state. The total nuclear, coal, and gas generation capacity provides 100% of annual peak load, to guarantee system reliability in existence of stochastic wind generation. If the availability of each generation unit is 90%, then the installed capacity is required to be 11% (which is 1 over 90%) more to be able to provide the desired generation capacity throughout the year.

Modeling parameters for mechanical energy storage units (CAES and PHES) and large scale batteries are presented in Table 3-2, and Table 3-3, respectively. As shown, CAES requires at least 20-minute idle time to switch between charging and discharging modes, while PHES requires at least 4-minute idle time. PHES are either fixed speed or adjustable speed. Fixed speed PHES can only pump at a constant power (which is rated power capacity), while adjustable speed one pumps for a specific range (which is 100% to 40% of rated power capacity). Generating power ranges between 100% and 50% for fixed speed PHES, while it is between 100% and 30% for adjustable speed PHES. The rated energy and power capacities for both CAES and PHES are considered to be 6000 MWh and 300 MW, respectively, for better comparison between these two technologies.

Characteristics of large-scale batteries including NaS, and Lead acid are shown in Table 3-3. As shown, all three have the same power capacity which is 50 MW. NaS battery has the highest energy capacity which is 300 MWh and Lead acid battery has the lowest energy capacity which is 200 MWh. Vanadium redox energy capacity is between the other two batteries which is 250 MWh. Lead acid battery has the highest efficiency which is 85%, while Vanadium redox has the lowest efficiency as 70%. All batteries are operated in such a way that their state of charge do not exceed 90%, nor get below 10% of their rated energy capacity. Another important parameter for battery operation is the life cycle, which is shown in the last row of Table 3-3.

DR potential can be estimated by aggregating the amount of electric water heater and air conditioning, participation factor, and capacity response ratio [108]. Total demand response capacity in PJM Interconnection is about 10 GW (considering both demand

resources and energy efficiency) [109], which is 6% of its annual peak load in 2013 [110].

This research assumes 5% and 10% of load at that time for DR maximum amount as shown in Table 3-4. Minimum load reduction is defined to be 0.5 of the maximum load reduction. This parameter is added to DR modeling to avoid zero values to be counted in DR periods. If time resolution of simulation is less than one hour, ramping constraints is required for DR modeling [118]. DR ramp rate in 15 minutes is assumed to be half of DR value at that time, due to 30-minute DR response time and 15-minute time resolution of the study. Maximum and minimum DR durations are considered to be three and two hours, respectively. Minimum duration of idle time between DR events is considered to be three hours.

Table 3-1. Natural Gas, Coal, and Nuclear Units Modeling Parameters [107]

Unit Type	Capacity (%)	Min (%)	Ramp Rate	Min up/down time	Capacity Factor (%)
Nat Gas	38	20	8% up/down per min	2 hrs	---
Coal	42	30	1.5% up/down per min	12 hrs	45-70
Nuclear	20	80	20% down per hr, 20% up per 6 hrs	---	100-75

Table 3-2. Large-Scale Mechanical Energy Storage Modeling Parameters [12], [13], [117]

Energy Storage Technology	PHES		CAES
	Single Speed	Adjustable Speed	
Min Generating Power (%)	50	30	--
Min Pumping Power (%)	100	40	--
Power Capacity (MW)	600		300, 600
Energy Capacity (MWh)	6000		6000
Ramp Rate	4-6% (per second)		18 MW/min
Efficiency (%)	80		70
Required Idle Time (min)	--		20

Table 3-3. Large-Scale Battery Modeling Parameters [12], [13]

Grid-scale battery	NaS	Lead acid
Power (MW)	50	50
Energy (MWh)	300	200
Efficiency (%)	75	85
Max, Min SoC	0.9,0.1	0.9,0.1

Table 3-4. DR and RE Modeling Parameters

Max Load Reduction Power to Load Ratio	0.05, 0.10
Min Load Reduction Power to Load Ratio	0.01
Max Ramp Up/Down Rate of DR to Max Load Reduction Ratio	0.5
Max Duration of DR (hrs)	3
Min Duration of DR (hrs)	2
Min Duration of Idle Time from Last DR (hrs)	3
Duration of Rebound Effect (HRS)	2
Max Rebound Effect Power to Load Ratio	0.05, 0.10
Min Rebound Effect Power to Load Ratio	0.01
Max Ramp Up/Down Rate of Rebound Effect to Load Reduction Ramp Up/Down Rate Ratio	0.5
Ratio of Rebound Effect Energy to Load Reduction Energy	0.5, 1,1.5
Max Number of DR Events in a Week	3
Max Number of DR Events in a Day	1

Three different rebound effect scenarios are considered based on the ratio of rebound effect energy to DR energy and rebound effect energy duration. For example, if rebound to DR energy ratio is 0.5, then cutting 1000MWh of energy results in a rebound of 500MWh energy. These scenarios are listed below:

1. Rebound effect energy to DR energy ratio is 0.5 with 1 hour duration of rebound.
2. Rebound effect energy to DR energy ratio is 1 with 2 hours duration of rebound.
3. Rebound effect energy to DR energy ratio is 1.5 with 2 hours duration of rebound.

The maximum rebound effect quantity is considered to be the same as the maximum DR quantity. The minimum rebound effect quantity is defined to be 0.5 of the maximum rebound effect quantity. This parameter is added to the rebound effect modeling to avoid zero values be counted as rebound effect in its duration. The ramp rate of rebound effect is considered to 0.5 of its maximum quantity. The last two parameters shown in Table 3-4, are maximum number of DR events per week and per day which are shown to be three and one, respectively.

Different case studies are simulated for the whole year to study the impact of generation mix, DR scenarios, energy storage technologies, and scheduling both DR and energy storage on reducing spilled wind energy. The impact of deploying different DR scenarios on reduction of total generation is also investigated. These case studies and their results are described as follows.

3.2.1 Impact of Generation Mix by Fuel Type

Four different generation mix scenarios including the projected generation in 2040 by U.S. EIA [106] are used to study their impacts on wind spill energy. These percentages are calculated as if nuclear, coal, and natural gas are the only generating units in addition to wind generation, as shown in Fig. 3-2. The total generation mix capacity provides 100% of annual peak load to guarantee system reliability, considering the stochastic nature of wind generation.

The spilled wind energy for each generation mix scenario is shown in Fig. 3-2 as a result of the proposed mixed integer linear programming to minimize spilled wind energy. As shown, the base case results in 952 GWh spilled wind energy. This spillage is 7% of the annual wind energy generation. The base case has the highest spilled wind energy due to having the highest nuclear and coal capacity comparing to the other cases. Then, case 1 with 10% less coal generation and 10% more gas generation units while having the same capacity comparing to the base case, results in 552 GWh spilled wind energy. Hence, the spilled wind energy has reduced by 400 GWh for case 1 as compared to the base case. The nuclear capacity has reduced by 10% and gas has increased by 10% as compared to

base case. This generation mix results in 667 GWh less spilled wind energy as compared to base case. The spilled wind energy of case 3 is the least which is 84 GWh due to having the lowest nuclear and coal generation capacity.

As a result, wind spill energy depends on the percentage of both nuclear and coal generation capacities due to their technical and economic barriers as shown in Table 3-1. The minimum loading level of nuclear and coal generation units are 80% and 30% of their nominal rated power capacities, respectively. The other limiting characteristic is the high capacity factor, which is 75-100% for nuclear generation unit and 45-70% for coal generation unit. The other two technical barriers are ramp rate and minimum up/down time of these units as shown in Table 3-1

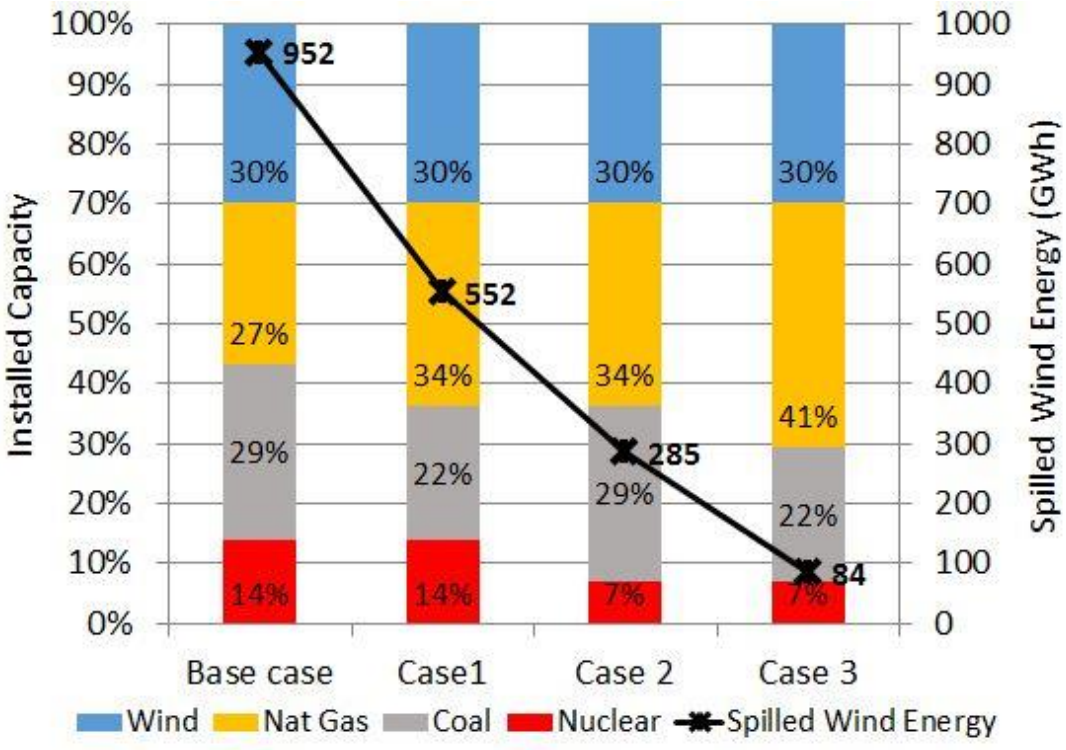

Fig. 3-2. Different generation mix by fuel type and their resultant spilled wind energy

The generation mix for the rest of case studies is based on U.S. EIA projected generation mix for 2040, which results in 952 GWh wind spill energy without considering energy storage and DR.

3.2.2 Impact of Different DR Scenarios

The novel idea presented in this research is modeling DR rebound effect such that it can reduce spilled wind energy, which is a challenge in utilities with high wind energy penetration levels. The implementation of this idea is achieved by the proposed mixed integer linear programming. The sample result of the optimization problem for a week is shown in Fig. 3-3 to illustrate the proposed DR scheduling. As shown, DR is scheduled prior to high wind energy penetration periods such that its rebound effect is aligned with the time of high wind generation period. This unique DR scheduling can reduce spilled wind energy by adjusting the rebound effect occurring time.

As shown in Fig. 3-3, there are three DR events scheduled right before the time when wind power is high but load is low, to reduce spilled wind energy. The number of events is limited to the constraint defined in DR modeling which was not more than three times per week and once per day. The negative part of the green line shown in Fig. 3-3 is DR (load reduction) and the positive one is related to the rebound effect (load compensation). The simulation result shown in Fig. 3-3 is when the rebound effect energy to DR energy ratio is 1.5 with the rebound effect duration of two hours. As illustrated in Fig. 3-3, solving the proposed optimization result in scheduling DR such that rebound effect is aligned with the time when wind power is high and load is low, to minimize the wind spillage. Results for different scenarios of DR and rebound effect are simulated for the whole year and explained as follows.

The impact of DR scheduling is investigated by simulating the whole year with 15-minute time intervals. It is important to note that since each week scheduling is independent of the other week, optimization problem is simulated for fifty-two weeks (one year) separately and results presented, are the summation of all these fifty-two weeks. Different DR scenarios as 5% and 10% amount, with 0.5, 1, and 1.5 rebound effect energy ratios, are simulated. The impact of these DR scenarios on wind spill energy is shown in Fig. 3-4.

As shown in Fig. 3-4, 5% DR amount with 0.5 rebound energy ratio, results in 48 GWh in spilled wind energy. While, 5% DR with 1 rebound effect energy ratio, results in 61 GWh reductions in wind spill energy. On the other hand, 5% DR amount with 1.5 rebound effect energy ratio reduced spilled wind energy by in 63 GWh. As shown in Fig. 3-4, spilled wind energy is reduced by 30 GWh, 44 GWh, and 50 GWh for 0.5, 1, and 1.5 rebound effect energy ratios, respectively, if DR amount is increased from 5% to 10%.

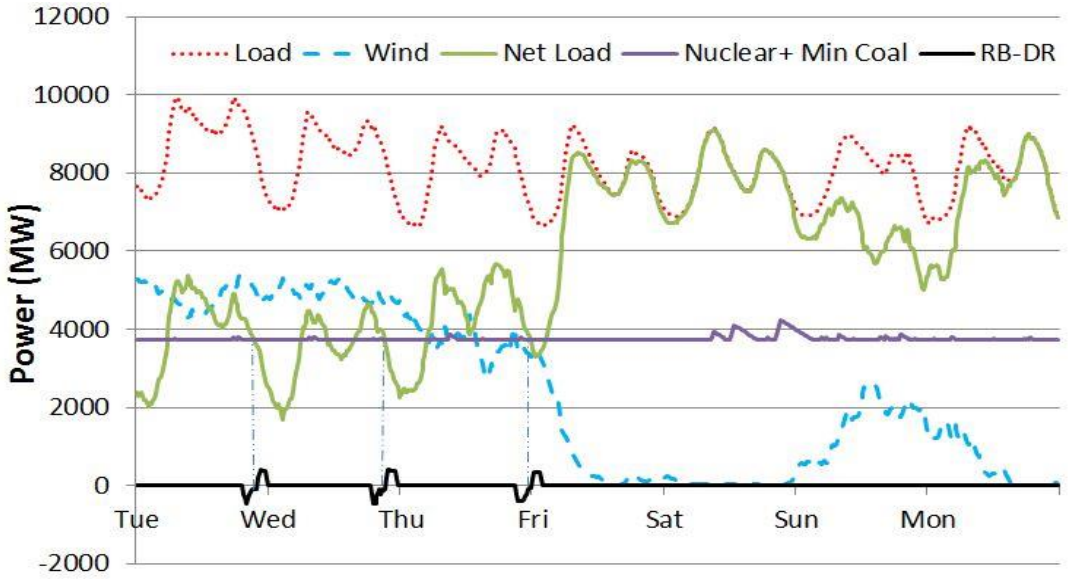

Fig. 3-3. Load, wind, and DR followed by rebound effect (Rb) for a week

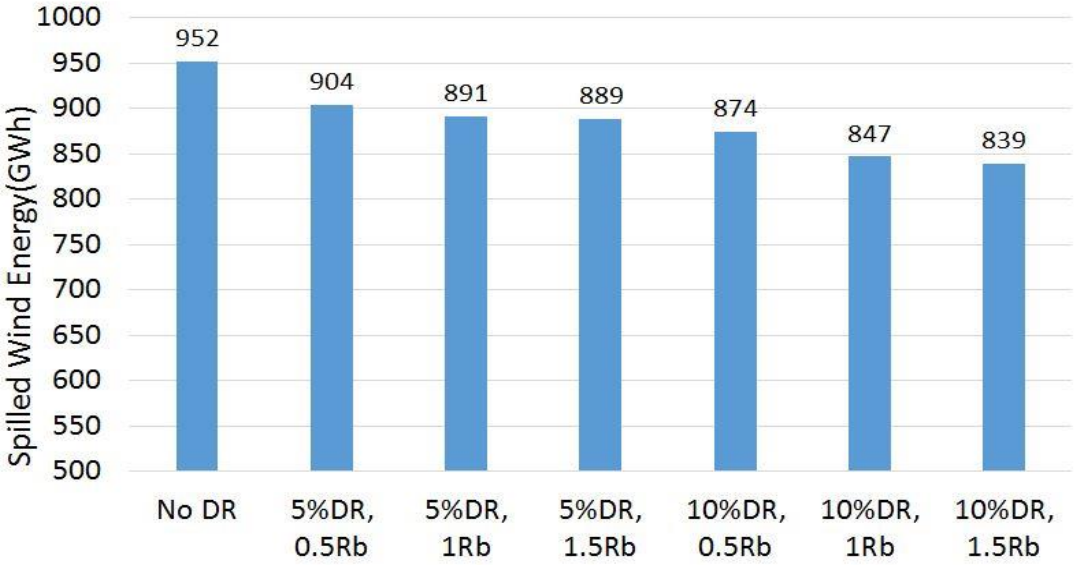

Fig. 3-4. Spilled wind energy for different DR scenarios

3.2.3 Impact of Different Energy Storage Technologies

The impact of large-scale energy storage technologies on spilled wind energy reduction are shown in Fig. 3-5. Large-scale mechanical energy storage technologies such as CAES and PHES have 20 to 30 times more rated energy capacity than mentioned large-scale batteries. The rated power capacity of CAES and PHES is 6 times more than the considered large-scale batteries. Hence, mechanical energy storage technologies results in less wind spill energy as compared to large scale batteries. This can be observed in Fig. 3-5.

The wind spill energy without inserting any type of energy storage technology is 952 GWh. If one NaS battery is inserted, spilled wind energy reaches 912 GWh. Wind spill energy reaches 923 GWh when one Lead acid battery is inserted, due to its lower energy capacity as compared to the other two large-scale batteries. If two NaS batteries are inserted, then spilled wind energy reaches 873 GWh. If two Lead acid batteries are inserted, then spilled wind energy reaches 894 GWh.

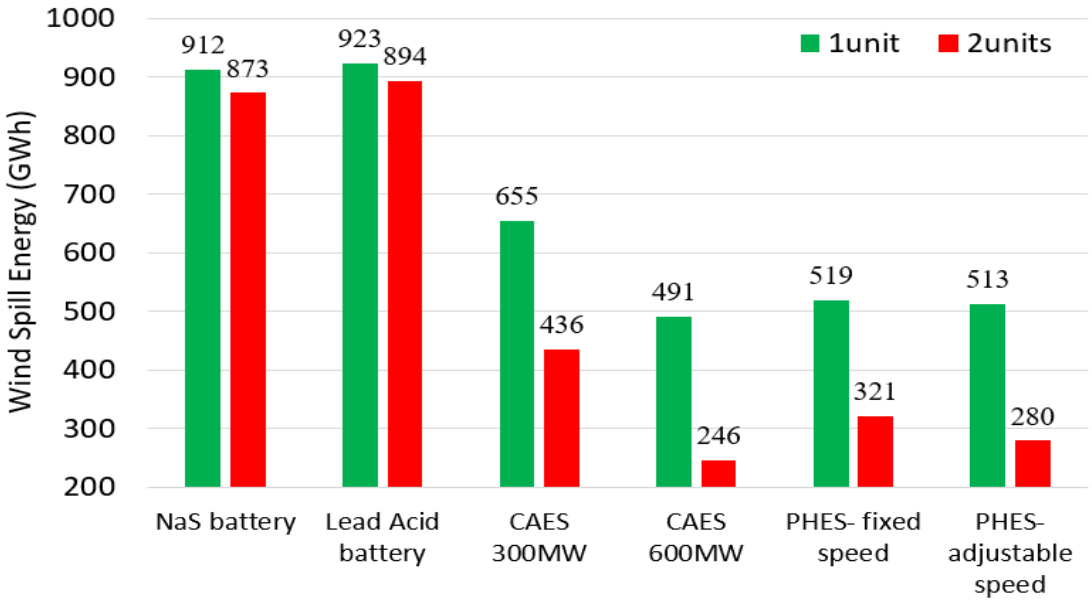

Fig. 3-5. Wind spill energy for different energy storage technologies.

If one 300 MW CAES is inserted, wind spill energy reaches 655 GWh, as opposed to 952 GWh for no energy storage scenario. When two 300 MW CAES units are inserted wind spill energy reaches 436 GWh. The reason why wind spill energy reduction is not doubled by adding an additional CAES is because the remaining wind spill available is less than what was available to charge the first CAES. This is important to take into consideration for investing on adding more energy storage units. When one 600 MW CAES is inserted with the same rated energy capacity as the 300 MW CAES, then spilled wind energy reaches 491 GWh. Hence, doubling the rated power capacity while keeping the rated energy capacity the same reduce more 164 GWh in spilled wind energy. This shows the impact of rated power capacity on spilled wind energy.

When two fixed speed PHES units are inserted, wind spill energy reaches 321 GWh. If two adjustable speed PHES units are inserted, then spilled wind energy reduces to 280 GWh. Hence, variable speed PHES results in 41 GWh less wind spill energy as compared to fixed speed one. This is due to fixed pumping power of fixed speed PHES and lower range of generating power as compared to adjustable PHES.

Although 600 MW CAES and both PHES technologies have the same rated power and energy capacity values, the spilled wind energy is reduced more by CAES as compared to PHES. This is because CAES has larger range of pumping and generating powers as compared to PHES, although it has longer required idle time and less efficiency comparing to PHES.

3.2.4 Impact of scheduling both DR and energy storage

The impact of scheduling both energy storage and DR on reducing wind spillage is depicted in Fig. 3-6. The 10% DR amount with 1 rebound effect energy ratio (which keeps load consumption the same before and after DR) is considered for this case study. Two types of energy storage units – including CAES, as a mechanical energy storage technology, and NaS battery, as a chemical energy storage technology – are selected for this study. These two energy storage technologies are selected because they can provide less wind spillage, as compared to their own group shown in the previous section.

Selection of a hybrid energy storage configuration including mechanical and chemical energy storage technologies result in better performance by getting benefit from characteristic of each energy storage technology category.

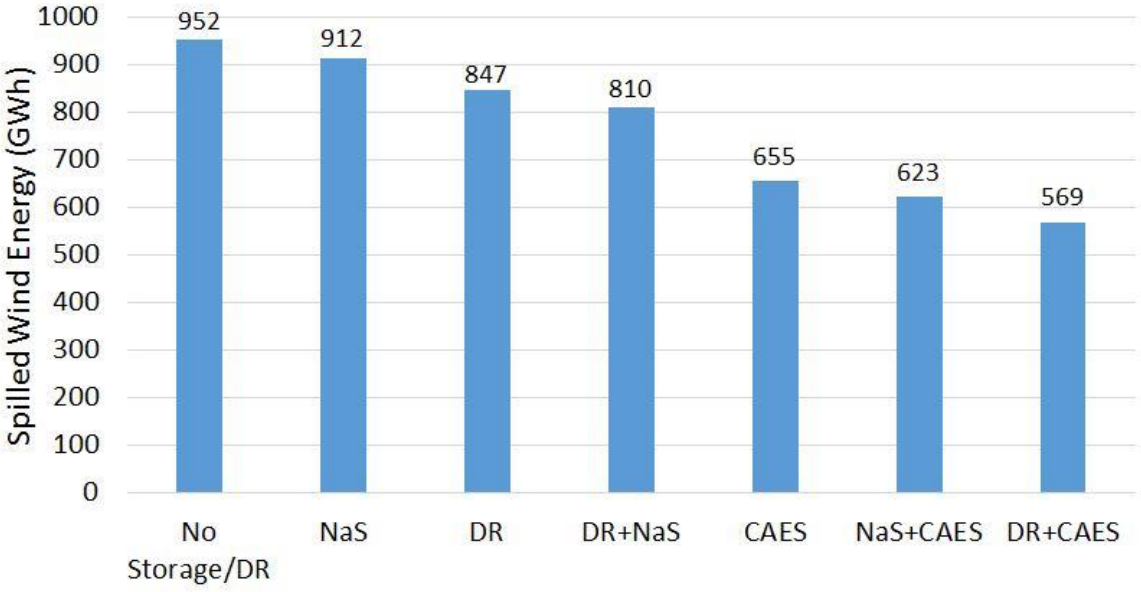

Fig. 3-6. Spilled wind energy for different DR and energy storage scenarios

As shown, if one NaS battery is inserted spilled wind energy reaches 912 GWh as opposed to 952 GWh seen earlier without energy storage or DR. The impact of DR is seen in the following way. When the load is shifted through DR with 1 rebound effect ratio, the spilled wind energy decreases by 105 GWh (from 952 GWh to 847 GWh). If both DR and NaS battery are scheduled, wind spill energy reaches 810 GWh as opposed to 847 GWh when only DR is scheduled. If one CAES is inserted, spilled wind energy reaches 655 GWh. By inserting one CAES, and one NaS batetry, spilled wind energy reaches 623 GWh. Scheduling one CAES (but no NaS) and DR, reduces spilled wind energy to 569 GWh. This means 383 GWh reduction of wind spill energy by scheduling CAES and DR as compared to 329 GWh less in spilled wind energy by scheduling CAES and NaS battery. This better overall result in terms of lesser spilled wind energy is achieved with 10% DR with 1 rebound effect energy ratio, but without NaS battery.

The overall decision depends on taking into account the cost issues such as battery investment and operational costs, incentive payments by utility to customers allowing

load reduction, and the cost of utilizing less wind generation and having spilled wind energy from the wind farm operator point of view.

3.3 Conclusion

The amount of spilled wind energy depends on wind power output, load level, generation mix, DR properties, and energy storage characteristics as found in our research. The generation mix by fuel type includes nuclear, coal, and natural gas. Since nuclear generation has the highest capacity factor and the lowest cycling capability, greater amount of nuclear generation results in higher wind power spillage. On the other hand, coal generation also needs to be taken into consideration for spilled wind energy, because coal generation has higher capacity factor and lower cycling capability than gas-fired generation.

Wind spill energy reduction also depends on energy storage and DR characteristics. Energy storage with higher rated power and energy capacity can reduce more of the wind spillage. On the other hand, implementing demand response with higher rebound effect energy ratio results in less wind spillage.

4. Energy Storage for Mitigating Wind Power Forecast Error Impacts

The wind power forecast error is a challenge that requires more reserve in the system. Energy storage units can be used to mitigate wind forecast error by allowing the storage to be charged when actual wind power output is more than the forecasted one and discharged when actual wind power output is less than the forecasted one. An energy storage sizing problem can be solved by signal processing approaches which are based on the concept that the efficient operation of energy storage or conventional units depends on their cycling. This is the advantage of signal processing techniques that extract control signals with appropriate cycling for a specific type of energy storage technology.

Wind power forecast error can be considered as a fluctuating signal that can be decomposed into different components with signal processing approaches. These components are defined based on appropriate cycling of energy storage technologies (e.g., intra-hour, intra-day and slow cycling components) to control the hybrid configuration of energy storage units. The intra-hour and intra-day components are time-varying periodic components that have the total energy of zero in a cycle. These components are suitable to control Sodium Sulfur battery (NaS) and Compressed Air Energy Storage (CAES), respectively. The slow cycling component is supposed to be supplied by conventional generators which are more efficient while operating at high mean generation levels.

The contributions and advantages of the proposed method in this chapter compared with other existing signal processing techniques in [57], [58], [60] are summarized as follows.

- Considering the detailed properties of each energy storage technology: These properties include ramp rate, idle time for CAES to switch between charge and discharge modes, maximum and minimum state of charge, besides efficiency and rated power and energy capacity.
- Choosing a specific wavelet function for DWT: The wavelet function in [60] is chosen based on correlation with the net load signal. Haar wavelet function is

selected in this dissertation because; this step-shape wavelet function results in intra-day components that are constant for a specific duration. This characteristic is convenient to schedule mechanical energy storage units as CAES. DFT and DWT with other non-haar wavelet functions change the control command at every time interval, which is too frequent for a CAES unit to operate.

- Analyzing the impacts of energy storage by different scenarios: Results presented in [57], [58], [60] are based on the concept that energy storage units are required to fully compensate for the wind power forecast error values, even if they are infrequent. This chapter analyzes impacts of different combinations of energy storage units on reducing wind spill, back up energy, and the standard deviation of the residual forecast error signal. Back-up energy is total additional energy provided by thermal or hydro generators to make up for the generation shortage.
- Calculating the service life of NaS: The battery service life is very important in long-term planning. The impact of increasing the number of energy NaS and CAES units on NaS cycle life is investigated in this chapter.
- Considering frequency bias constant: This factor can alleviate the wind power forecast error impacts. It allows small frequency deviation (0.1 Hz) from 60Hz to reduce wind spill and back-up energy. The rest of this chapter is organized as follows: the methodology and the storage sizing algorithm, case study and discussion.

4.1 DFT and DWT Analysis

The DFT analysis changes time domain to frequency domain with a sinusoidal basic function. First the DFT of the signal is derived as shown in Eq. 4-1, and then it is passed through high-pass, band-pass and low-pass filters to get different components. Finally, the resultant components are converted into the time domain using inverse DFT as shown in Eq. 4-2.

$$X_k = \sum_{n=0}^{N-1} x_n . e^{-i 2\pi k n / N}, k \in Z \qquad \text{Eq. 4-1}$$

$$x_n = \frac{1}{N}\sum_{n=0}^{N-1} X_k . e^{i2\pi kn/N}, n \in Z \qquad \text{Eq. 4-2}$$

The DWT changes the signal domain to the time-frequency plane by scaling and shifting the basic wavelet function. The set of basic wavelet functions are defined as Eq. 4-3.

$$\Psi_{j,k,t} = \frac{1}{\sqrt{2^j}} \Psi(\frac{t - k2^j}{2^j}) \qquad \text{Eq. 4-3}$$

Where Ψ is the wavelet function and 2^j is the scaling factor of t, $2^{-j}k$ is the translation in t. The factor $2^{j/2}$ maintains the norm of the wavelet at different scales.

The "haar" wavelet function is described in Eq. 4-4.

$$\Psi_{Haar,t} = \begin{cases} 1, if\ 0 < t < 0.5 \\ -1, if\ 0.5 < t < 1 \\ 0, otherwise \end{cases} \qquad \text{Eq. 4-4}$$

The DWT decomposition with "haar" wavelet function is used among other wavelet functions. Hence, the decomposed signals are shifted and scaled version of "haar" wavelet function, which has step shape and is constant for each half period as shown in Eq. 4-4. This characteristic may be desirable to control a large-scale mechanical energy storage unit with barriers to allow frequent switch of their operating mode. The signal can be represented as shown in Eq. 4-5.

$$f_t = \sum_{j,k} a_{j,k} \Psi_{j,k,t} \qquad \text{Eq. 4-5}$$

Where the two dimensional coefficient $a_{j,k}$ is called DWT of f_t. It is calculated by inner products as shown in Eq. 4-6.

$$a_{j,k} = \left\langle \Psi_{j,k,t}, f_t \right\rangle \qquad \text{Eq. 4-6}$$

The signal is decomposed into approximate and detailed signals as shown in Eq. 4-7.

$$f_t = A_{n,t} + \sum_{j=1}^{n} D_{j,t} \qquad \text{Eq. 4-7}$$

Where,

$A_{n,t}$: approximate signal at level n decomposition at time t

$D_{j,t}$: detailed signal at level j decomposition (j=1,…,n) at time t

n : level of DWT decomposition

4.2 Energy Storage Sizing Algorithm

The difference between wind power and its hour-ahead forecast represents the wind power forecast error as shown in Eq. 4-8.

$$p_{wfe,t} = p_{aw,t} - p_{fw,t}, \forall t \qquad \text{Eq. 4-8}$$

Where,

$p_{wfe,t}$: Wind power forecast error signal at time t

$p_{aw,t}$: Actual wind power signal at time t

$p_{fw,t}$: Forecasted wind power signal at time t

The wind power forecast error is formulated in an area control error (ACE) as expressed in Eq. 4-9. The balancing authority is expected to return the ACE to zero by utilizing its contingency reserves to compensate for the error.

$$\text{ACE} = -(I_a - I_s) + 10\beta(f_a - f_s) \qquad \text{Eq. 4-9}$$

Where,

I_a : Actual interchange in MW

I_s : Scheduled interchange in MW

f_a : Actual system frequency in Hz

f_s : Scheduled system frequency in Hz

β : System frequency bias constant in MW/0.1Hz

The frequency bias constant allows the incorporation of intermittent renewable energy sources into a power system with a small frequency deviation of up to 0.1 Hz. Many balancing authorities take a simple approach and calculate their bias as 1% of their forecasted peak load of the year [111].

The detailed energy storage sizing algorithms for DWT and DFT methods are defined as follows.

4.2.1 Energy Storage Sizing Algorithm Based on DWT

Step1 – Find $p_{wfe,t}$ as described in Eq.4-8.

Step2 – Decompose the $p_{wfe,t}$ using "haar" as a wavelet function to approximate and detailed signals as shown in Eq.4-7. The period of the j^{th} detailed signal is 2^j times the data time resolution. The duration of its constant command is 2^{j-1} times the data time resolution. The approximate signal with n level of decomposition is constant for 2^n times the data time resolution. Hence, if the data time resolution is 5 minutes and the level of DWT decomposition is chosen to be 8, then the approximate signal changes every 21 hours and 20 minutes. This decomposition level keeps the period of detailed signals less than a day. As a result, intra-hour and intra-day components are extracted from detailed signals with 8 level of decomposition.

Step3 – Derive high, medium and low frequency decomposed signals as intra-hour, intra-day and slow cycling components, respectively, as expressed in Eq. 4-10 to Eq. 4-12.

$$p_{hf,t} = \sum_{j=1}^{3} D_{j,t} \quad \text{Eq. 4-10}$$

$$p_{mf,t} = \sum_{j=4}^{8} D_{j,t} \quad \text{Eq. 4-11}$$

$$p_{lf,t} = A_{8,t} \quad \text{Eq. 4-12}$$

The $p_{hf,t}$ is the high frequency or intra-hour component as presented in Eq. 4-10. As shown, it is the summation of 1st to 3rd detailed signals. Hence, it changes every 5 minutes and its period is 40 minutes which is less than an hour. This signal is appropriate to control large-scale batteries, like NaS that has high ramp rates and less energy capacity comparing to CAES. The $p_{mf,t}$ is the medium frequency or intra-day component as defined in Eq. 4-11. This signal changes every 40 minutes and its period is 21 hours and 20 minutes which is less than a day. Hence, it is a good candidate for intra-day component to charge/discharge mechanical large-scale energy storage units as CAES. The $p_{lf,t}$ is the low frequency/slow-cycling component that changes every 21 hours and 20 minutes as shown in Eq. 4-12. This can be easily followed by conventional generators, which also has high mean value.

4.2.2 Energy Storage Sizing Algorithm Based on DFT

Step1 - Find $p_{wfe,t}$ as described in Eq. 4-8.

Step2 - Find the DFT of the $p_{wfe,t}$ to project the signal from time domain to frequency domain by using Eq. 4-1.

Step3 - Use the high pass, band pass and low pass filters, as described in Table 4-1, to extract high, medium and low frequency components. Cut-off frequencies were chosen to match the DWT method. Hence, results of the two methodologies can be compared and the trade-off can be discussed.

Step4 - Take the inverse DFT of decomposed components in the previous step and change them from the frequency domain to the time domain by using Eq. 4-2.

Table 4-1. DFT Methodology Filters

Filter	f_l (mHz)	f_u (mHz)	$1/f_l$ (Hrs:Min)	$1/f_u$ (Hrs:Min)
High Pass	0.208	--	2^4×5min=01:20	--
Band Pass	0.208	0.013	2^4×5min=01:20	2^8×5min=21:20
Low Pass	--	0.013	--	2^8×5min=21:20

4.2.3 Applying Large-Scale Energy Storage Properties

Each energy storage technology has its own operating limits as rated power and energy capacity, efficiency, ramp rate, etc. These characteristics are shown in Table 4-2 for NaS and CAES. In particular, CAES needs at least 20 minutes to remain idle for switching between charging and discharging modes [13].

Table 4-2. Energy Storage Technology Characteristics [12]-[13]

Energy Storage Technology	NaS	CAES
Power Capacity (MW)	50	300
Energy Capacity (MWh)	300	6000
Max Ramp up/down rate (MW/min)	50	18
Efficiency (%)	75	70
Required idle Time to switch mode (min)	---	20
Max state of charge (%)	90	100
Min state of charge (%)	10	0

In the literature, the sizing based on signal processing approach neglects all energy storage characteristics. Hence, the rated power and energy capacity are sized to follow

the decomposed components completely as shown in Eq. 4-13 to Eq. 4-15, respectively, which result in oversized energy storage units that can provide infrequent required power.

$$P = \max(|c_t|) \quad \text{Eq. 4-13}$$

$$SoC_t = \sum_{i=1}^{t} c_i, \forall t \quad \text{Eq. 4-14}$$

$$E = \max(SoC_t) - \min(SoC_t) \quad \text{Eq. 4-15}$$

Where,

c_t : Decomposed component at time t in MW.

P : Rated power capacity in MW.

SoC_t : State of charge at time t in MW.

E : Rated energy capacity in MWh.

Energy storage characteristics, that prevent the storage to closely follow the control signals, are considered. The intra-day component controls CAES operation. NaS battery follows the intra-hour component and also the difference between CAES output and the intra-day component. The detailed steps of the algorithm are described as follows.

Step 1 – Consider medium frequency (intra-day) signal to control the CAES operation as shown in Eq. 4-16.

$$p_t = p_{mf,t}, \forall t \quad \text{Eq. 4-16}$$

Where,

p_t : Energy storage operation at time t in MW.

Step2 – Set t=1 to start scheduling. The initial state of the charge before running the simulation is assumed to be 50% of the full energy capacity.

Step 3 – Operational power limit: the charge/discharge power of any energy storage unit is limited to its rated power capacity.

$$if\left|p_t\right| > P_r N, then, p_t = sign(p_t) P_r N \quad \text{Eq. 4-17}$$

Where,

P_r : Rated energy storage power capacity.

N : Number of energy storage units.

Step 4 – ramp rate limit: when t>1.

$$r_t = (p_t - p_{t-1}) / \Delta t \quad \text{Eq. 4-18}$$

$$if\left|r_t\right| > R_r N, then, p_t = p_t + sign(r_t) R_r N \quad \text{Eq. 4-19}$$

Where,

r_t : Energy storage ramp rate at time t in MW/min.

R_r : Rated ramp rate in MW/min.

Step 5 – Remain idle for switching between charging/discharging modes: (this is only applicable to CAES)

$$ifp_t p_{t-1} < 0, then, p_k = 0, k \in [t, t + idletime] \quad \text{Eq. 4-20}$$

Step 6 – State of the charge limit:

$$SoC_t = \begin{cases} (p_t \eta \Delta t) / E_r + SoC_{t-1}, ifp_t > 0 \\ (p_t \Delta t) / E_r + SoC_{t-1}, ifp_t < 0 \end{cases} \quad \text{Eq. 4-21}$$

$$ifSoC_t > SoC_{\max}, then$$
$$SoC_t = SoC_{\max}, p_t = (SoC_t - SoC_{t-1}) / (\eta \Delta t) \quad \text{Eq. 4-22}$$

$$if SoC_t < SoC_{\min}, then$$
$$SoC_t = SoC_{\min}, p_t = (SoC_t - SoC_{t-1}) / \Delta t \quad \text{Eq. 4-23}$$

Where,

$SoC_{\min}$: Minimum state of charge in %.

$SoC_{\max}$: Maximum state of charge in %.

E_r : Rated energy capacity in MWh.

η : Efficiency in %

Step 7 – Check if the simulation has reached the end:

If t<T, then, t=t+1, go to step 3, else, $p_{C,t} = p_t, \forall t$ and go to step8.

Where,

T : Whole period of simulation.

$p_{C,t}$: CAES operation at time t in MW.

Step 8 – NaS battery is supposed to provide the high frequency (intra-hour) component and also the difference between CAES operation and the medium frequency component as shown in Eq. 4-24.

$$p_t = p_{hf,t} + (p_{mf,t} - p_{C,t}), \forall t \quad \text{Eq. 4-24}$$

Where,

p_t : NaS control signal at time t in MW.

Step 9-12– This is the same as steps 2 to 6 except for step 5.

Step 13 – Check if the simulation has reached the end:

If t<T, then, t=t+1, go to step 9, else, $p_{N,t} = p_t, \forall t$ and go to step14. Where,

$p_{N,t}$: NaS operation at time t in MW.

Step 14 – Calculating the wind spill and back-up energy: The residual forecast error signal is defined in Eq.4-25. It is the difference between summation of high and medium frequency components with the summation of NaS and CAES operation. The wind spill and back-up energy are defined as positive and negative parts of this signal, respectively as shown in Eq. 4-26 to Eq. 4-27.

$$p_{r,t} = p_{hf,t} + p_{mf,t} - (p_{N,t} + p_{C,t}) \quad \text{Eq. 4-25}$$

$$p_{ws,t} = (|p_{r,t}| + p_{r,t})/2 \quad \text{Eq. 4-26}$$

$$p_{rs,t} = (|p_{r,t}| - p_{r,t})/2 \quad \text{Eq. 4-27}$$

Where,

$p_{r,t}$: Residual power at time t in MW.

$p_{ws,t}$: Wind spill power at time t in MW.

$p_{rs,t}$: Back-up power at time t in MW.

4.3 Battery Life Cycle Analysis

When batteries are used to mitigate renewable generation fluctuations and forecast errors, these have to cycle frequently to keep up with renewable ramp rates and mitigate the forecast error. Battery service life depends on cycles at various depths of discharge (DOD). Hence studying the number of cycles at each DOD is important when considering batteries as a solution to mitigate wind power forecast error impacts. Cycle counting has different methods as described in American Society for Testing and Materials (ASTM) - E 104985 [112]. Rain-flow cycle counting is used to count the life cycle of NaS battery, which was first proposed by Downing [113]. The result of this

approach is the number of cycles at each depth of discharge which includes complete cycles and partial cycles.

The rain-flow cycle counting is used in fatigue analysis. This algorithm is summarized in the following six steps.

Let X denotes the range under consideration; Y, previous range adjacent to X; and S, starting point in the history.

Step1) Read next peak or valley. If out of data, go to Step 6.

Step2) If, there are less than three points, go to Step 1. Form ranges X and Y using the three most recent peaks and valleys that have not been discarded.

Step3) Compare the absolute values of ranges X and Y.

a) If $X < Y$, go to Step 1.
b) If $X \geq Y$, go to Step 4.

Step4) If, the range of Y contains the starting point S, go to Step 5; otherwise, count range Y as one cycle; discard the peak and valley of Y; and go to Step 2.

Step5) Count range Y as one-half cycle; discard the first point (peak or valley) in range Y; move the starting point to the second point in range Y; and go to Step 2.

Step6) Count each range that has not been previously counted as one-half cycle.

The number of cycles to failure at each DOD for NaS battery is depicted in Fig. 4-1.

To study the impact of cycles on battery service life, the DOD is divided into m intervals. Then, the number of cycles in a year for each range of DOD is extracted. Finally, the battery life-time in years is calculated as follows [114].

$$Life_{NaS} = 1 / \sum_{i=1}^{m} {}^{N_i}\!/_{CF_i} \qquad \text{Eq. 4-28}$$

Where,

$Life_{NaS}$: NaS battery Life-time in years.

N_i : Number of Cycles at each DOD.

CF_i : Number of Cycles to Failure at each DOD.

m : Number of DOD ranges.

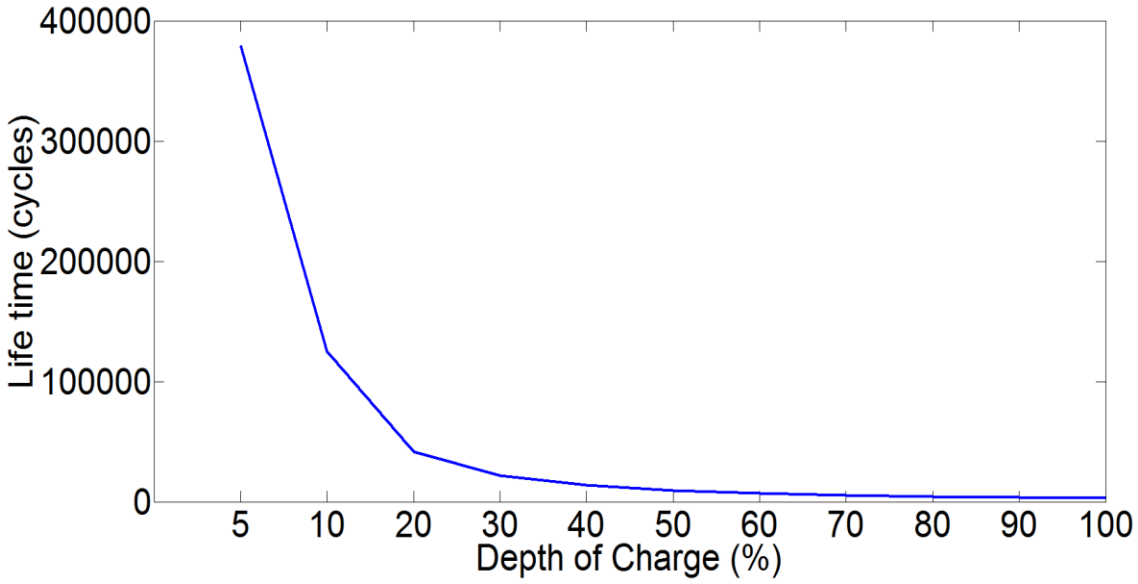

Fig. 4-1. NaS Battery Number of Cycles to Failure with Respect to DOD.[115]

4.4 Case Study and Discussion

The wind power forecast error is determined by the actual and hour-ahead wind power forecast data with 5-minute intervals in the BPA area in 2013 [54]. The BPA installed wind capacity was 4.5GW in 2013. The wind power forecast error signal is shown in Fig. 4-2 for the whole year of 2013, which oscillates between 1.76 and -1.32 GW. The normalized histogram of this signal and the normal distribution function that fits, are depicted in Fig. 4-3. The wind power forecast error signal characteristics are summarized in Table 4-3. As shown, the standard deviation of the wind power forecast error signal is 216 MW with the mean value of 28 MW. Hence by considering the three-sigma rule, 99% of the time the forecast error is between 676 MW and -620 MW.

Table 4-3. Wind Power Forecast Error Signal Characteristics

Max (MW)	MIN (MW)	Max ramp up/down (MW/5min)	Mean (MW)	Sigma (MW)
1763	-1316	805/-875	28	216

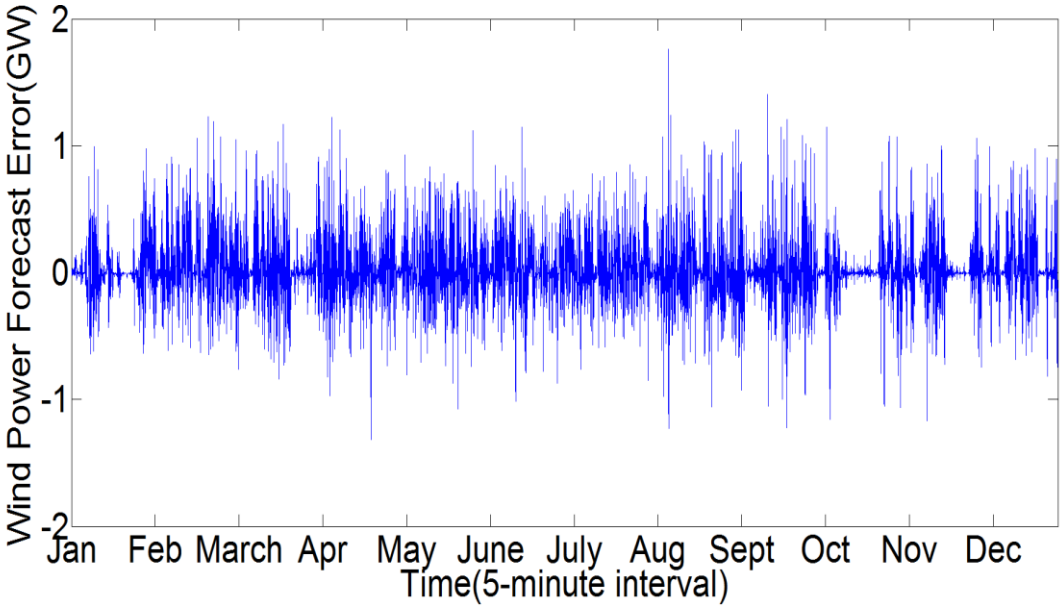

Fig. 4-2. The BPA Wind Power Forecast Error of BPA for 2013.

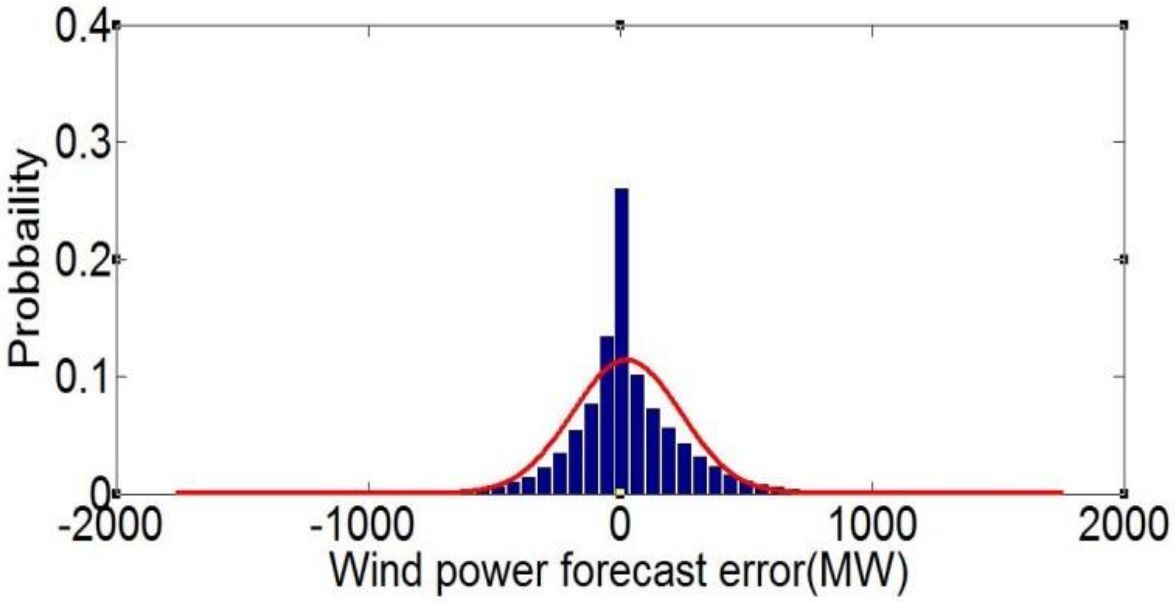

Fig. 4-3. BPA Wind Power Forecast Error Histogram for 2013

The intra-hour, intra-day and slow-cycling components of the wind power forecast error signals are extracted and shown in Fig. 4-4 and Fig. 4-10 by DWT and DFT, respectively. The difference between DFT and DWT methodologies is the shape of the decomposed components as shown in Fig. 4-5 to Fig 4-10.

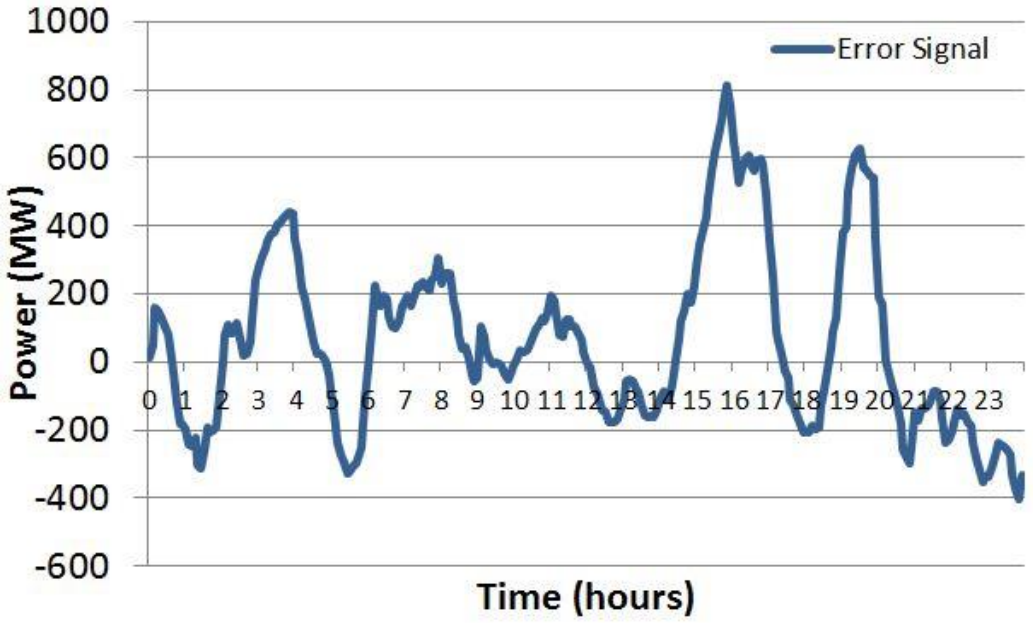

Fig. 4-4. Wind Power Forecast Error Signal for a Day in 2013.

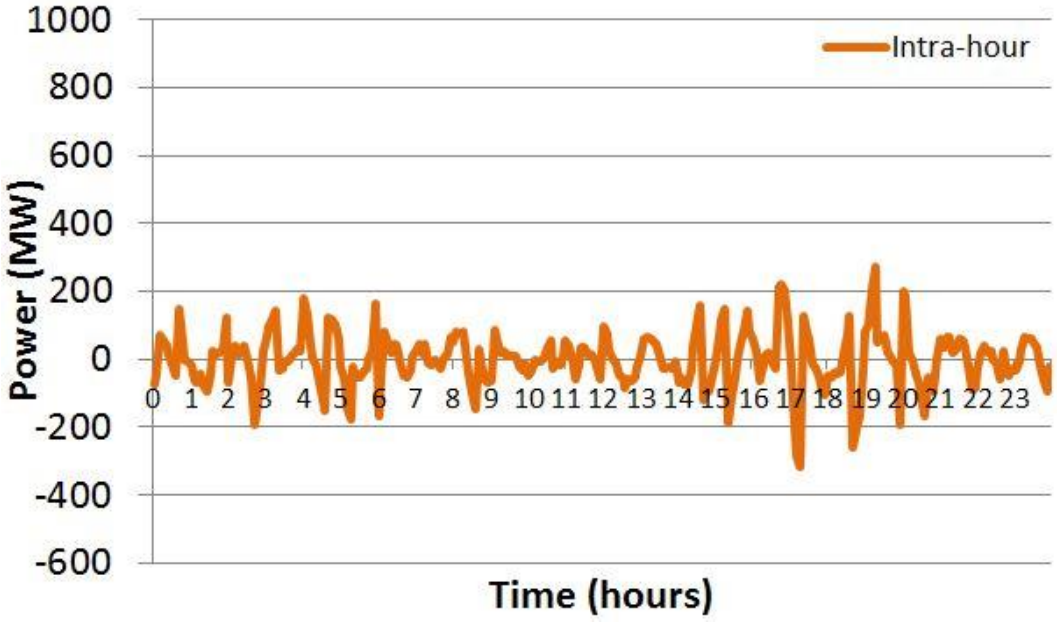

Fig. 4-5. DWT intra-hour component of the forecast error signal for a Day in 2013

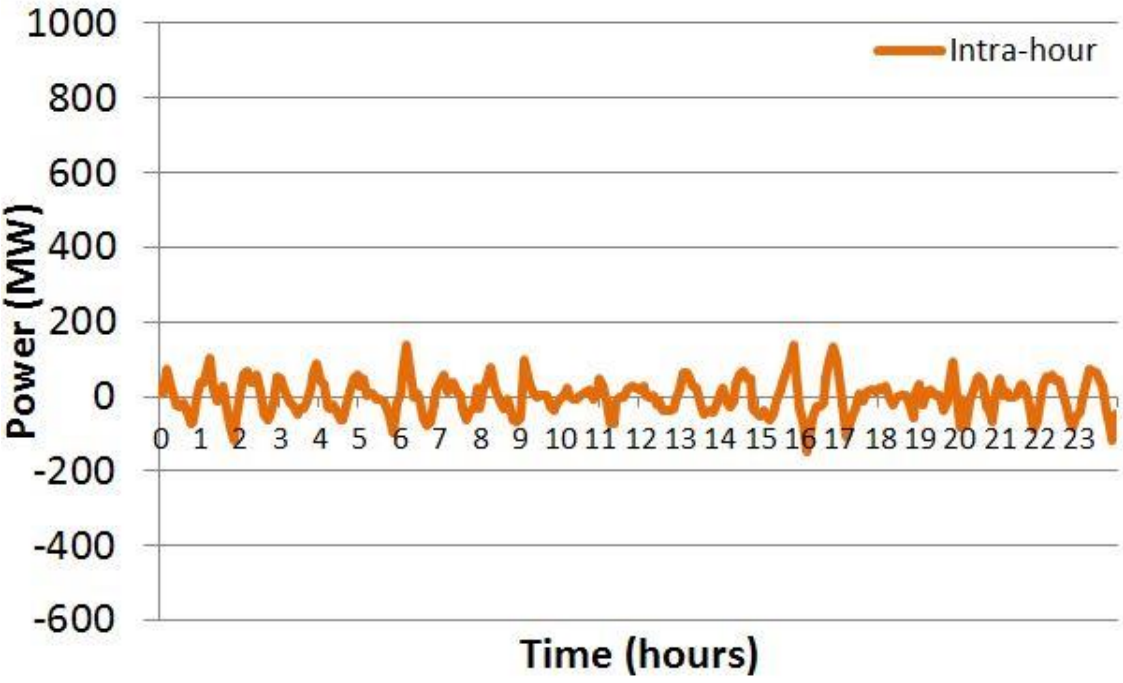

Fig. 4-6. . DFT intra-hour component of the forecast error signal for a Day in 2013

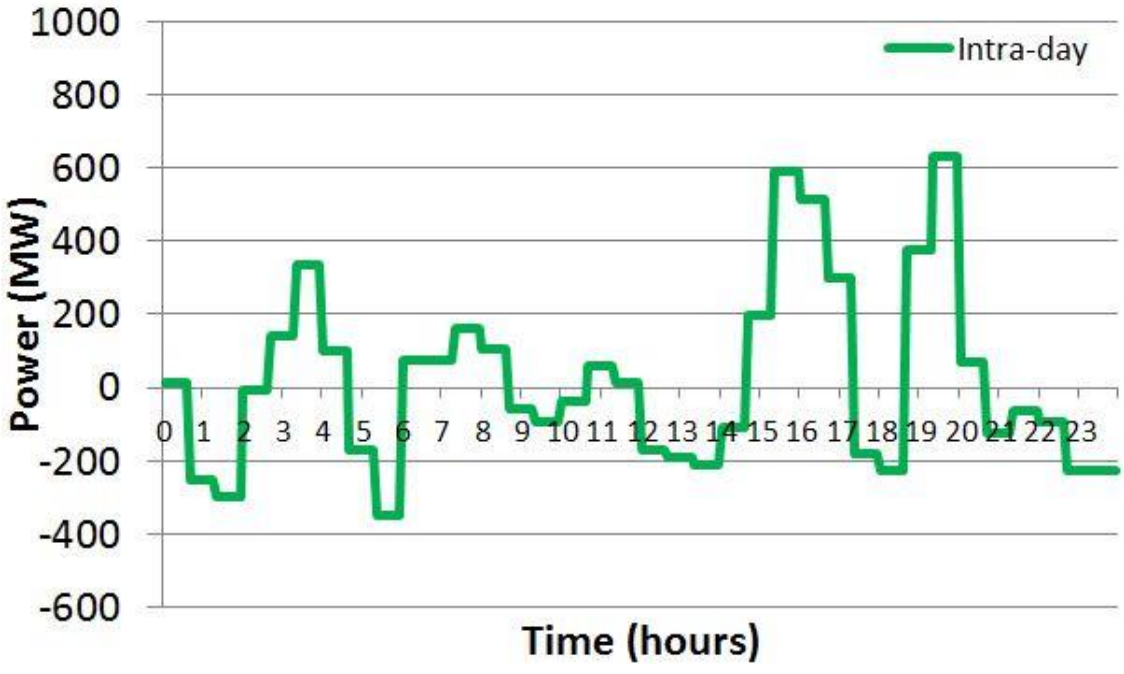

Fig. 4-7. DWT intra-day component of the forecast error signal for a Day in 2013

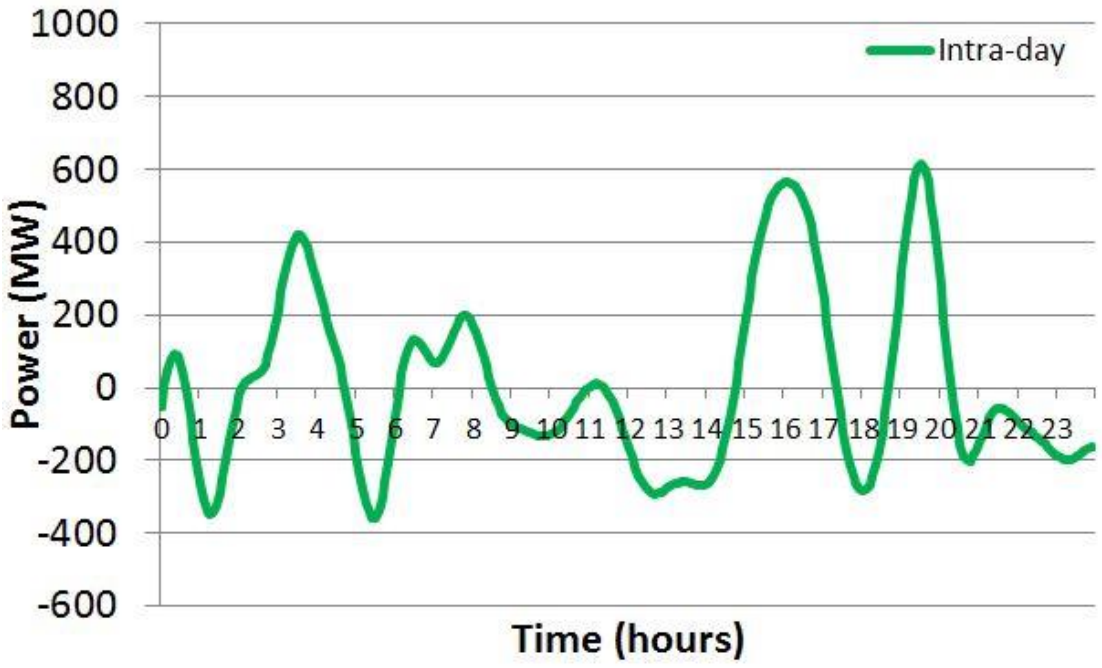

Fig. 4-8. DFT intra-day component of the forecast error signal for a Day in 2013

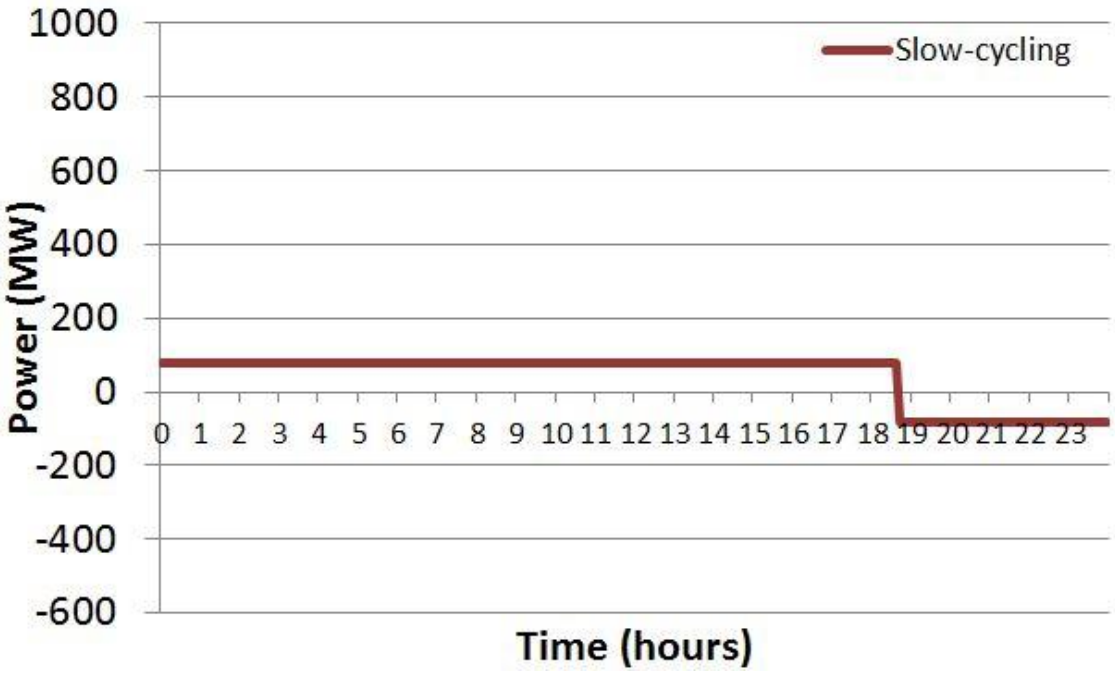

Fig. 4-9. DWT slow cycling component of the forecast error signal for a Day in 2013

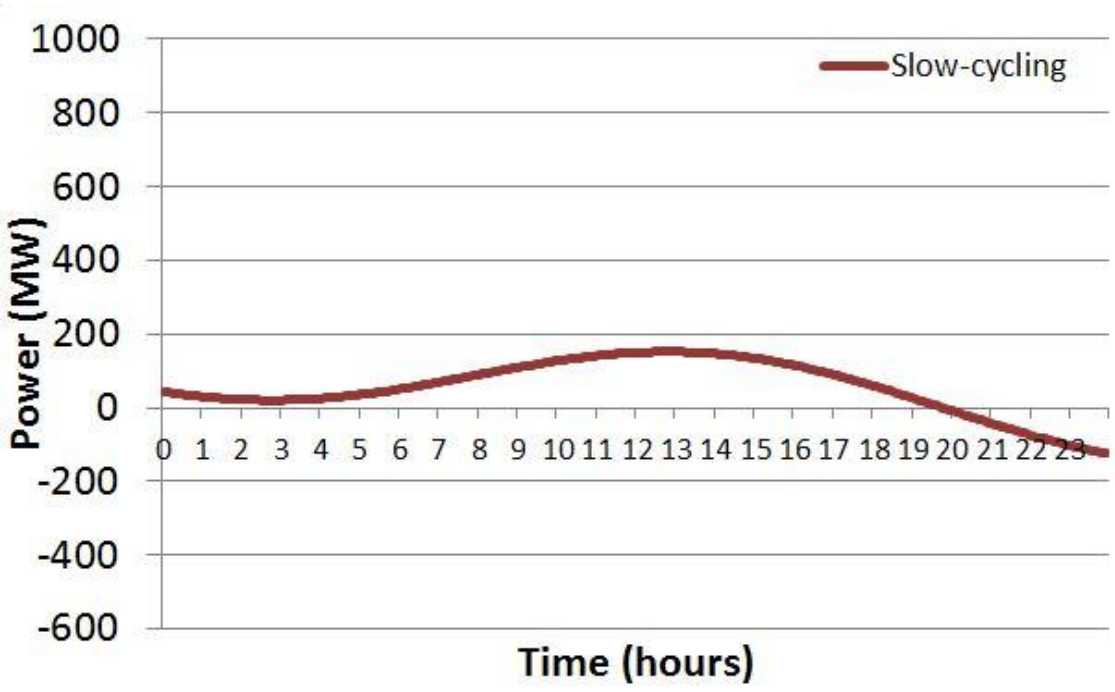

Fig. 4-10. DFT slow cyling component of the forecast error signal for a Day n 2013

The properties of decomposed components are shown in Table 4-4. As shown, the mean values of the intra-hour and intra-day components are zero, which is desirable to control energy storage. The mean of the slow-cycling component for both methods is 28, which is equal to the wind power forecast error mean shown in Table 4-3.

According to the three sigma rule, 99% of the time the value of the intra-day component is between ±573 MW for DWT method and ±546 MW for DFT method. According to the CAES unit described in Table 3-2, the rated power of one unit is 300MW. Hence for running the described algorithm, two units are required neglecting the energy storage operational limits. Also, 99% of the time the value of intra-hour component is between ±201 MW for the DWT method and ±138 MW for the DFT method. Hence, four and three 50MW NaS are required for DWT and DFT methods, respectively, while neglecting the operational limits and only based on standard deviation analysis.

Table 4-4. DWT and DFT Component Characteristics

Method	Component	Max (MW)	MIN (MW)	Max ramp up/down (MW/5min)	M (MW)	Σ (MW)
DWT	Intra-hour	912	-779	966/-936	0	67
	Intra-day	964	-1065	987/-1394	0	191
	Slow-cycling	275	-153	296/-312	28	74
DFT	Intra-hour	978	-572	778/-749	0	46
	Intra-day	972	-1048	207/-160	0	182
	Slow-cycling	382	-303	6/-6	28	106

In the literature, the required energy storage power capacity has been derived from maximum absolute value of the decomposed components. While energy capacity is sized to satisfy that at each interval, the state of charge remains positive as stated. Table 4-5 shows results based on the literature approach that fully compensates the decomposed components. As shown in Table 4-5, twenty 50 MW NaS units are required to follow the intra-hour component. Also, four 300 MW CAES units are required to follow the intra-day component. This approach results in oversizing energy storage units while neglecting all of their characteristics. Hence, these over-sized energy storage units cannot even fully compensate the control signals due to operational barriers.

Table 4-5. DWT and DFT Sizing Results Based on Literature Approach

Method	Component	Power (MW)	Energy (MWh)
DWT	Intra-hour	912	279
	Intra-day	1,065	4,776
DFT	Intra-hour	978	187
	Intra-day	1,048	2,265

The proposed approach study the energy storage sizing by evaluating the impacts of different combination of 50 MW NaS and 300 MW CAES units on reducing wind spill and required back-up energy. Hence, 25 different combinations of CAES and NaS battery units are considered as scenarios. The standard deviation, spilled wind energy and required back-up energy are depicted in Fig. 4-11 to Fig. 4-13. The DWT and DFT results are shown in the transparent and colored surfaces, respectively.

Due to more flexible components of DFT comparing to DWT, results related to DFT show better performance than DWT results. As shown in Fig. 4-11, by increasing the number of energy storage units, the standard deviation decreases from 202 MW to 70 MW for DWT by implementing four NaS and CAES units. It also decreases from 187 MW to 66 MW for DFT by implementing four NaS and CAES units. As shown, the standard deviation decrease becomes less by increasing energy storage units and be surface becomes flat eventually.

The wind spill and back-up energy are calculated from the residual wind power forecast error signal after scheduling storage units. The wind spill energy shown in Fig. 4-12 reduces from 600 GWh to 11 GWh for the DWT method by increasing the number of energy storage units. It also reaches 4 GWh from 600 GWh for the DFT method by increasing the number of energy storage units. The impact of energy storage on decreasing the required back-up energy is shown in Fig. 4-13.

The required back-up energy decreases from 600 GWh to 198 GWh for the DWT method and reduces to 178 GWh for the DFT approach. The reason why back-up energy reduction is less than wind spill energy reduction is because of considering energy storage efficiency. Hence, the storage is able to charge the excess wind energy but since its efficiency is not 100% it cannot discharge as required. As shown, the slope of the surfaces decreases and becomes flat by increasing the number of energy storage units.

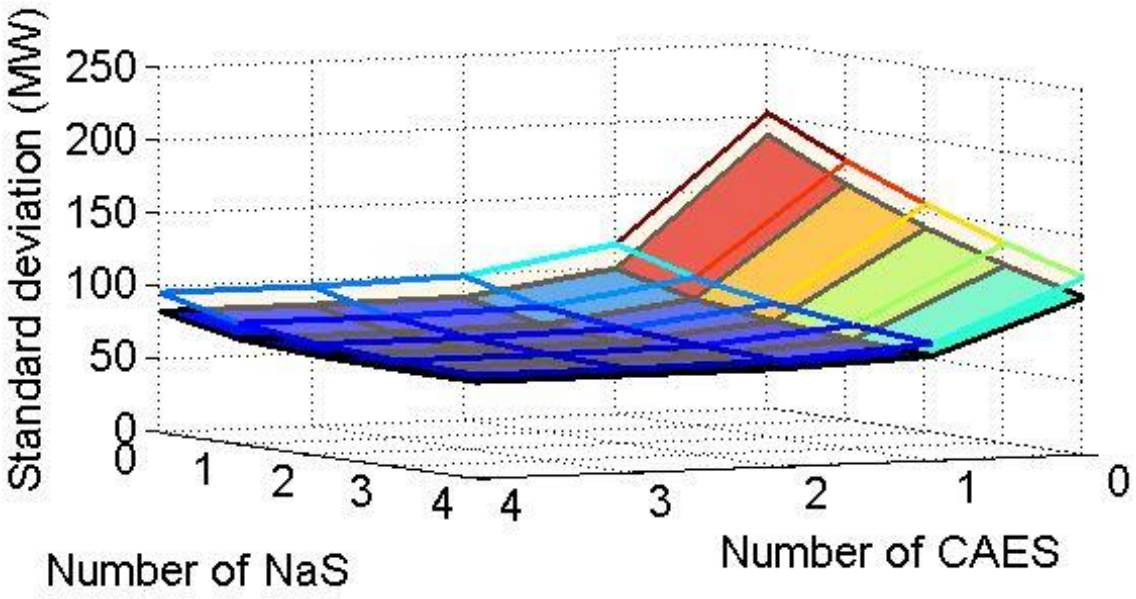

Fig. 4-11. Standard Deviation of Residual Forecast Error by DWT and DFT

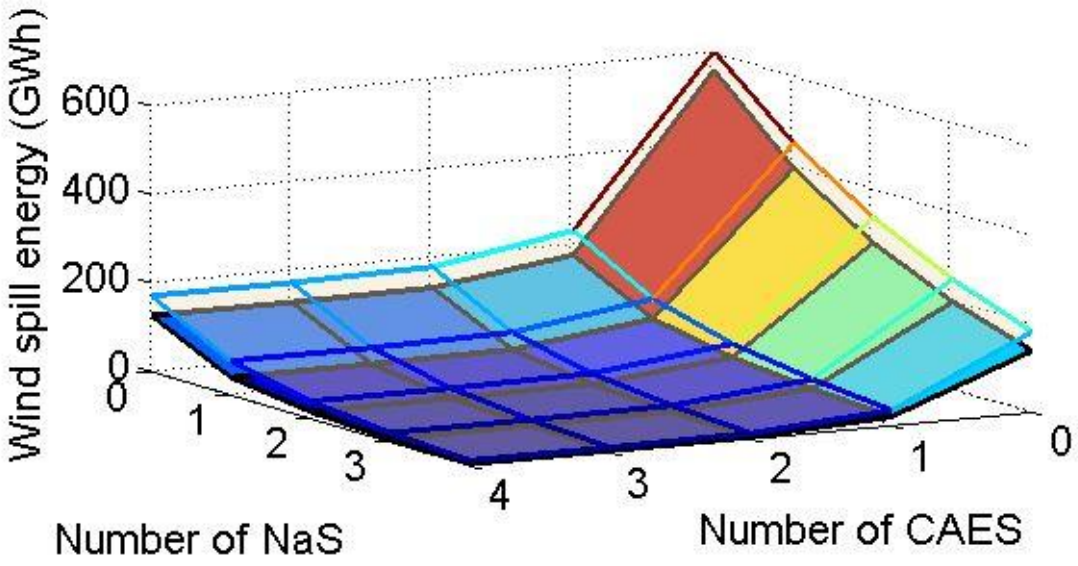

Fig. 4-12. Wind Spill Energy by DWT and DFT Methods

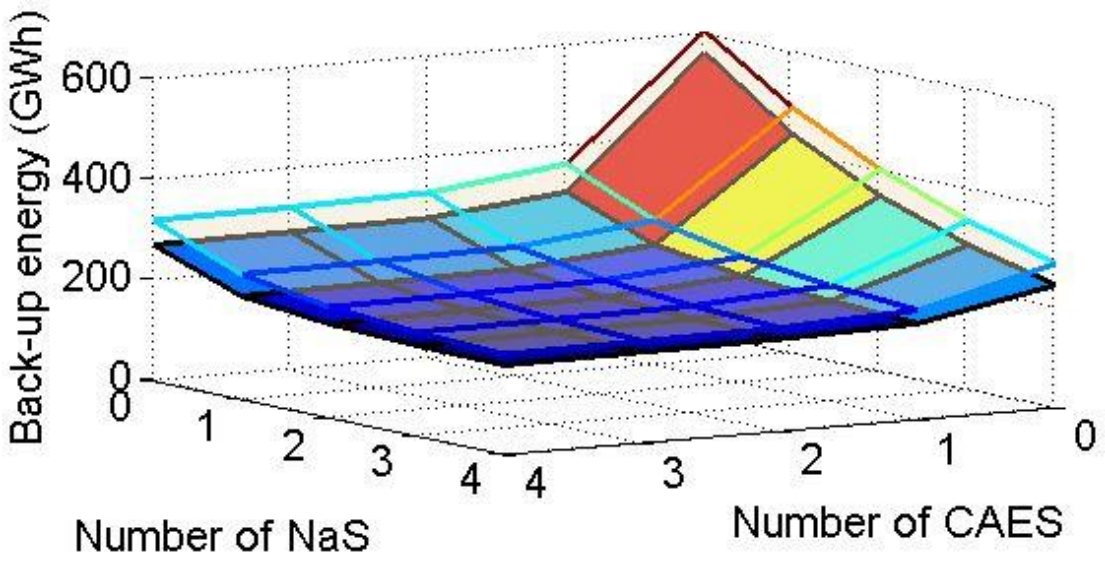

Fig. 4-13. Back-up Energy by DWT and DFT Methods

The impact of energy storage size on the NaS battery life-time is analyzed and shown in Table 4-6. The cycle counting and battery life-time estimation is very important for planning large-scale batteries. Results show that, by increasing the number of NaS battery units, their life-time increases. This is due to increasing the energy capacity of the total batteries. Hence, there is less number of cycles at each range of Depth of Discharge. This number increases from 20 years to 28 years for DWT, and 25 years to 32 years for the DFT method by increasing number of NaS battery units from one to four while operating one CAES units. As one can observe from Table 4-6, the NaS battery lifetime for DWT method is less than DFT method.

With an increasing number of CAES, NaS battery life-time increases. The NaS battery life-time increases by CAES contribution which can follow the intra-day component. NaS battery life-time increases from 20 years to 30 years for DWT and 25 years to 35 years for DFT, while increasing the CAES units from zero to four and NaS units from one to four. This result is very beneficial for calculating the net present value of battery investment for a long-time project by knowing the number of battery replacements during the whole project.

Table 4-6. NaS life-time in years by DFT and DWT methods

		1 CAES	2 CAES	3 CAES	4 CAES
DWT	1 NaS	20.65	23.29	23.63	23.64
	2 NaS	23.62	26.27	26.72	26.72
	3 NaS	26.17	28.73	29.14	29.15
	4 NaS	28.01	30.18	30.55	30.50
DFT	1 NaS	25.40	28.64	29.02	29.02
	2 NaS	28.89	32.71	33.19	33.29
	3 NaS	30.78	34.32	34.75	34.76
	4 NaS	32.31	35.08	35.34	35.37

The impact of considering 100 MW frequency bias constant on reducing the wind power forecast error impacts are shown in Fig. 4-14 to Fig. 4-16. This allowable mismatch is considered for the residual of wind power forecast error after implementing energy storage units. As shown in Fig. 4-14, the standard deviation of wind power forecast error without implementing energy storage is 145 MW for DWT and 131 MW for DFT, which was about 200 MW before considering frequency bias constant. It will reduce to 48 MW for DWT and 46 MW for DFT by implementing four CAES and NaS units.

As shown in Fig. 4-15, wind spill energy without energy storage is 320 GWh for DWT and 275 GWh for DFT method. As shown in Fig. 4-16, the required back-up energy considering frequency bias constant is 300 GWh for DWT and 267 GWh for DFT. Hence, by considering the frequency bias constant, wind spill and required back-up energy decreases about 300 GWh for the no-storage case.

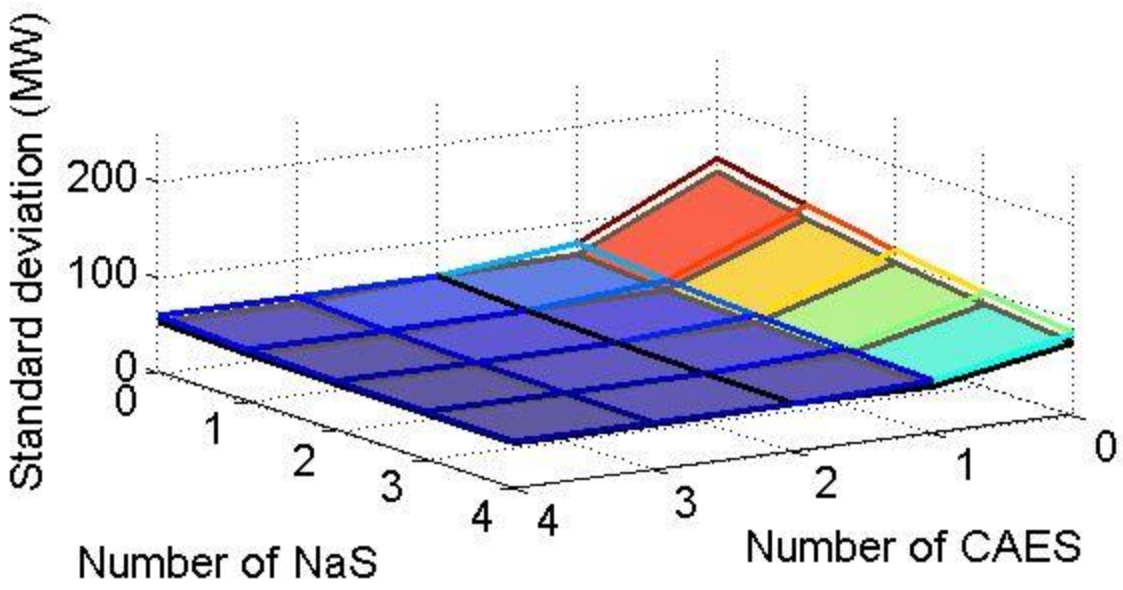

Fig. 4-14. Standard deviation of the residual forecast error considering 100 MW bias for DWT and DFT

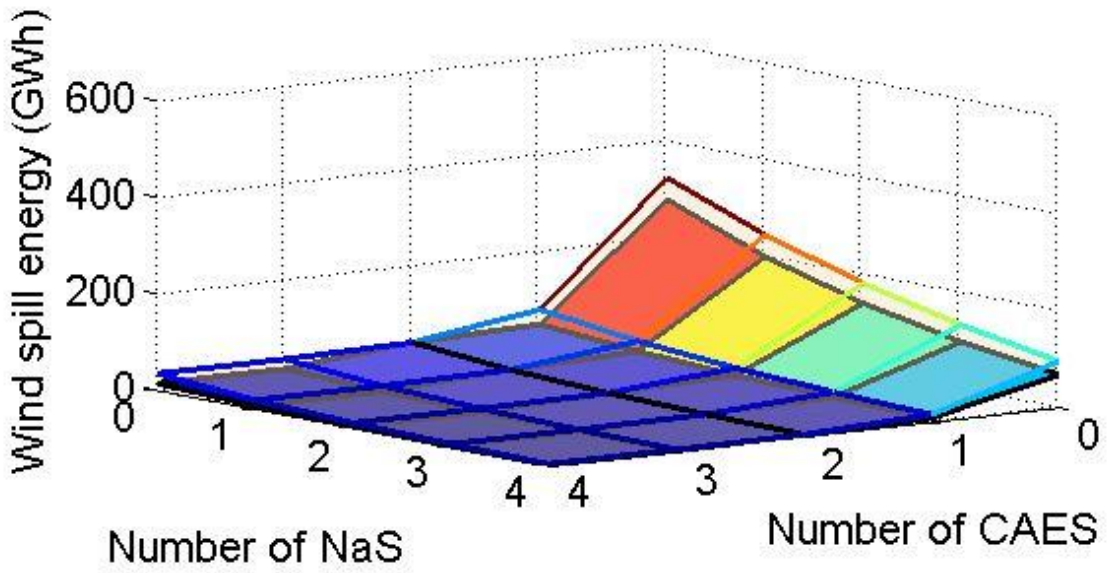

Fig. 4-15. Wind spill energy considering 100 MW bias for DWT and DFT

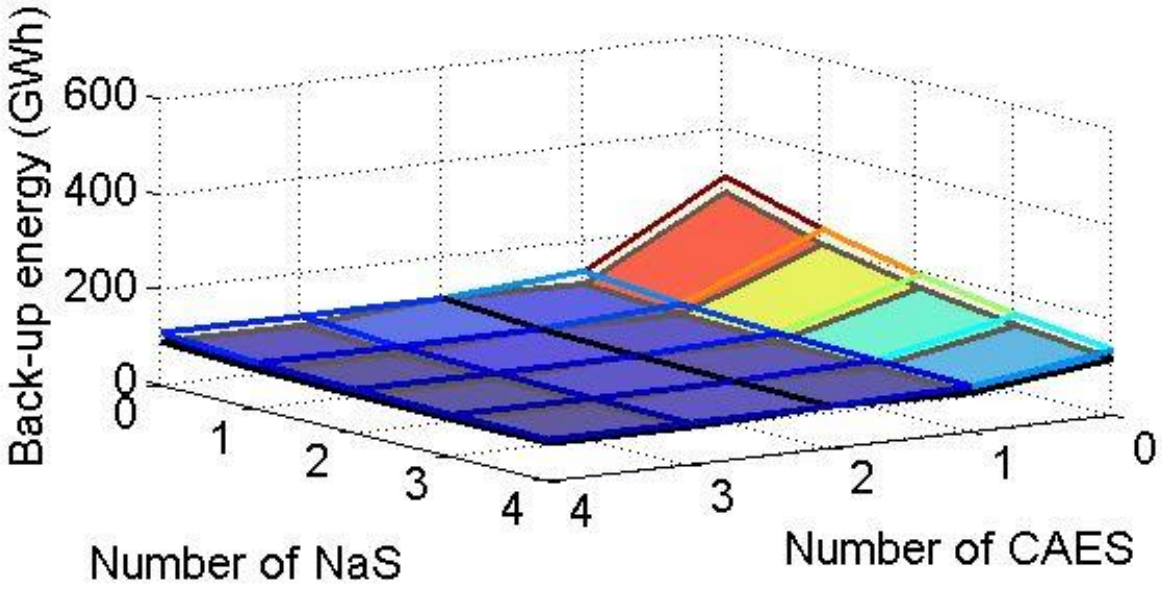

Fig. 4-16. Back-up energy considering 100 MW bias for DWT and DFT

4.5 Conclusion

This research proposes and compares two signal processing methods (based on DFT and DWT) to schedule the hybrid configuration of energy storage technologies (e.g., NaS battery and CAES) and conventional generators. The defined DWT method results in step-shape components, which are more appropriate for controlling large-scale mechanical energy storage units that cannot change their output frequently. Hence, scheduling based on DWT results in more spilled wind energy and requires more back-up energy comparing to DFT method that varies every interval.

The proposed approach is based on analyzing impacts of increasing the number of energy storage units on reducing spilled wind energy and the required back-up energy. Also, the standard deviation of the residual wind power forecast signal is studied, which is an important factor for planning the additional system flexibility required. This approach avoids oversizing the required energy storage by implementing different combinations of

energy storage units and analyzing their impacts. Frequency bias constant is considered to reduce the final wind spill and needed back-up energy.

The detailed properties of CAES and NaS units, including efficiency, rated power and energy capacity, DoD (only applied to NaS), required idle time for switching between charging and discharging modes (only applied to CAES) are considered. NaS battery service life depends on the cycles at each DoD. The NaS battery life-time increases by adding more NaS and CAES units.

The information provided is beneficial for investors in energy storage and wind sectors. The overall energy storage sizing depends on the economic issues of energy storage operation, investment costs, and wind production tax credit in addition to analyzing the technical issues.

5. Mitigating Spilled Wind Energy and Forecast Error by Energy Storage

Among different challenges related to utilities with high wind energy penetration levels, non-correlation between wind and load profiles, and wind power forecast errors have been discussed separately in previous chapters. Chapter 3 proposed an optimization problem modeling various scenarios for energy storage technologies and demand response programs to minimize spilled wind energy due to the non-correlation between wind and load profiles [119]. That analysis was based on using actual wind generation for scheduling energy storage, demand response, and generation units, while neglecting the wind power forecast error. Chapter 4 presented a method based on signal processing techniques (e.g. Discrete Wavelet Transform (DWT)) to mitigate the error between hour-ahead wind power forecast and actual wind power by scheduling Sodium Sulfur (NaS) battery and compressed air energy storage (CAES) [120]. That study neglected differences between day-ahead and hour-ahead wind power forecasts, while only using energy storage technologies for the application of mitigating wind power forecast error.

The algorithm presented in this chapter is the upgraded and expanded version of what has been presented in [119], and [120], while using optimization approach in [119] to schedule energy storage technologies day-ahead and then update their schedules in hour-ahead and 5 minutes ahead by proposed signal processing technique [120]. Contributions and novelties of this chapter are summarized as follows.

- Present an algorithm for optimal operation of energy storage that addresses both applications – minimizing spilled wind energy and mitigating wind power forecast errors, in three steps. First, schedule energy storage day-ahead to minimize spilled wind energy due to non-correlation between load profile and day-ahead wind power forecast range by MILP. Then, update energy storage operation by DWT to mitigate errors between day-ahead wind power forecast, hour-ahead wind power forecast, and actual wind power in two steps.

- Compare final spilled wind energy and back-up generation for different energy storage units when their operation is not updated, with the case that their operation is updated based on the proposed algorithm.
- Compare final spilled wind energy and back-up generation when different day-ahead wind power forecast scenarios (e.g., maximum, average, and minimum values) are used to schedule energy storage units for day-ahead operation.

The rest of the chapter is organized as follows. Section 5.1 describes the scheduling algorithm. Case studies and conclusion are presented in Section 5.2 and Section 5.3, respectively. Section 5.4 discusses the convexity of the proposed mixed integer linear programming.

5.1. Energy Storage Scheduling Algorithm

The algorithm to schedule energy storage units for both applications of spilled wind energy and wind power forecast error is presented in three steps as shown in Fig. 5-1. As shown these three steps are defined in day-ahead, hour-ahead and 5 minutes ahead scheduling, which aligns well with electricity market that dispatch energy in day-ahead, hour-ahead, and 5 minutes ahead markets. In the first step, the optimization problem used for scheduling energy storage units is a simplified version of the one studied in Chapter 3. The algorithm used in steps two and three are based on the algorithm presented in Chapter 4.

The algorithm runs for each day, first energy storage units are scheduled based on day-ahead wind power forecast by MILP to minimize spilled wind energy. Then, their scheduling is updated in two steps using DWT based on the error between day-ahead, and hour-ahead wind power forecast, and actual wind power. The input for each step besides related wind power is the energy storage operation. Three steps of this algorithm are defined in details as follows.

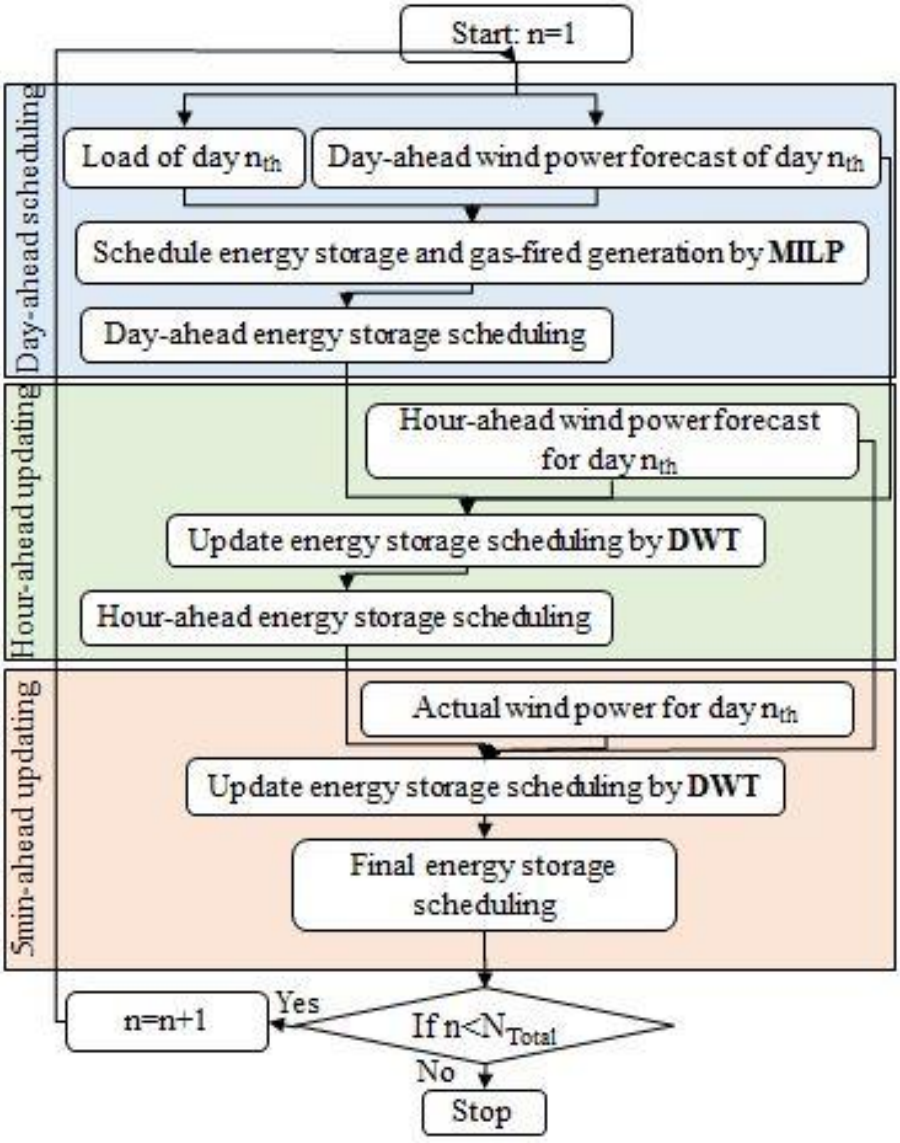

Fig. 5-1. Energy storage scheduling algorithm

5.1.1. Step 1) Day-ahead scheduling:

The whole system in this study includes fossil-fuel (gas-fired) generation, must-run or inflexible generation (power plants without cycling capability generating a constant power), wind farms, NaS battery, CAES, and load. As mentioned before, this is a simplified version of the optimization problem presented in Chapter 3 which is based on the model presented in [119]. The mixed integer linear programming (MILP) is defined by following constraints.

The mixed integer linear programming (MILP) defined in Chapter 3 for modeling energy storage units, and gas-fired generation is used in this research with following six differences.

1) Energy constraint: day-ahead wind power forecast is used instead of actual wind power in the power balance constraint. This constraint ensures that the total generation, equals to the total load, at each time interval as shown in Eq. 5-1.

$$p_{l,t} = P_{ig} + p_{dwf,t} + p_{fg,t} + p_{Cdchg,t} - p_{Cchg,t} + p_{Ndchg,t} - p_{Nchg,t} + p_{ws,t}, \forall t \quad \text{Eq. 5-1}$$

Where,

$p_{dwf,t}$: Continuous variable denoting the day-ahead wind power forecast at time t (MW).

$p_{l,t}$: Continuous variable denoting the quantity of load at time t (MW).

$p_{ws,t}$: Continuous variable denoting the wind spill power at time t (MW).

$p_{Cchg,t}$: Continuous variable denoting the CAES charging power at time t (MW).

$p_{Cdchg,t}$: Continuous variable denoting the CAES discharging power at time t (MW).

$p_{Nchg,t}$: Continuous variable denoting the NaS battery charging power at time t (MW).

$p_{Ndchg,t}$: Continuous variable denoting the NaS battery discharging power at time t (MW).

$p_{fg,t}$: Continuous variable denoting the quantity of fossil-fuel (gas fired) generation at time t (MW).

P_{ig} : Inflexible generation (MW).

2) The system is simulated for a month by running each day separately, while in Chapter 3 each week was simulated individually. The other difference is related to the time interval which is every 5 minutes in this chapter, while it was every 15 minutes in chapter 3.
3) The modeling constraints related to demand response and rebound effect is neglected in this chapter and load is assumed to be an inelastic load that has no contract to change its profile. It is important to note that, similar to Chapter 3, load forecast error is also neglected.
4) The generation unit in this chapter is an equivalent fossil-fuel (gas fired) generation unit and an inflexible generation providing constant power. This generation modeling is the simplified version of the one presented in Chapter 3 which includes nuclear, coal, and gas fired generation units. The equivalent fossil- fuel generation unit is modeled by Eq. 5-2 to Eq. 5-7.

Equivalent fossil-fuel unit power is limited to its minimum and maximum as shown in Eq.5-2.

$$P_{fg}^{\min} u_{th,t} \le p_{fg,t} \le P_{fg}^{\max} u_{fg,t}, \forall t \qquad \text{Eq. 5-2}$$

Where,

$p_{fg,t}$: Continuous variable denoting fossil-fuel unit generation at time t (MW).

$u_{fg,t}$: Binary variable denoting whether fossil-fuel unit is on or off at time t; 1 if on, 0 otherwise.

$P_{fg}^{\min}$: Minimum generation of fossil-fuel unit (MW).

$P_{fg}^{\max}$: Maximum generation of fossil-fuel unit (MW).

The relationship among binary variables for the equivalent fossil-fuel unit model denoting the starting and stopping indicators is shown in Eq. 5-3. While Eq. 5-4 shows that starting or stopping indicators happen once at a time.

$$y_{fg,t} - z_{fg,t} = u_{fg,t} - u_{fg,t-1}, t > 1 \quad \text{Eq. 5-3}$$

$$y_{fg,t} + z_{fg,t} \leq 1, \forall t \quad \text{Eq. 5-4}$$

Where,

$u_{fg,t}$: Binary variable denoting whether fossil-fuel unit is on or off at time t; 1 if on, 0 otherwise.

$y_{fg,t}$: Binary variable denoting the starting indicator of fossil-fuel unit start up at time t; if $u_{fg,t} = 1$ and $u_{fg,t-1} = 0$, then $y_{fg,t} = 1$,

$z_{fg,t}$: Binary variable denoting the stopping indicator of fossil-fuel unit at time t; if $u_{fg,t} = 0$ and $u_{fg,t-1} = 1$, then $z_{fg,t} = 1$,

The equivalent fossil-fuel unit ramp rate constraint is shown in Eq. 5-5.

$$-dP_{fg} \leq (p_{fg,t} - p_{fg,t-1}) / \Delta t \leq dP_{fg}, \forall t \quad \text{Eq. 5-5}$$

Where,

dP_{fg} : Fossil-fuel unit ramp rate limit (MW/min).

The equivalent fossil-fuel unit minimum up time constraint is stated in Eq. 5-6.

$$\sum_{t'=t}^{t+T_{fg,up}^{\min}-1} u_{fg,t'} \geq T_{fg,up}^{\min} y_{fg,t}, \forall t \quad \text{Eq. 5-6}$$

Where,

$T_{fg,up}^{\min}$: Fossil-fuel unit minimum up time (min).

The equivalent fossil-fuel unit minimum down time constraint is shown in Eq. 5-7.

$$\sum_{t'=t}^{t+T_{fg,dn}^{\min}-1}(1-u_{fg,t'}) \geq T_{fg,dn}^{\min} z_{fg,t}, \forall t \quad \text{Eq. 5-7}$$

Where,

$T_{fg,dn}^{\min}$: Fossil-fuel unit minimum down time (min).

5.1.2. Step 2) Hour-ahead updating:

The DWT method proposed in [120] is used to decompose the error between day-ahead and hour-ahead wind power forecast powers for scheduling CAES, and NaS battery. First, the error signal is derived as shown in Eq. 5-8.

$$p_{fe1,t} = p_{dwf,t} - p_{hwf,t}, \forall t \quad \text{Eq. 5-8}$$

Where,

$p_{fe1,t}$: Error between day-ahead and hour-ahead wind power forecast powers at time t (MW).

$p_{dwf,t}$: Day-ahead wind power forecast at time t (MW).

$p_{hwf,t}$: Hour-ahead wind power forecast at time t (MW).

Then, high, medium, and low frequency components are derived by using the DWT method. The difference between this research and the method proposed in [120] are defined below.

1) First, energy storage units are prescheduled by day-ahead wind power forecast, rather than only be used for mitigating forecast error. This modifies the control signal of energy storage units which are shown in Eq. 5-9 and Eq. 5-10 for CAES and NaS

battery, respectively. As shown in Eq. 5-9, the CAES control signal is the CAES day-ahead scheduling plus the medium frequency component of the error signal derived in Eq. 5-8.

$$p_{C,t} = (p_{Cdchg,t} - p_{Cchg,t}) + p_{mf,t}, \forall t \quad \text{Eq. 5-9}$$

Where,

$p_{C,t}$: CAES control signal at time t (MW).

$p_{mf,t}$: Medium frequency component at time t (MW).

$p_{Cchg,t}$: CAES charge power derived from step1 at time t (MW).

$p_{Cdchg,t}$: CAES discharge power derived from step1 at time t (MW).

2) Then this control signal Eq. 5-9 is the new input to the algorithm proposed in [120] that applies CAES properties such as power and energy limits, ramp rate, and required idle time at each time interval. The output is CAES discharge and charge power at each time interval. Then, the NaS battery control signal is determined as the summation of its day-ahead scheduling plus high frequency component and also the difference between CAES operation and its initial control signal as shown in Eq. 5-10.

$$p_{N,t} = (p_{Ndchg,t} - p_{Nchg,t}) + p_{hf,t} + (p_{CAES,t} - p_{C,t}), \forall t \quad \text{Eq. 5-10}$$

Where,

$p_{N,t}$: NaS control signal at time t (MW).

$p_{hf,t}$: High frequency component at time t (MW).

$p_{Nchg,t}$: NaS charge power derived from step1 at time t (MW).

$p_{Ndchg,t}$: NaS discharge power derived from step1 at time t (MW).

3) The control signal presented in Eq. 5-10 is the new input to the algorithm proposed in [120] that applies NaS battery properties such as power limit, energy capacity limit, and state of charge limit. The output is NaS discharge and charge power at each time interval.

5.1.3. Step 3) 5minute-ahead updating:

This step is the same as step 2, with following differences. First, the error signal is the difference between the hour-ahead wind power forecast and the actual wind power as Eq. 5-11.

$$p_{fe2,t} = p_{hwf,t} - p_{aw,t}, \forall t \qquad \text{Eq. 5-11}$$

Where,

$p_{fe2,t}$: Error between hour-ahead and actual wind power at time t (MW).

$p_{aw,t}$: Actual wind power at time t (MW).

Second, the energy storage control signal is the summation of energy storage scheduling derived from step 2 and the related decomposed component of error signal in Eq. 5-11 by DWT.

5.1.4. Step 4) calculating final spilled wind energy

The residual power is calculated as shown in Eq. 5-12, which equals to the total generation (inflexible generation, thermal units, energy storage discharging power, wind power, and low-frequency component) minus total load (load, and energy storage charging power) at each time interval.

$$p_{residual,t} = P_{ig} + p_{aw,t} + p_{gf,t} + p_{dchg,t} - p_{chg,t} + p_{lf,t} - p_{l,t}, \forall t \quad \text{Eq. 5-12}$$

Where,

$p_{residual,t}$	:	Residual power at time t (MW).
P_{ig}	:	Inflexible (must-run) generation (MW).
$p_{gf,t}$	:	Gas-fired generation at time t (MW).
$p_{lf,t}$	:	Low frequency components derived from DWT of step 2 and step 3 at time t (MW).
$p_{l,t}$	:	Load at time t (MW).

Spilled wind energy and back-up generation are the positive and negative quantities of this residual signal, respectively.

5.2. Case Studies and Discussions

To showcase the applicability of the proposed approach, different case studies based on wind and load data with 5-minute interval, obtained from the Bonneville Power Administration (BPA) in 2013 are investigated [54]. BPA day-ahead wind power is forecasted in a range identified by maximum, average, and minimum values as shown Fig. 5-2. The hour-ahead wind power forecast and actual wind power are also depicted in Fig. 5-2 for the same day. This figure shows the problem addressed by the proposed algorithm that mitigates errors between day-ahead forecast, hour-ahead forecast and actual wind power while energy storage units are scheduled based on day-ahead wind power forecast at its first step.

BPA peak load in 2013 is 10.6 GW, and installed wind capacity is 4.5 GW. Wind energy penetration is 20% in BPA, while neglecting net interchange. Nuclear generation and gas-fired generation are considered in this research to be able to provide 100% of annual peak load to guarantee system reliability. Nuclear generation is considered to be a must-run generation providing 20% of peak load with 95% availability. Hence, nuclear must-run

power is 2 GW. Gas-fired generation parameters are shown in Table 5-1. Modeling parameters for energy storage technologies including CAES and NaS battery are presented in Table 5-2.

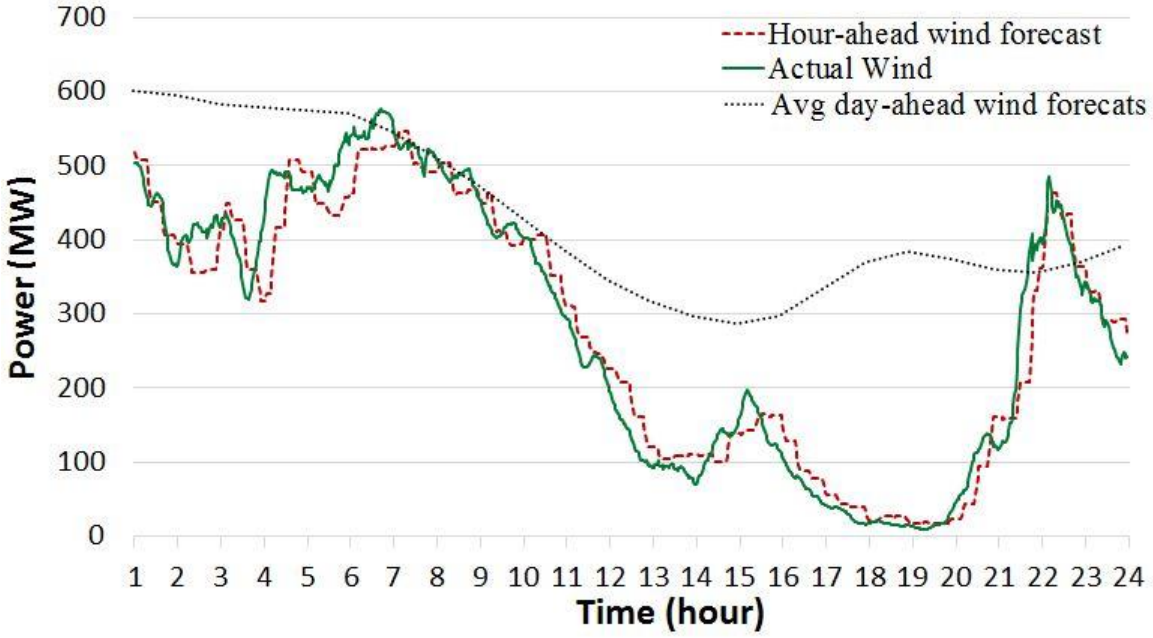

Fig. 5-2. A day in BPA 2013 showing actual wind generation, hour-ahead wind power forecast, and day-ahead wind power forecast range.

Different case studies are investigated by simulating BPA data for one month (April) in 2013 with 5-minute time interval. Characteristics of errors between maximum, average, minimum day-ahead wind power forecasts, and hour-ahead wind power forecast with actual (real-time) wind power is extracted and shown in Table 5-3. As shown, if energy storage units are only used for day-ahead scheduling, extra energy storage units are required to be installed for mitigating this error.

Table 5-1. Gas-fired Generation parameters [118]

Capacity (GW)	9
Min Stable Generation (%)	20
Ramp up/down (% of installed capacity per min)	8
Min up/down Time (hours)	2

Table 5-2. Large-scale energy storage parameters [12], [13]

Energy Storage Technology	CAES	NaS
Power Capacity (MW)	300	50
Energy Capacity (MWh)	6000	300
Ramp Rate (MW/min)	18	---
Efficiency (%)	70	75
Required Idle Time to Switch Modes (min)	20	---
Max and Min State of Charge	1,0	0.9,0.1

Table 5-3. Wind Power Forecast Error Analysis

	Mean (MW)	Sigma (MW)	Max (MW)	Min (MW)
Actual wind minus maximum day-ahead wind power forecast	-317	1131	3782	-3836
Actual wind minus average day-ahead wind power forecast	-12	1121	3891	-3609
Actual wind minus minimum day-ahead wind power forecast	310	1130	3974	-3374
Actual wind minus hour-ahead wind power forecast	34	236	1225	-1316

Proposed algorithm updates day-ahead energy storage operation to be able to mitigate wind power forecast errors. Hence, the objective of energy storage scheduling based on this algorithm is to address both challenges of systems with high wind energy penetration levels: spilled wind energy due to non-correlation between load and wind power forecast profile, as well as, wind power forecast errors. The results of this algorithm for final spilled wind energy of different energy storage technologies, and different scenarios are shown in Fig. 5-3.

As shown in Fig. 5-3, If day-ahead scheduling was based on actual wind data rather than day-ahead wind forecast then wind spillage would be 280 GWh. On the other hand, if day-ahead wind power forecast is used, then wind spillage reached 372 GWh. Inserting one NaS battery and one CAES while following the proposed updating algorithm results in 257 GWh. But, if energy storage units are not updated in hour-ahead and 5 minute ahead while being scheduled based on day-ahead wind power forecast, then wind spillage would have been 301 GWh. The ideal scenario for one NaS battery and one CAES is the result of scheduling based on actual wind generation shown in grey columns which results in 142 GWh. By increasing the number of energy storage units, wind spillage decreases as shown in Fig. 5-3.

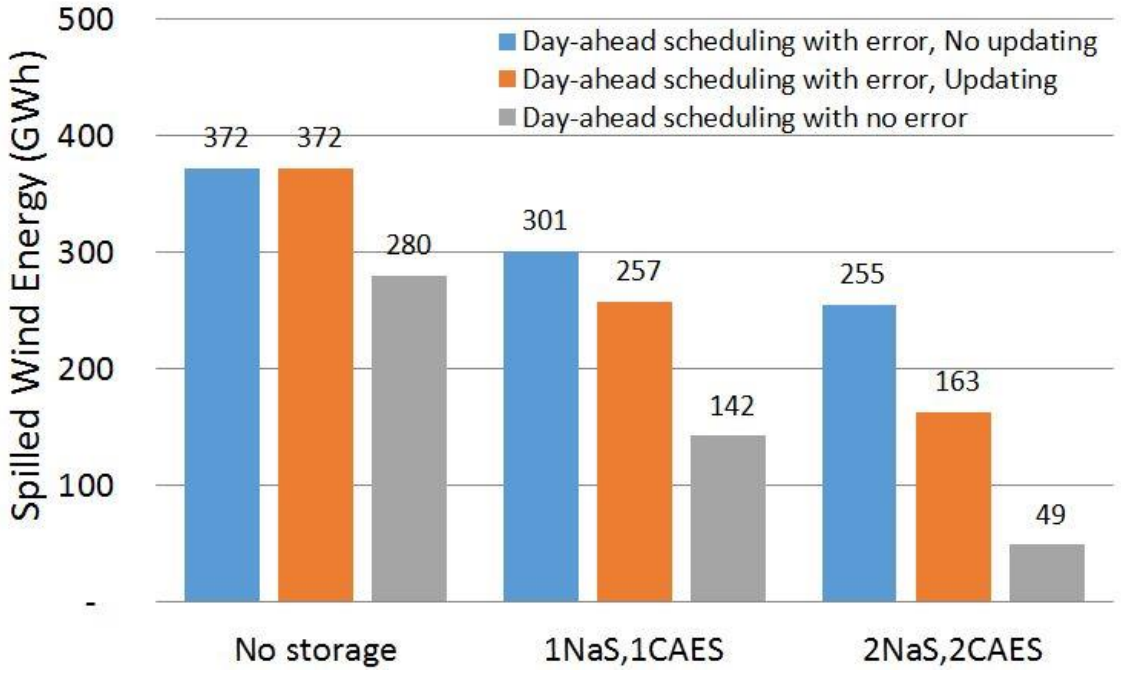

Fig. 5-3. Final spilled wind energy based on different scenarios

5.3. Conclusion

This chapter presents an algorithm to optimally operate energy storage units based on the day-ahead wind power forecast and then update it to mitigate wind power forecast errors. This scheduling uses energy storage technologies to mitigate both high wind energy penetration challenges - spilled wind energy and wind power forecast error.

Tradeoffs between different algorithms and number of energy storage technologies are investigated on final spilled wind energy. The proposed algorithm results in less wind spillage due to updating energy storage scheduling based on the proposed algorithm. Hence, updating based on the proposed algorithm reduces the need to install more energy storage units by updating energy storage operation based on wind power forecast error signals.

5.4. Analyzing Convexity of Proposed Optimization Problem

The optimization problem proposed is a mixed integer linear programming. Hence, it has both continuous and integer variables, but all constraints are presented in the linear format. All integer parameters in the model are related to on or off values which are decision variables presented by binary values (zero or one). This type of optimization problem is non-convex by nature due to having integer values. The solution to solve this type of optimization problem is to use the branch-and-bound method [116] that is also used by IBM CPLEX software.

The output of the optimization problem is the vector called x for each time interval as shown in Eq. 5-15. It contains both continuous and integer variables as shown below. As shown, the vector x at each time interval has six continuous variables and eight integer variables. On the other hand, the optimization problem presented in this chapter is simulated for a day with 5 minutes time interval. This results in 288 time intervals. As a result, each optimization has 1728 (288 times 6) continuous variables and 2304 (288 times 8) integer variables.

$$x_t = [x_{Continous,t}, x_{Integer,t}] \forall t \quad \text{Eq. 5-13}$$

$$x_{Continous,t} = [p_{fg,t}, p_{Cdchg,t}, p_{Cchg,t}, p_{Ndchg,t}, p_{Nchg,t}, p_{ws,t}] \forall t \quad \text{Eq. 5-14}$$

$$x_{Integer,t} = [\alpha_{C,t}, \beta_{C,t}, \gamma_{C,t}, \rho_{C,t}, \varphi_{C,t}, u_{fg,t}, y_{fg,t}, z_{fg,t}] \forall t \quad \text{Eq. 5-15}$$

Where,

χ_t	:	Output of optimization problem for each time interval t
$x_{Continous,t}$	:	Continuous component of the optimization problem output for each time interval t
$x_{Integer,t}$	:	Integer component of the optimization problem output for each time interval t

The fact that the optimization problem has reached its optimal solution when starting from different weeks of the year shows the convex nature of this problem. Also, random initial values are given to the optimization solver to see if the objective function values differ or not, as defined below.

Random initial variables are derived to be within the upper and lower limits of each variable, as shown in Eq. 5-18. Random variables have the uniform distribution function as defined for random function in MATLAB. To extract random binary values, the random variable between zero and one is rounded which results in 0 if the random variable is less than 0.5, otherwise it would be 1.

$$x^{rand}{}_{t} = [x^{rand}{}_{Continous,t}, x^{rand}{}_{Integer,t}] \forall t \quad \text{Eq. 5-16}$$

$$x^{rand}{}_{Continous,t} = [rand(size(x_{Continous,t})).\times U(x_{Continous,t})] \forall t \quad \text{Eq. 5-17}$$

$$x^{rand}{}_{Integer,t} = [round(rand(size(x_{Integer,t})))] \forall t \quad \text{Eq. 5-18}$$

Where,

$x^{rand}{}_{t}$	:	Random initial input of optimization problem for each time interval t
$x^{rand}{}_{Continous,t}$	:	Random initial continuous component of the optimization problem input for each time interval t
$x^{rand}{}_{Integer,t}$	:	Random initial integer component of the optimization problem input for each time interval t
$rand(j)$	:	Random vector with uniform distribution function with size j
$U(x)$	:	Upper limit of optimization problem output as x
$round(y)$	:	Round function of input y

The objective function for 100 random initial input vectors is simulated for three days with the highest wind energy penetration level. The objective function for all these initial values for each day is plotted in Fig.5-5 for 170th , 162th, and 110th days of the year which have the first three highest wind energy penetration levels. The optimization problem is solved when there is one 50 MW NaS battery and one 300 MW CAES in the system. As

shown, all 100 random vectors result in the same value for the objective function for each week that is shown in three lines for each week. This shows the convexity of the proposed mixed integer linear programming.

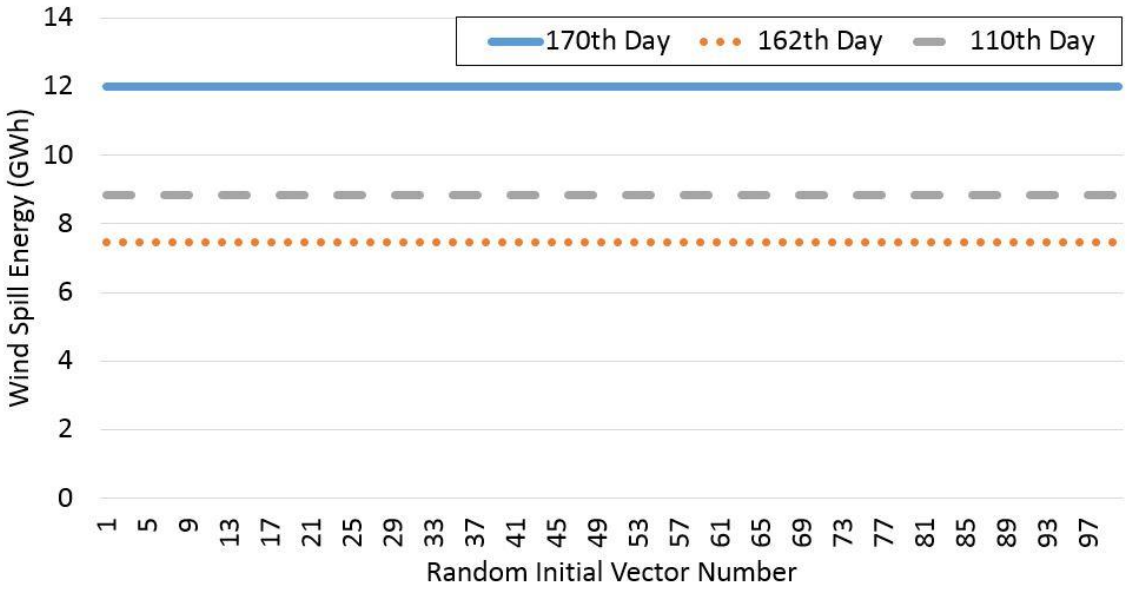

Fig. 5-4. Objective functions for random initial values of three different weeks

5.5. The Branch-and-Bound Method

In IBM CPLEX, integer programming is solved by using the technique called the branch-and-bound method. The branch-and-bound method finds the optimal solution to an integer programming by efficiently enumerating the points in a sub problem's feasible region. A solution obtained by solving a sub problem in which variables have integer values is a candidate solution. Because the candidate solution may be optimal, the candidate solution must be kept till a better feasible solution to the integer programming (if any exists) is found [116].

The key aspects of the branch-and-bound method for solving integer programming problems are summarized as follows [116]:

Step 1) if it is unnecessary to branch on a sub problem, then it is fathomed. The following three situations result in a sub problem being fathomed: (1) The sub problem is infeasible; (2) the sub problem yields an optimal solution in which all variables have integer values; and (3) the optimal value of the objective function for the sub problem does not exceed the current value of the objective function for the best candidate to date.

Step 2) a sub problem may be eliminated from consideration in the following situations: (1) The sub problem is infeasible; (2) the current value of the objective function for the best candidate to date is at least as large as the value of the objective function for the sub problem.

In a mixed integer programming, some variables are required to be integers and others are allowed to be either integers or non-integers. To solve a mixed integer programming, using the branch-and-bound method, modify the method described by branching only on variables that are required to be integers. Also, for a solution to a sub problem to be a candidate solution, it needs only assign integer values to those variables that are required to be integers [116].

To illustrate, let us solve the following mixed integer programming [116]:

$$\max z = 2x_1 + x_2 \qquad \text{Eq. 5-19}$$

$$\textit{s.t.} \quad 5x_1 + 2x_2 \le 8 \qquad \text{Eq. 5-20}$$

$$x_1 + x_2 \le 3 \qquad \text{Eq. 5-21}$$

$$x_1, x_2 \ge 0; x_1 : \textit{Integer} \qquad \text{Eq. 5-22}$$

Solving the integer programming begins with linear programming relaxation (this method solve the problem while assuming all variables are allowed to be either integers or non-integers). The optimal solution of the linear programming relaxation is z=11/3, x_1=2/3, x_2=7/3. Because x_2 is allowed to be fractional, branching on x_2 is discontinued; otherwise, points having x_2 values between 2 and 3 would be excluded, which is not wanted. Thus, branching on x_1 is continued. This yields sub problems 2 and 3 in Figure 5-4.

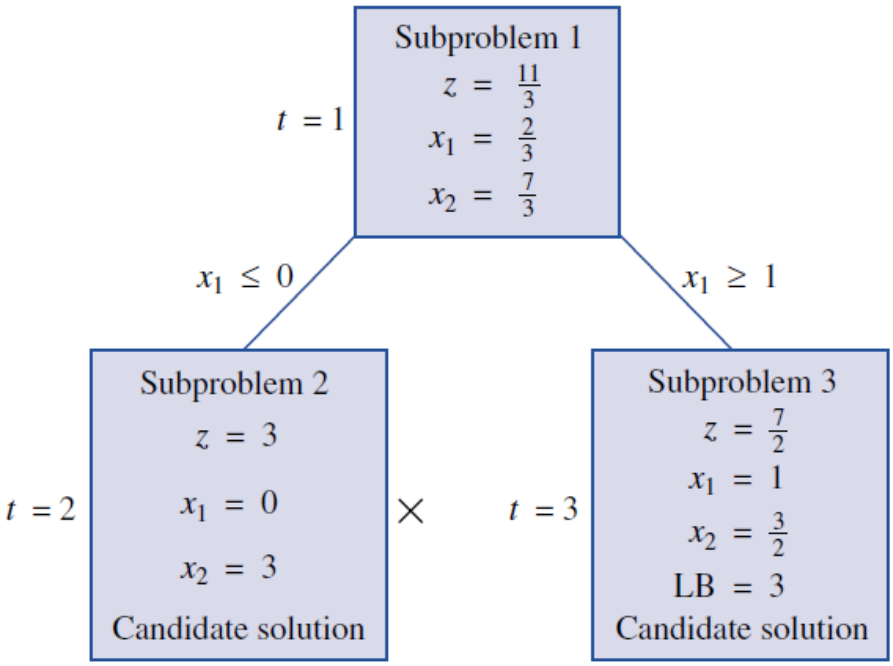

Fig. 5-5. Branch-and-bound tree for mixed integer programming [116]

Next sub problem 2 is chosen to solve. The optimal solution to sub problem 2 is the candidate solution z = 3, x_1 = 0, x_2 = 3. Then, sub problem 3 is solved and the candidate solution z = 7/2, x_1 = 1, x_2 = 3/2 is obtained. The z-value from the sub problem 3

candidate exceeds the z-value for the sub problem 2 candidate, so sub problem 2 can be eliminated from consideration, and the sub problem 3 candidate ($z = 7/2$, $x_1 = 1$, $x_2 = 3/2$) is the optimal solution to the mixed linear programming.

6. Summary, Conclusion, and Future Work

6.1. Summary

The objective of the dissertation is to propose a planning tool for electric utility operators to provide an insight into the sizing and operation of grid-scale energy storage equipment, and demand response programs to mitigate challenges of power systems with high wind energy penetration levels. The proposed planning tool comprises algorithms that are designed to schedule energy storage units and demand response programs to minimize wind spillage and mitigate wind power forecast errors. The three main contributions and novelties of this dissertation are summarized below:

First, different energy storage technologies and demand response options are taken into account in the proposed mixed integer linear programming method to minimize wind spillage due to the non-correlation between wind and load profiles. The objective function is to minimize the wind spillage due to the non-correlation between wind and load profiles. The contribution is the detailed model of each energy storage technology, including CAES, PHES, and different large-scale batteries including NaS, Lead acid, and Vanadium redox batteries. DR is scheduled prior to high wind and low load periods, to adjust its rebound occurring at this duration, to reduce wind spillage.

Second, the algorithm based on signal processing techniques is proposed to schedule different types of energy storage technologies and conventional generation units for mitigating the wind power forecast error. The idea is to decompose the wind power forecast error signal using signal processing techniques (e.g. Discrete Wavelet Transform and Discrete Fourier Transform) to time-varying periodic components that have specific cycling, which is appropriate for the operation of each energy storage technology and conventional units.

Third, an algorithm is presented to mitigate the spilled wind energy due to non-correlation as well as wind power forecast error impacts in day-ahead, hour-ahead and five-minute ahead situations. This algorithm uses day-ahead wind power forecast and

load data to schedule energy storage units for minimizing wind spill energy due to the non-correlation between these two profiles. Then, energy storage scheduling is updated in the hour-ahead time frame using proposed signal processing techniques to mitigate the error between day-ahead wind power forecast and hour-ahead wind power forecast profiles. Finally, it is updated in 5 minutes ahead to mitigate the error between hour-ahead wind power forecast and actual wind power generations using the same signal processing techniques.

6.2. Conclusion

High renewable energy penetration is designed to achieve the goal of reducing carbon emissions through proactive environmental and energy policies. The leading source for renewable electricity generation today is wind energy. But the downside is spilled wind energy resulting from the non-correlation between wind and load profiles. The stochastic nature of wind energy, causing wind power forecast error, is another challenge that makes high wind energy penetration cases more complicated to manage. The planning tool proposed in this dissertation mitigates these two challenges as highlighted by the following findings and conclusions.

The amount of wind spill energy depends on wind power generation, load level, and generation mix as presented in this dissertation. The generation mix studied in this research includes nuclear, coal, and natural gas. Since nuclear and coal generation units have higher capacity factors and lower cycling capability as compared to a natural gas generation units, greater amount of nuclear and coal generation results in higher wind spill energy. Energy storage and demand response are flexible resources that can be scheduled to reduce wind spill energy.

A system's ability to minimize the wind energy spillage depends on the type of energy storage technology used, as well as, the characteristics of demand response program (contract) deployed. Energy storage technologies with higher energy capacity, like CAES, are able to absorb more energy, which results in less spilled wind energy. But, these energy storage technologies have their own barriers to cope with intermittent

variable wind generation, such as required idle time to switch between the charge and discharge modes. Hence, combination of large-scale batteries with mechanical energy storage technologies as PHES and CAES is a good option that can benefit from characteristics of both technologies.

In high wind energy penetration scenarios, the peak demand is not the usual peak load. It rather depends on the net load, which is the system load minus the wind output. As a result, the conventional approach of using demand response at peak load time just to reduce peak load needs to be changed. This dissertation proposes a new approach for demand response implementation by matching the rebound effect to coincide with a high wind power output period, thus potentially reducing wind spill energy. This research shows that if DR is scheduled before high wind generation periods, then its rebound during the high wind generation period can reduce spilled wind energy significantly. The amount of this reduction depends on the rebound effect of demand response and the frequency of demand response events, which are based on the contract between a grid operator and energy customers.

The two signal processing techniques proposed in this dissertation are Discrete Wavelet Transform (DWT) and Discrete Fourier Transform (DFT). The proposed DWT method decomposes the wind power forecast error signal to components with step shape (which do not change at each time interval and remain constant for a specific duration). The trade-off between scheduling energy storage technologies with DWT as compared to DFT is more spilled wind energy and required back-up generation, but the DWT result is more appropriate signal to control mechanical energy storage technologies as compared to the DFT result. This approach avoids oversizing the required energy storage by implementing different combinations of energy storage units and analyzing their impacts. Frequency bias constant is considered to reduce the final wind spill and needed back-up energy.

Finally, an algorithm is presented to optimally operate energy storage units based on the day-ahead wind power forecast while updating it to mitigate wind power forecast errors. Tradeoffs between different case studies such as energy storage technologies are investigated on final spilled wind energy and back-up generation required. More energy

storage technologies and using minimum day-ahead wind power forecast have better overall results in terms of lower spilled wind energy as compared to the case when energy storage is not updated. This algorithm reduces the need to install more energy storage units by updating energy storage operation based on wind power forecast error signals.

The information provided in this dissertation is beneficial for investors in energy storage and wind sectors. The overall energy storage sizing depends on the economic issues of energy storage operation, investment costs, and wind production tax credit in addition to analyzing the technical issues.

6.3. Future Work

The proposed planning tool can facilitate additional energy storage and demand response research to mitigate challenges in utilities with high wind energy penetration levels. This dissertation solved the optimization problem to minimize spilled wind energy using branch-and-bound method. One future work is to elaborate more about the proposed optimization problem. For example, minimax algorithm, which is a decision rule in game theory, can be used for solving other complex objective functions to minimize the possible loss for the worst case (maximum loss) scenario. Other possible objective functions are stated below.

The dissertation has analyzed the technical part of this issue while neglecting required market infrastructure and economic tradeoffs. One potential future work may be to evaluate the impact of energy storage and demand response on increasing wind energy penetration from the economic point of view while considering all investment and operational costs of different energy storage technologies and demand response programs.

This dissertation has considered high wind penetration challenges and scheduling of both energy storage and demand response from the grid (utility) operator point of view. Several possible future research works can come from looking at this problem from

distribution system level, to accommodate a higher level of renewable energy penetration in distribution networks.

References

[1] Lauha, F., S. Steve, S. Sgruti, and Q. Limig. Global Wind Report - Annual Market Update 2013. Global Wind Energy Council, Brussels, Belgium, 2012.

[2] Meibom, Peter, Klaus Baggesen Hilger, Henrik Madsen, and Dorthe Vinther. "Energy Comes Together in Denmark: The Key to a Future Fossil-Free Danish Power System." Power and Energy Magazine, IEEE 11, no. 5 (2013): 46-55.

[3] A. I. Estanqueiro, J.M. F. de Jesus, J. Ricardo, A. dos Santos, and J. A. P. Lopes, "Barriers (and solutions...) to very high wind penetration in power systems" in Proc. IEEE Power Eng. Soc. General Meeting, Jun. 24–28, 2007, pp. 1001–1012.

[4] T. Mai, M. Hand, S.F. Baldwin, R. H. Wiser, G.L. Brinkman, P. Denholm, D.J. Arent, G. Porro, D. Sandor, D. Hostick, M. Milligan, E.A. DeMeo, M. Bazilian, "Renewable Electricity Futures for the United States," IEEE Trans. on Sustainable Energy, vol.5, no.2, pp. 372-378, April 2014.

[5] C. Brandstätt, G. Brunekreeft, and K. Jahnke. "How to deal with negative power price spikes?—Flexible voluntary curtailment agreements for large-scale integration of wind." Energy Policy, vol.39, no.6, pp.3732-3740, June 2011

[6] L. Jin, S. Yuan-zhang, P. Sørensen, L. Guo-jie, and G. Weng-zhong,, "Method for Assessing Grid Frequency Deviation Due to Wind Power Fluctuation Based on "Time-Frequency Transformation"," IEEE Trans. on Sustainable Energy, vol. 3, no. 1, pp. 65-73, Jan. 2012.

[7] H. Banakar, C. Luo, and B. T. Ooi "Impacts of wind power minute-to-minute variations on power system operation", IEEE Trans. on Power System, vol. 23, no. 1, pp.150 -160, Feb. 2008.

[8] Changling Luo; Far, H.G.; Banakar, H.; Keung, Ping-Kwan; Boon-Teck Ooi, "Estimation of Wind Penetration as Limited by Frequency Deviation," IEEE Trans. on Energy Conversion, vol. 22, no.3, pp.783,791, Sept. 2007

[9] J. Bebic, G.Hinkle, S. Matic, and W. Schmitt, Grid of the Future: Quantification of Benefits from Flexible Energy Resources in Scenarios With Extra-High Penetration of Renewable Energy, ARPA-e Project Report, GE Energy Consulting, Ver. 1.2, Jan 15, 2015.

[10] L. Bird, M. Milligan, and D. Lew, Integrating Variable Renewable Energy: Challenges and Solutions, National Renewable Energy Laboratory (NREL) technical report, September 2013, Denver, Colorado.

[11] L. Bird, J. Cochran, and X. Wang., Wind and solar energy curtailment: Experience and practices in the United States, National Renewable Energy Laboratory (NREL) technical report, March 2014, Denver, Colorado.

[12] R. Carnegie, D. Gotham, D. Nderitu, and P. V. Preckel. Utility Scale Energy Storage Systems: Benefits, Applications, and Technologies. Perdue University, State Utility Forecasting Group, West Lafayette, Indiana, June 2013.

[13] Barnes, Frank S., and Jonah G. Levine, eds., large energy storage systems handbook. CRC Press, 2011.

[14] NAS Battery Energy Storage System, NGK presentation, available online at http://www.eei.org/about/meetings/meeting_documents/abe.pdf, Viewed on 15 May 2015

[15] Exploding Sodium Sulfur Batteries from NGK Energy Storage, available online at http://www.greentechmedia.com/articles/read/Exploding-Sodium-Sulfur-Batteries-From-NGK-Energy-Storage

[16] H. T. Le; S. Santoso, T. Q. Nguyen, "Augmenting Wind Power Penetration and Grid Voltage Stability Limits Using ESS: Application Design, Sizing, and a Case Study," IEEE Trans. on Power Systems , vol.27, no.1, pp.161-171, Feb. 2012

[17] C. Abbey, and G. Joos, "A stochastic optimization approach to rating of energy storage systems in wind-diesel isolated grids," IEEE Trans. on Power Systems, vol. 24, no. 1, pp. 418-426, Apr. 2009.

[18] Y. Levron, J. M. Guerrero, and Y. Beck, "Optimal power flow in micro grids with energy storage," IEEE Trans. on Power Systems, vol. 28, no. 3, pp. 3226-3234, Apr. 2013.

[19] D. Gayme, and U. Topcu, "Optimal power flow with large-scale storage integration," IEEE Trans. on Power Systems, vol. 28, no. 2, pp. 709-717, May. 2013.

[20] S. Teleke, M. E. Baran, S. Bhattacharya, and A. Q. Huang, "Rule-based control of battery energy storage for dispatching intermittent renewable sources," IEEE Trans. on Sustainable Energy, vol. 1, no. 3, pp. 117-124, Oct. 2010.

[21] L. Xu, X. Ruan, Ch. Mao, B. Zhang and Y. Luo, “An Improved Optimal Sizing Method for Wind-Solar-Battery Hybrid Power System,” IEEE Trans. on Sustainable Energy, vol. 4, no. 3, pp. 774-785, July. 2013.

[22] T. K. A. Brekken, A. Yokochi, A. V. Jouanne, Z. Z. Yen, H. M. Hapke, and D. A. Halamay, “Optimal energy storage sizing and control for wind power applications,” IEEE Trans. on Sustainable Energy, vol. 2, no. 1, pp. 69-77, Jan. 2011

[23] S. Teleke, M. E. Baran, A. Q. Huang, S. Bhattacharya, and L. Anderson, "Control strategies for battery energy storage for wind farm dispatching," IEEE Trans. on Energy Conversion., vol. 24, no. 3, pp.725-732, Sep. 2009.

[24] P. Wang, Z. Gao, and L. Bertling, “Operational adequacy studies of power systems with wind farms and energy storages,” IEEE Trans. on Power Systems, vol. 27, no. 4, pp. 2377-2384, Nov. 2012.

[25] C. Wang, Z. Lu, and Y. Qiao, “A consideration of the wind power benefits in day-ahead scheduling of wind-coal intensive power systems,” IEEE Trans. on Power Systems, vol. 28, no. 1, pp. 236-245, Feb. 2013.

[26] M. Ghofrani, A. Arabali, M. Etezadi-Amoli and M. S. Fadali, “Energy Storage Application for Performance Enhancement of Wind Integration,” IEEE Transaction on Power Systems, vol. 28, no. 4, pp. 4803-4811, Nov. 2013.

[27] S. Teleke, M. E. Baran, S. Bhattacharya, and A. Q. Huang, “Rule-based control of battery energy storage for dispatching intermittent renewable sources,” IEEE Trans. on Sustainable Energy, vol. 1, no. 3, pp. 117-124, Oct. 2010.

[28] Y. A. Katsigiannis, P. S. Georgilakis, and E. S. Karapidakis, “Hybrid Simulated Annealing–Tabu Search Method for Optimal Sizing of Autonomous Power Systems With Renewables,” IEEE Trans. on Sustainable Energy, vol. 3, no. 3, pp. 330-338, July. 2012.

[29] Z. Zhang, Q. Zhou, and A. Kusiak, “Optimization of Wind Power and Its Variability With a Computational Intelligence Approach,” IEEE Trans. on Sustainable Energy, vol. 5, no. 1, pp. 228-236, Jan. 2014.

[30] S. Mei, Y. Wang, F. Liu, X. Zhang, and Z. Sun, “Game Approaches for Hybrid Power System Planning,” IEEE Trans. on Sustainable Energy, vol. 3, no. 3, pp. 506-517, July. 2012.

[31] Z. Zhang, Q. Zhou, and A. Kusiak, “Optimization of Wind Power and Its Variability With a Computational Intelligence Approach,” IEEE Trans. on Sustainable Energy, vol. 5, no. 1, pp. 228-236, Jan. 2014.

[32] Sh. Mei, D. Zhang, Y. Wang, F. Liu, and W. Wei, “Robust Optimization of Static Reserve Planning With Large-Scale Integration of Wind Power: A Game Theoretic Approach,” IEEE Trans. on Sustainable Energy, vol. 5, no. 2, pp. 535-545, April. 2014.

[33] X. Ke, N. Lu, C. Jin, "Control and Size Energy Storage Systems for Managing Energy Imbalance of Variable Generation Resources," IEEE Trans. on Sustainable Energy, vol.6, no.1, pp.70, 78, Jan. 2015.

[34] F. Luo, K. Meng, Z.Y. Dong, Y. Zheng, Y. Chen, K.P. Wong, "Coordinated Operational Planning for Wind Farm With Battery Energy Storage System," IEEE Trans. on Sustainable Energy, vol.6, no.1, pp.253, 262, Jan. 2015.

[35] A. Ingram, “Storage options and sizing for utility scale integration of wind energy plants,” in Proc ASME. Int. Solar Energy Conf. 2005, Orlando, FL, Aug. 2005, pp. 843–851.

[36] H. Bludszuweit and J. A. Domínguez-Navarro, “A Probabilistic Method for Energy Storage Sizing Based on Wind Power Forecast Uncertainty,” IEEE Trans. on Power Systems, vol. 26, no. 3, pp. 1651-1658, Aug. 2011.

[37] N. Zhang, Ch. Kang, D. S. Kirschen, Q. Xia, W. Xi, J. Huang and Q. Zhang, “Planning Pumped Storage Capacity for Wind Power Integration,” IEEE Trans. on Sustainable Energy, vol. 4, no. 2, pp. 393-401,April. 2013.

[38] Faias, Sergio; de Sousa, J.; Reis, F.S.; Castro, R., "Assessment and Optimization of Wind Energy Integration Into the Power Systems: Application to the Portuguese System," IEEE Trans. on Sustainable Energy, vol.3, no.4, pp.627,635, Oct. 2012

[39] M. Dicorato, G. Forte, M. Pisani, and M. Trovato, “Planning and Operating Combined Wind-Storage System in Electricity Market,” IEEE Trans. on Sustainable Energy, vol. 3, no. 2, pp. 209-217, April. 2012.

[40] M.E. Khodayar, M. Shahidehpour, "Stochastic Price-Based Coordination of Intrahour Wind Energy and Storage in a Generation Company," IEEE Trans. on Sustainable Energy, vol.4, no.3, pp.554,562, July 2013

[41] H. Akhavan-Hejazi and H. Mohsenian-Rad, “Optimal Operation of Independent Storage Systems in Energy and Reserve Markets With High Wind Penetration,” IEEE Trans. on Smart Grid, vol. 5, no. 2, pp. 1088-1097, March. 2014.

[42] M. Parvania, M. Fotuhi-Firuzabad and M. Shahidehpour, “Comparative Hourly Scheduling of Centralized and Distributed Storage in Day-Ahead Markets” IEEE Trans. on Sustainable Energy, vol. 5, no. 3, pp. 729-737, July. 2014.

[43] L. Xu, X. Ruan, Ch. Mao, B. Zhang and Y. Luo, “An Improved Optimal Sizing Method for Wind-Solar-Battery Hybrid Power System,” IEEE Trans. on Sustainable Energy, vol. 4, no. 3, pp. 774-785, July. 2013.

[44] Y. Levron, J. M. Guerrero and Y. Beck, “Optimal power flow in micro grids with energy storage,” IEEE Trans. on Power Systems, vol. 28, no. 3, pp. 3226-3234, Apr. 2013.

[45] D. Gayme and U. Topcu, “Optimal power flow with large-scale storage integration,” IEEE Trans. on Power Systems, vol. 28, no. 2, pp. 709-717, May. 2013.

[46] P. Wang, Z. Gao and L. Bertling, “Operational adequacy studies of power systems with wind farms and energy storages,” IEEE Trans. on Power Systems, vol. 27, no. 4, pp. 2377-2384, Nov. 2012.

[47] C. Wang, Z. Lu and Y. Qiao, “A consideration of the wind power benefits in day-ahead scheduling of wind-coal intensive power systems,” IEEE Trans. on Power Systems, vol. 28, no. 1, pp. 236-245, Feb. 2013.

[48] J. Mitra, M.R. Vallem, "Determination of Storage Required to Meet Reliability Guarantees on Island-Capable Microgrids With Intermittent Sources," IEEE Trans. on Power Systems, vol.27, no.4, pp.2360,2367, Nov. 2012

[49] C. M. Colson, M. H. Nehrir, R. K. Sharma, and B. Asghari, “Improving Sustainability of Hybrid Energy Systems Part I: Incorporating Battery Round-Trip Efficiency and Operational Cost Factors,” IEEE Trans. on Sustainable Energy, vol. 5, no. 1, pp. 37-45, Jan. 2014.

[50] L. Zhang; Y. Li, "Optimal Energy Management of Wind-Battery Hybrid Power System With Two-Scale Dynamic Programming," IEEE Trans. on Sustainable Energy, vol.4, no.3, pp.765,773, July 2013

[51] A. Damiano, G. Gatto, I. Marongiu, M. Porru, A. Serpi, "Real-Time Control Strategy of Energy Storage Systems for Renewable Energy Sources Exploitation," IEEE Trans. on Sustainable Energy, vol.5, no.2, pp.567,576, April 2014

[52] E. Hajipour, M. Bozorg, M. Fotuhi-Firuzabad, "Stochastic Capacity Expansion Planning of Remote Microgrids With Wind Farms and Energy Storage," IEEE Trans. on Sustainable Energy, vol.6, no.2, pp.491,498, April 2015

[53] R. Doherty and M. O'Malley, "A new approach to quantify reserve demand in systems with significant installed wind capacity," IEEE Trans. on Power Systems, vol. 20, no. 2, pp. 587–595, May 2005.

[54] Historical BPA wind data 2013, [on-line]. Available : http://transmission.bpa.gov/Business/operations/Wind/default.aspx , Viewed on 15 May 2015

[55] H. Holttinen, M. Milligan, E. Ela, N. Menemenlis, J. Dobschinski, B. Rawn, R.J. Bessa, D. Flynn, E. Gomez-Lazaro, N.K. Detlefsen, "Methodologies to Determine Operating Reserves Due to Increased Wind Power," IEEE Trans. on Sustainable Energy, vol.3, no.4, pp.713-723, Oct. 2012

[56] B. Hartmann, and A. Dan, "Methodologies for Storage Size Determination for the Integration of Wind Power," IEEE Trans. on Sustainable Energy, vol. 5, no. 1, pp. 182-189, Jan. 2014.

[57] Y. V. Makarov, P. Du, M. C. W. Kintner-Meyer, J. Chunlian and H. F. Illian, "Sizing energy storage to accommodate high penetration of variable energy resources," IEEE Trans. on Sustainable Energy, vol. 3, no. 1, pp. 34-40, Jan. 2012.

[58] J. Xiao, L. Bai, F. Li, H. Liang and C. Wang, "Sizing of Energy Storage and Diesel Generators in an Isolated Microgrid Using Discrete Fourier Transform (DFT)," IEEE Trans. on Sustainable Energy, vol. 5, no. 3, pp. 907-916, July. 2014.

[59] P. Mandal, A.U. Haque, J. Meng, A.K. Srivastava and R. Martinez, "A novel hybrid approach using wavelet, firefly algorithm, and fuzzy ARTMAP for day-ahead electricity price forecasting," IEEE Trans. on Power Systems, vol. 28, no. 2, pp. 1041-1051, May. 2013

[60] Q. Jiang and H. Hong, “Wavelet-based capacity configuration and coordinated control of hybrid energy storage system for smoothing out wind power fluctuations,” IEEE Trans. on Power Systems, vol. 28, no. 2, pp. 1363-1372, May. 2013.

[61] R. Chen; H. Sun; Q. Guo; Z. Li; T. Deng; W. Wu; B. Zhang, "Reducing Generation Uncertainty by Integrating CSP With Wind Power: An Adaptive Robust Optimization-Based Analysis," IEEE Trans. on Sustainable Energy, vol.6, no.2, pp.583,594, April 2015

[62] U.S. Department of Energy. (2006, February). Benefits of Demand Response in Electricity Markets and Recommendations for Achieving Them: A Report to the United States Congress Pursuant to Section 1252 of the Energy Policy Act of 2005.

[63] Assessment of Demand Response and Advanced Metering, FERC Staff Report, 2008

[64] Assessment of Demand Response and Advanced Metering, FERC Staff Report, 2010

[65] Assessment of Demand Response and Advanced Metering, FERC Staff Report, 2012

[66] G. C. Heffner, C. A. Goldman, and M. M. Moezzi. "Innovative approaches to verifying demand response of water heater load control." IEEE Trans. on Power Delivery, vol.21, no.1, pp. 388 - 397, Dec. 2006

[67] Black, Jason W., and Rajesh Tyagi. "Potential problems with large scale differential pricing programs." 2010 IEEE PES Transmission and Distribution Conference and Exposition, 5p, 19-22 April 2010, New Orleans, LA.

[68] R.F. Bischke, and R. A. Sella. "Design and controlled use of water heater load management." IEEE Trans. on Power Apparatus and Systems, vol. PAS-104, no.6, pp. 1290-1293, June 1985.

[69] R. L. W. Analytics, and C. Goldman. "Deemed Savings Estimates for Legacy Air Conditioning and Water Heating Direct Load Control Programs in PJM Region." Lawrence Berkeley National Laboratory, Berkeley, CA, April 2007.

[70] K. Kalsi, M. Elizondo, J. Fuller, L. Shuai, D. Chassin, "Development and Validation of Aggregated Models for Thermostatic Controlled Loads with Demand

Response," in 2012 45th Hawaii International Conference on System Science (HICSS) , pp.1959-1966, 4-7 Jan. 2012, Maui, HI.

[71] W. Zhang, K. Kalsi, J. Fuller, M. Elizondo, D. Chassin, "Aggregate model for heterogeneous thermostatically controlled loads with demand response," in 2012 IEEE Power and Energy Society General Meeting, 8p, 22-26 July 2012, San Diego, CA.

[72] G. C. Heffner, and D. A. Kaufman. "Distribution substation load impacts of residential air conditioner load control." IEEE Trans. on Power Apparatus and Systems, vol.PAS-104, no.7, pp.1602-1608, July 1985.

[73] G. Papaefthymiou, B. Hasche, C. Nabe, "Potential of Heat Pumps for Demand Side Management and Wind Power Integration in the German Electricity Market," IEEE Trans. on Sustainable Energy, vol.3, no.4, pp.636,642, Oct. 2012

[74] M. Parvania, M. Fotuhi-Firuzabad. M. Shahidehpour, "Optimal Demand Response Aggregation in Wholesale Electricity Markets". IEEE Trans. on Smart Grid, vol.4, no.4, pp.1957-1965, Dec. 2013

[75] P. Cappers, C. Goldman, and D. Kathan,"Demand response in U.S. electricity markets: Empirical evidence," Energy, vol. 35, no. 4, pp. 1526–1535, 2010.

[76] M. Parvania, M. Fotuhi-Firuzabad, M. Shahidehpour, "ISO's Optimal Strategies for Scheduling the Hourly Demand Response in Day-Ahead Markets," IEEE Trans. on Power Systems,, vol.29, no.6, pp.2636-2645, Nov. 2014

[77] W. Hongyu, M. Shahidehpour, A. Alabdulwahab, A. Abusorrah, "Demand Response Exchange in the Stochastic Day-Ahead Scheduling With Variable Renewable Generation," IEEE Trans. on Sustainable Energy, , vol.6, no.2, pp.516-525, April 2015

[78] M. Milligan and B. Kirby, Utilizing Load Response for Wind and Solar Integration and Power System Reliability NREL Rep. CP-550-48247, May 2010.

[79] M. LeMay, R. Nelli, G. Gross, C.A. Gunter, "An Integrated Architecture for Demand Response Communications and Control," in Proceedings of the 41st Annual Hawaii International Conference on System Sciences, pp.174-174, 7-10 Jan. 2008, Waikoloa, HI.

[80] J. A. Short, D. G. Infield and L. L. Freris, “Stabilization of Grid Frequency Through Dynamic Demand Control” IEEE Trans. on Power Systems, vol. 22, no. 3, pp. 1284-1293, Aug. 2007.

[81] A.J. Conejo, J. M. Morales, and L. Baringo. "Real-time demand response model." IEEE Trans. on Smart Grid, vol.1, no.3, pp.236-242, Dec. 2010

[82] S.A. Pourmousavi, M.H. Nehrir, "Real-Time Central Demand Response for Primary Frequency Regulation in Microgrids," IEEE Trans. on Smart Grid, vol.3, no.4, pp.1988-1996, Dec. 2012

[83] K. Dietrich, J.M. Latorre, L. Olmos, A. Ramos, "Demand Response in an Isolated System With High Wind Integration," IEEE Trans. on Power Systems, vol.27, no.1, pp.20-29, Feb. 2012

[84] A. Khodaei, M. Shahidehpour, S. Bahramirad, "SCUC With Hourly Demand Response Considering Intertemporal Load Characteristics," IEEE Trans. on Smart Grid, vol.2, no.3, pp.564-571, Sept. 2011

[85] S.H. Madaeni, R. Sioshansi, "Measuring the Benefits of Delayed Price-Responsive Demand in Reducing Wind-Uncertainty Costs," IEEE Trans. on Power Systems, vol.28, no.4, pp.4118-4126, Nov. 2013

[86] S.H. Madaeni, R. Sioshansi, "Using Demand Response to Improve the Emission Benefits of Wind," IEEE Trans. on Power Systems, vol.28, no.2, pp.1385-1394, May 2013

[87] N. Cicek, H. Delic, H., "Demand Response Management for Smart Grids With Wind Power," IEEE Trans. on Sustainable Energy, vol.6, no.2, pp.625,634, April 2015

[88] N. Lu, P. Du, Y.V. Makarov, "The potential of thermostatically controlled appliances for intra-hour energy storage applications," 2012 IEEE Power and Energy Society General Meeting, 6p, 22-26 July 2012, San Diego, CA

[89] N. Lu, D.P. Chassin, "A state-queueing model of thermostatically controlled appliances," IEEE Trans. on Power Systems, vol.19, no.3, pp.1666-1673, Aug. 2004

[90] N. Lu, D.P. Chassin, S.E. Widergren, "Modeling uncertainties in aggregated thermostatically controlled loads using a State queueing model," IEEE Trans. on Power Systems, vol.20, no.2, pp.725-733, May 2005

[91] M. Hamdi and G. Lachiver, “A fuzzy control system based on the human sensation of thermal comfort,” in Proc. IEEE World Congress on Computational Intelligence, vol.1, no., pp.487-492 vol.1, 4-9 May 1998, Anchorage, AK

[92] F. Calvino, M. La Gennusa, G. Rizzo, and G. Scaccianoce. "The control of indoor thermal comfort conditions: introducing a fuzzy adaptive controller." Energy and Buildings, vol.36, no.2, pp.97-102, Feb. 2004

[93] Chen, Kuentai, Yue Jiao, and E. Stanley Lee. "Fuzzy adaptive networks in thermal comfort." Applied Mathematics Letters, vol. 19, no. 5, pp. 420-426, May 2006.

[94] Liang, Jian, and Ruxu Du. "Thermal comfort control based on neural network for HVAC application." In Proceedings of IEEE Control Applications Conference, pp. 819-824., 28-31 Aug 2005, Toronto, Ont.

[95] S.M. Hakimi, S.M. Moghaddas-Tafreshi "Optimal Planning of a Smart Microgrid Including Demand Response and Intermittent Renewable Energy Resources," IEEE Trans. on Smart Grid, vol.5, no.6, pp.2889-2900, Nov. 2014

[96] Torgeir Ericson “Direct load control of residential water heaters”, Energy Policy, Volume 37, Issue 9, September 2009, pp 3502–3512

[97] Wenbo Shi; Na Li; Xiaorong Xie; Chi-Cheng Chu; Gadh, R., "Optimal Residential Demand Response in Distribution Networks," IEEE Journal on Selected Areas in Communications, vol.32, no.7, pp.1441-1450, July 2014

[98] N. Motegi, M.A. Piette, D.S. Watson, S. Kiliccote, P. Xu, “Introduction to commercial building control strategies and techniques for demand response.” Lawrence Berkeley National Laboratory, 22 May 2007, LBNL-59975, Berkeley, CA.

[99] Dan Wang ; Shaoyun Ge ; Hongjie Jia ; Chengshan Wang ; Yue Zhou ; Ning Lu ; Xiangyu Kong “A Demand Response and Battery Storage Coordination Algorithm for Providing Microgrid Tie-Line Smoothing Services,” IEEE Trans. on Sustainable Energy, vol. 5, no. 2, pp. 476-486, April. 2014.

[100] D. Pudjianto, M. Aunedi, P. Djapic, G. Strbac, “Whole-Systems Assessment of the Value of Energy Storage in Low-Carbon Electricity Systems,” IEEE Trans. on Smart Grid, vol. 5, no. 2, pp. 1098-1109, March. 2014.

[101] H.S.V.S. Kumar Nunna, S. Doolla, L. Ning, K. Xiangyu "Energy Management in Microgrids Using Demand Response and Distributed Storage—A Multi agent Approach," IEEE Trans. on Power Delivery, vol. 28, no. 2, pp. 939-947, April. 2013.

[102] W. Alharbi, K. Bhattacharya, "Demand response and energy storage in MV islanded microgrids for high penetration of renewables," IEEE Electrical Power & Energy Conference (EPEC), 6p, 21-23 Aug. 2013, Halifax, NS

[103] K. Mackey, R. McCann, K. Rahman, R. Winkelman, "Evaluation of a battery energy storage system for coordination of demand response and renewable energy resources," 4th IEEE International Symposium on Power Electronics for Distributed Generation Systems (PEDG), 8p, 8-11 July 2013, Rogers, AR

[104] S. Pazouki, M.R. Haghifam, "Comparison between demand response programs in multiple carrier energy infrastructures in presence of wind and energy storage technologies," Smart Grid Conference (SGC), 6p, 9-10 Dec 2014, Tehran, Iran.

[105] Longbo Huang; J. Walrand, K. Ramchandran, "Optimal demand response with energy storage management," IEEE Third International Conference on Smart Grid Communications (SmartGridComm), 6p, 5-8 Nov. 2012, Tianan, Taiwan

[106] J. J. Conti, P. D. Holtberg, J. R. Diefenderfer, "Annual Energy Outlook 2015, with projections to 2040", U.S. Energy Information Administration Office of Integrated and International Energy Analysis, U.S. Department of Energy Washington, DC [Online]. Available: eia.gov/forecasts/aeo/pdf/0383(2015).pdf

[107] I. Perez-Arriaga: Managing Large Scale Penetration of Intermittent Renewables, MITEI Symposium on Managing Large-Scale Penetration of Intermittent Renewables, Cambridge, U.S.A, 20 April 2011, 43p.

[108] J.E. Runnels, M.D. Whyte, "Evaluation of demand-side management," Proceedings of the IEEE, vol.73, no.10, pp.1489-1495, Oct. 1985.

[109] PJM Interconnection capacity by fuel type 2013, [on-line]. Available : http://www.pjm.com/~/media/markets-ops/ops-analysis/capacity-by-fuel-type-2013.ashx Viewed on 6 July 2015

[110] PJM Interconnection hourly Load data 2013 [on-line]. Available : http://www.pjm.com/markets-and-operations/ops-analysis/historical-load-data.aspx Viewed on 6 July 2015

[111] Personal Communication, email with Clyde Loutan, California ISO, date, April 11, 2014.

[112] ASTM-E1049-85. (Re-approved 2011). Standard Practices for Cycle Counting in Fatigue Analysis. American society for testing and materials (ASTM) International, West Conshohocken, PA, 2011.

[113] S. D. Downing and D. F. Socie, "Simple rain flow counting algorithms," Int. J. Fatigue, vol. 4, pp. 31–40, 1982.

[114] R. Dufo-López, J.L. Bernal-Agustín, and José A. Domínguez-Navarro, "Generation management using batteries in wind farms: Economical and technical analysis for Spain", IET Energy Policy, Volume 37, Issue 1, August 2009, Pages 126-139.

[115] N. Lu, M.R. Weimar, Y.V. Makarov, J. Ma, and V.V. Viswanathan, "The Wide-Area Energy Storage and Management System – Battery Storage Evaluation," PNNL-18679, Pacific Northwest National Laboratory, Richland, Washington, 2009.

[116] Wayne L. Winston, Operations Research Applications and Algorithms, fourth edition, Brooks/Cole, a division of Thomson Learning Inc., 2004.

[117] S. J. Hayes. Technical Analysis of Pumped Storage and Integration with Wind Power in the Pacific Northwest, Final report for Hydroelectric Design Center, Aug 2009, 166p.

[118] D. K. Critz, "Power system balancing with high renewable penetration: The potential of demand response," M.S. thesis, Eng. Syst. Div., Mass. Inst. Technol., Cambridge, MA, USA, 2011.

[119] H. Bitaraf, H. Zhong, and S. Rahman, "Managing Large Scale Energy Storage Units to Mitigate High Wind Penetration Challenges", IEEE Power and Energy Society General Meeting, 6p, 22-26 July 2015, Denver, Colorado.

[120] H. Bitaraf, S. Rahman, M. Pipattanasomporn, "Sizing Energy Storage to Mitigate Wind Power Forecast Error Impacts by Signal Processing Techniques," IEEE Trans. on Sustainable Energy, vol.6, no.4, pp.1457-1465, Oct. 2015